九州大学学術情報リポジトリ
Kyushu University Institutional Repository

A study on EEG based motion intention estimation techniques for control of upper limb wearable robots

ダンワッタ サンジャヤ ヴィプラ バンダーラ

https://hdl.handle.net/2324/1959100

出版情報：Kyushu University, 2018, 博士（工学）, 課程博士
バージョン：
権利関係：

KYUSHU UNIVERSITY

A study on EEG based motion intention estimation techniques for control of upper limb wearable robots

DANWATTA SANJAYA VIPULA BANDARA

A dissertation submitted in partial
fulfillment of the requirements for the
Doctor of Philosophy degree in
Mechanical Engineering, Department of
Mechanical Engineering, Graduate School
of Engineering, Kyushu University, Japan

九州大学

Supervisor: Prof. Kazuo Kiguchi

Acknowledgement

“Strong people don't put others down... They lift them up.”

During the time of my PhD, I was lucky to be surrounded by strong people who did not let me down, instead lift me up. This is a small not of acknowledgement for them.

First and foremost, my supervisor Prof. Kazuo Kiguchi is one of the greatest human beings I have met in my life and without his patience, guidance and advices, completion of this thesis would not have been possible. I am really thankful to him for all the support and guidance given to me, leading by example as a successful researcher and an academic. In a similar manner, I want to thank Prof. Ruwan Gopura of University of Moratuwa, Sri Lanka for introducing to my PhD supervisor. Prof. Gopura was my advisor for the master’s thesis and meeting him was a key point in my life. Further, I need to extend my thanks to Associate Prof. Jumpei Arata of my laboratory. His kind and friendly helps and advices to achieve success in this thesis were invaluable. I also need to convey my gratitude to the members of the dissertation committee Prof. Ryo Kurazume and Prof. Motoji Yamamoto for their valuable suggestions and comments.

I would like to especially acknowledge; Ministry of Education, Science, and Culture, Japanese Government, for the financial support granted me under the Monbukagakusho scholarship scheme for my studies at Kyushu University.

Next, I want to thank my lab mates, Koki Honda, Kaori Tamura, Kurahachchi, Kanazawa, Kamura, Hora for their immense support during the experiments and other day to day activities in Japan. Further, I owe a big thanks to Ms. Ayako Kashiwagi, Ms. Nami Murakami and Ms. Kumiko Uchida, administrative staff of my laboratory. Their great helps during the affairs outside the laboratory to make the living easy in Japan for me and my family will never be forgotten.

I also convey my thanks to the Sri Lankan community in Fukuoka, especially Dhammika, Prof. Athula, Naamal, Ranga & Samindi, Buddhika and Dassanayaka for their company during my stay for the PhD in Fukuoka. I never felt like I am living

outside from Sri Lanka, when I am with them. I would like to thank all the other unnamed Sri Lankan, Japanese, and foreign friends in Fukuoka for making my life an enjoyable one.

Last but not least, I need to thank to my family. For the last 32 years, my parents were my biggest supporters. My father was a role model for me and his guidance until now has never let me down in my life. On the other hand, my mother was right next to me giving me the courage to get success in every tasks I have being doing. I need to thank my father and mother. In the same manner, my brother was there with me always supporting my every endeavor. I need thank him for his great support. This thesis reflects the patience and courage of my wife, Manosha. I need to thank my wife for being with me and all the support given to me during this journey. Finally, I need to thank my beautiful daughter, Nuvini. Her smile and words were the greatest motivation to complete this thesis.

Abstract

In todays' world, aging population or disabilities due to accidents, war or congenital diseases have created a society with different abilities which needs a special attention and care. Recently, introduction of robotic technologies to the available traditional assistive and care taking methodologies, draws more attention from the community, due to their intuitiveness and the effective in use. Wearable robots such as prostheses or exoskeleton robots are worn by human operators, to supplement the function of a limb or to replace it completely. In order for better use of these wearable robotic systems, its mechanical design is utmost important. Similarly, in order to control the robots according to their wearer's motion intention, understanding of the wearer's motion intention is also extremely important, yet challenging. Amongst different biological and no-biological methods for motion intention identification, Electroencephalography (EEG) signals recorded from the scalp of the human head are expected to contain information related to motion intention of the wearer. The objective of this thesis is to study different approaches to estimate the motion intention using EEG signals, towards real-time control of a wearable robot using EEG signals.

In this thesis, a new approach to control several degrees of freedoms (DoF) in a wearable robot is proposed by estimating the users motion intention in real-time, in terms of the user's intended tasks to perform, by using EEG signals measured from the scalp of the user. A time-delayed feature matrix constitutes of the power band features of EEG signals is introduced to provide inputs to neural network and support vector machine (SVM) based classifiers that harvest the dynamic nature of the EEG signals for motion intention prediction. In order to estimate the motion intention, individual classifiers are trained for each individual subject for both types of classifiers. At the same time, another two different classifiers are trained with data from all the subjects. The results show that the SVM based classifiers perform better in terms of the prediction accuracies. Conversely, quicker predictions were obtained from the neural network based classifiers. As a conclusion, the experimental results indicate the effectiveness of the proposed methodology in the prediction of user's motion intention.

In addition, an EEG based hierarchical two-stage approach is proposed to achieve multi-DoF control of a transhumeral prosthesis. In the proposed method, the motion intention for arm reaching or hand lifting is identified using classifiers trained with motion-related EEG features. For this purpose, neural network and *k*-nearest neighbor classifiers are used. Then, elbow motion and hand endpoint motion is estimated using a different set of neural-network-based classifiers, which are trained with motion information recorded using healthy subjects. The predictions from the classifiers are compared with residual limb motion to generate a final prediction of motion intention. This can then be used to realize multi-DoF control of a prosthesis. The experimental results show the feasibility of the proposed method for multi-DoF control of a transhumeral prosthesis. This proof of concept study was performed with healthy subjects.

Conversely, the feasibility of using two different approaches to estimate the user's motion intention in terms of velocity are also evaluated in this thesis. In the first method, the activation of the brain is identified in an offline study and the results are used to train a neural network based classifiers to estimate the 2 DoF motion velocity. This will enable the control of similar number of DoFs of the robot. In the latter method, to estimate the velocity of the hand end point, root mean square (RMS) based feature matrix introduced as input to the nonlinear autoregressive network with an exogenous input. Experiments results show that the proposed methods are capable of estimating the user's motion intention in terms of velocity.

Table of Contents

Chapter 1 Introduction 1

1.1 Motivation 2

1.1.1 Caretaking and assistance 5

1.2 Wearable Robots 6

1.2.1 Upper Limb Exoskeleton 6

1.2.2 Upper Limb Prosthesis 7

1.2.3 Controlling of Wearable Robots 8

1.3 Brain Computer Interface Systems 10

1.3.1 Human Brain 11

1.3.2 Categorization of BCI techniques 13

1.3.4 Invasive BCI techniques. 14

1.3.5 Noninvasive BCI techniques 18

1.4 Setup of experimental platform 23

1.4.1 Electrode placement for EEG recording 23

1.4.2 Recording of EEG signals 24

1.4.3 Recording of motion 25

1.5 Contribution of the thesis 26

1.6 Thesis Overview 27

Chapter 2 Estimation of Motion Intention of ADL Tasks for Upper-Limb Wearable Robot with EEG Signals 35

2.1 Introduction 36

2.2 Method 39

2.2.1 Experimental setup 41

2.2.2 Offline analysis 43

2.2.3 Real-time prediction 44

2.3 Results 49

2.3.1 Frequency analysis 49

2.3.2 Neural network-based prediction 51

2.3.3 SVM-based prediction 53

2.3.4 Latency 55

2.4 Discussion 56

2.5 Conclusions 59

Chapter 3 EEG Based Control Approach for a Transhumeral Prosthesis 65

3.1 Introduction 66

3.2 Methodology 69

3.2.1 EEG based motion intention identification 69

3.2.2 Experimental Setup.....70

3.2.3 Data processing 73

3.2.4 Feature extraction.....72

3.2.5 Neural Network based motion intention estimation 76

3.2.6 k- nearest neighbor based motion intention estimation……..….77

3.2.7 Comparison.....78

3.2.8 Motion analysis 78

3.3 Results 80

3.3.1 Neural network based motion intention estimation 80

3.3.2 k-nn based motion intention estimation…….81

3.3.2 Motion relationships 81

3.3.3 Motion estimation 83

3.4 Discussion 84

3.5 Conclusions 88

Chapter 4 Velocity based Estimation of Motion Intention of Wearable Robot Users 93

4.1 Introduction 94

4.2 Methodology 96

4.2.1 Joint based velocity estimation.....97

4.2.2 Trajectory based velocity estimation 100

4.3 Results 103

4.3.1 Joint based velocity estimation 103

4.3.2 Trajectory based velocity estimation 106

4.4 Conclusions 107

Chapter 5 Conclusion and Future Work 110

5.1 Conclusion 110

5.2 Future Directions……..…….……...114

List of figures

Fig. 1.1: Percentage of population aged 60 years or over by region, from 1980 to 2050 (reproduced from [1]) ……..……...03

Fig. 1.2: Old age dependency ration by region, from 1980 to 2050 (reproduced from [1]……04

Fig. 1.3: Exoskeleton Robots (a)LIMPACT[17] (b) HEXAR[18] (c) SUEFUL – 7[19] …….07

Fig. 1.4: Robotic Prostheses (a) DEKA Arm (b) UOM – Arm (c) Smarthand…….... 08

Fig. 1.5: Structure of the Controller for SEUFUL – 7 (reproduced from [19])……..10

Fig. 1.6 : Lobes of the brain (reproduced from [42])…….……11

Fig. 1.7: Functional Cortical Areas of the left Cerebral hemisphere (reproduced from [42])…….....12

Fig. 1.8: Functional area map of motor cortex for different motor actions of the body (reproduced from [42])…….....13

Figure 1.9: Classification of Brain Computer Interface Techniques…….….14

Fig. 1.10: Micro Electrode Array (reproduced from[48])……..15

Fig. 1.11: Patient with tetraplegia (a) access method to the implanted electrodes array (b) activations of the patient's brain – black squares approximate postions of the electrode arrays on the motor cortex (reproduced from [38])…….……...…15

Fig. 1.12: Placement of ECoG electrodes in the cortices (reproduced from [49])....16

Fig. 1.13: NIRS based hand rehabilitation robot (a) Hand exoskeleton robot (b) experimental setup……..……...19

Fig. 1.14: Nomenclature and electrode locations of 10 – 20 electrode system (reproduced from [59])……..…….23

Fig. 1.15: (a) g.LADYbird electrode (b) g.gammacap……..…..…24

Fig. 1.16: Electrical connection system for the EEG recordings……..…...25

Figure 1.17: Thesis Overview…….…….....27

Fig. 2.1: Proposed approach for wearable robot control (dark background – offline analysis ⟶ - raw EEG ⟹ - preprocessed EEG ⟹ - filtered EEG)…..39

Fig. 2.2: Selected channel locations according to the 10 – 20 system……..…..…..41

Fig. 2.3: Experimental setup (a) Moving (b) Drinking……..42

Fig. 2.: Task schedule for twenty-four tasks in the experiment (1: movement; −1: drinking; 0: resting)……...43

Fig. 2.5: Different activation functions for neural networks (a) Step (b) Arbitrary are used to perform arithmetic summing that will be followed by an activation function [32]. Accordingly, the network (*N*) will be Step (c) Threshold Linear (d) Sigmoid…45

Fig. 2.6.: Structure of the trained neural network……..……47

Fig. 2.7: Linear classifier and margins (Reproduced from [33])……...…...48

Fig. 2.8: FFT results for electrodes (a) F7 and (b) C5 for subject 1…..……..50

Fig. 2.9: Activation of electrodes F7 and F8 (where D is drinking and M is moving..50

Fig. 2.10: Comparison of actual velocities of elbow flexion/extension with predicted velocities for two subjects. (a) Actual output from the neural network. (b) Corresponding Rounded output. (c) Actual output from the neural network(d) Corresponding Rounded output.....…….51

Fig. 2.11: Comparison of actual tasks with predicted tasks for the SVM for four subjects (a) Subject 1 (b) Subject 2 (c) Subject 3 (d) Subject 5……53

Fig. 2.12: Analysis of results for all six subjects with four different types of

prediction……..….56

Fig. 2.13: Comparison of results for different subjects……...57

Fig. 2.14. Latency of predicted motion relative to the expected motion for all six subjects……58

Fig. 3.1: Targeted Muscle Reinnervation (reproduced from [11])…….……66

Fig. 3.2: Proposed Hierarchical Approach…….…….68

Fig. 3.3: Proposed approach for the motion identification, CAR – Common average reference…….…….……69

Fig. 3.4: Electrode layout for experiment……69

Fig. 3.5: Recording of the motion data (a)Motion Capture System (b)Reflective Markers attached to the upper limb of the subject……..……..……..70

Fig. 3.6: Motions used in the experiment. (a) Arm lifting. (b) Hand reaching……..71

Fig. 3.7: Motion schedule (1 = arm lifting motion, 0 = rest, −1 = hand reaching motion)…….……...71

Fig. 3.8: Feature plots for channel selection. (a) MRCP. (b) Delta band power. (c) RMS……74

Fig. 3.9: Proposed approach for estimation of identified motion (Sn—healthy individuals, n—1, 2, 3, …, Ux—residual limb joint angle of the transhumeral amputee)…77

Fig. 3.10: Prediction from the system with MRCP for subject 1 (1 = lifting motion, −1 = reaching motion, 0 = rest, blue line = prediction, orange line = subject motion)……..……..81

Fig. 3.11: Motion relationships. (a) Elbow flexion/extension angle to the shoulder flexion/extension angle for reaching. (b) Variation of the endpoint with the shoulder flexion/extension angle…….……..81

Fig. 3.12: Comparison of data measured experimentally (blue line) and those generated by the neural network classifier (orange line). (a) Estimated elbow flexion/extension angle. Hand trajectory in the (b) x direction and (c) y direction……..……83

Fig. 3.13: Summary of the results of the motion intention classifiers (error bars show the standard deviation)……85

Fig. 3.14: Comparison of the estimation results for neural network based estimation before and after the gating method ……86

Fig. 3.15: Comparison of the estimation results for k–nn based estimation before and after the gating method……..….87

Fig. 4.1: Velocity estimation approaches (a)Joint based velocity estimation (b)End – point velocity estimation…….96

Fig. 4.2: Proposed approach for motion intention estimation…….97

Fig. 4.3: Experimental setup (a) Electrode layout (b) Recording environment with motion capture system ……..……...98

Fig. 4.4: Proposed approach for motion estimation……...…….…….100

Fig. 4.5: Experimental Conditions (a)Electrode Layout (b) Different motion steps of reaching motion……..……..….101

Fig. 4.6: Representation of RMS in multiple time widows……102

Fig. 4.7: Structure of the neural network used for trajectory estimation……..103

Fig. 4.8: Power spectrum analysis (a) P3 (b) F4…….……104

Fig. 4.9: Time series data of selected electrodes……..……..105

Fig 4.10: Comparison of actual velocity with predicted velocity (a) Elbow flexion/ extension (b) wrist flexion/ extension……105

Fig 4.11: Feature Plot for CP1……..…….106

Fig 4.12: Comparison of predicted velocity with real velocity of end point of hand (blue – prediction, orange – real) (a) Subject 1 (b) Subject 2, (smoothed for clarity……..……..…107

List of tables

Table 1.1: Summary of BCI systems in use……...22

Table 2.1: Results for six subjects produced by the neural networks (Individual Training.....52

Table 2.2: Results for six subjects produced by the neural networks (Collective Training)……...…..52

Table 2.3: Results for six subjects produced by the SVM (Individual Training)…….……...54

Table 2.4: Results for six subjects produced by the SVM (Collective Training)…….……...54

Table 2.5: Latency of real motion onset and estimated motion onset ……...55

Table 3.1: Summary of configuration of proposed Neural Networks (NN) ……..76

Table 3.2: Rules of comparison for residual limb motion and the Neural Network (NN) output……..78

Table 3.3: Summarized results for 5 subjects for neural networks…..……80

Table 3.4: Summarized results for 5 subjects for k-nn classifiers…..……81

Chapter 1

Introduction

Chapter Overview

In todays' world, aging population or disabilities due to accidents, war or congenital diseases have created a society with different abilities which needs a special attention and care. Due to the deficiencies, their independency is diminished and the social and economic contribution is deteriorated. Providing a special care or assistance by human beings for these individuals further become an obligation for the demanding life styles of the healthy individuals having a bad impact to their socio-economic states. As a results, the requirement of developing assistive and care taking technologies has become a demand towards enabling the differently able community to have an individual life style of their own. Among available different assistive technologies, wearable devices such as prostheses and orthoses are popular among their users due to the easiness of use and the effectiveness. Prostheses are the replacement for lost limb parts and orthoses are worn form outside of the body being a support to the weak body parts. With the improvement of the technology, prostheses and orthoses which can be actuated electrically have being developed. These are known as wearable robotic devices that replace the body powered or non – actuated counterparts. With the introduction of the robotic technologies, the capabilities of these wearable devices have drastically increased by enabling their wearers to perform multi degrees of freedom motions simultaneously to assist their activities of daily living. Similar to the improvement to their mechanical aspects, control aspects of these robotic systems also demands improvements in catering the requirement for more intuitive control of these devices according to the movement intentions of their users. This chapter initially introduces available wearable robotic technologies. It will be followed by the information of available control approaches for identification of motion intention from the human subjects. This will include an explanation about the available BCI based control techniques that will be followed by a description of the behavior of the brain.

Chapter 1

1.1 Motivation

In 2017, the report on World Population Ageing by the department of economic and social affairs of united nations presents the existing status of population growth as follows [1].

> "The world's population is ageing: older persons are increasing in number and make up a growing share of the population in virtually every country, with implications for nearly all sectors of society, including labor and financial markets, the demand for goods and services such as housing, transportation and social protection, as well as family structures and intergenerational ties. Preparing for the economic and social shifts associated with an ageing population is thus essential to fulfil the pledge of the 2030 Agenda for Sustainable Development that "no one will be left behind". Trends in population ageing are particularly relevant for the Sustainable Development Goals (SDGs) related to poverty eradication, the promotion of health, gender equality, employment and sustainable human settlements, as well as those on reducing inequality within and across countries and promoting peaceful and inclusive societies."

In addition, following key points were highlighted in the same report, as the current trends with growing of the elderly population.

- The global population aged 60 years or over numbered 962 million in 2017, more than twice as large as in 1980 when there were 382 million older persons worldwide. The number of older persons is expected to double again by 2050, when it is projected to reach nearly 2.1 billion.
- Across 143 countries or areas with available data, the proportion of persons aged 60 or over who live "independently" —alone or with a spouse only—varied widely, ranging from a low of 2.3 per cent in Afghanistan to a high of 93.4 per cent in the Netherlands.

- In Asia, in Africa and in Latin America and the Caribbean, well over half of persons aged 60 or over co-resided with a child circa 2010; by contrast, in Europe and in Northern America only around 20 per cent of older persons co-resided with their children.

According to the above status, it is evident that the current phase of ageing population is increasing over the time as predicted in Figure 1.1., globally. Not only that, the dependency of the elderly population also keeps growing with the increment in population with time by 2050 as shown in Figure 1.2.

In addition to this, disability and limb loss also affect the independency of an individual. According to the recent census studies based in United States, approximately 5.4 million people have some kind of disability caused majorly by stroke, multiple sclerosis, spinal cord injury or cerebral palsy [2], whereas an estimated

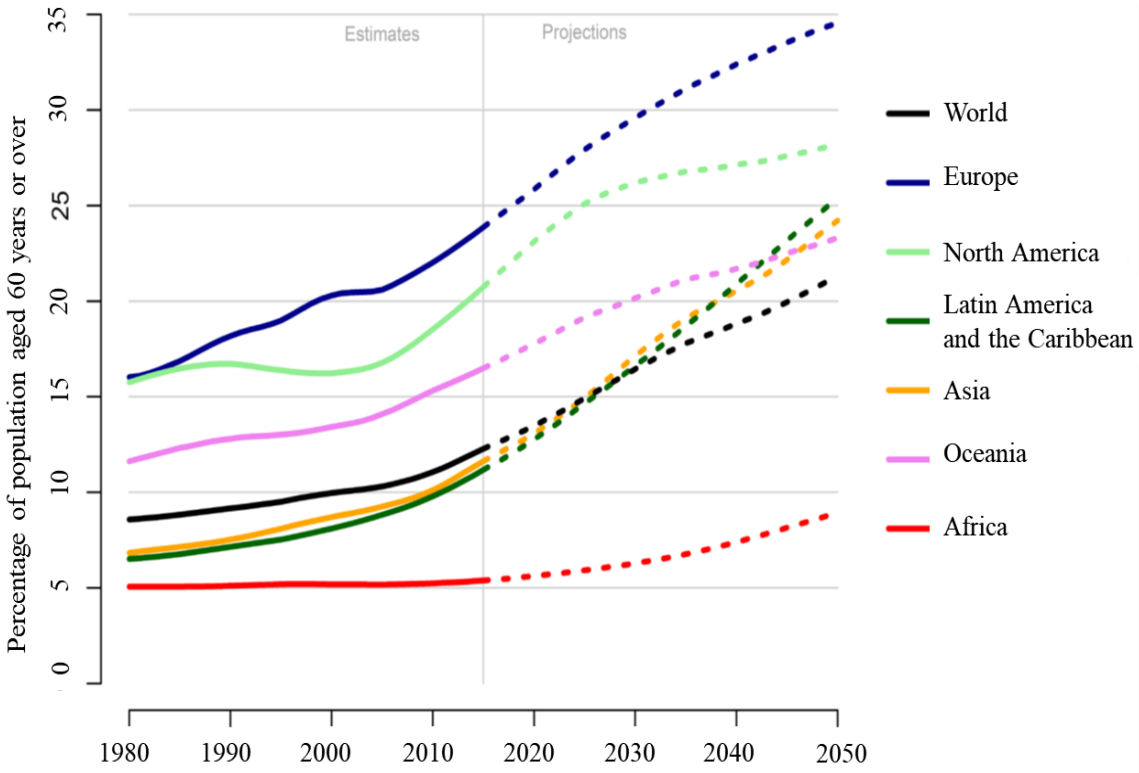

Fig. 1.1: Percentage of population aged 60 years or over by region, from 1980 to 2050 (reproduced from [1])

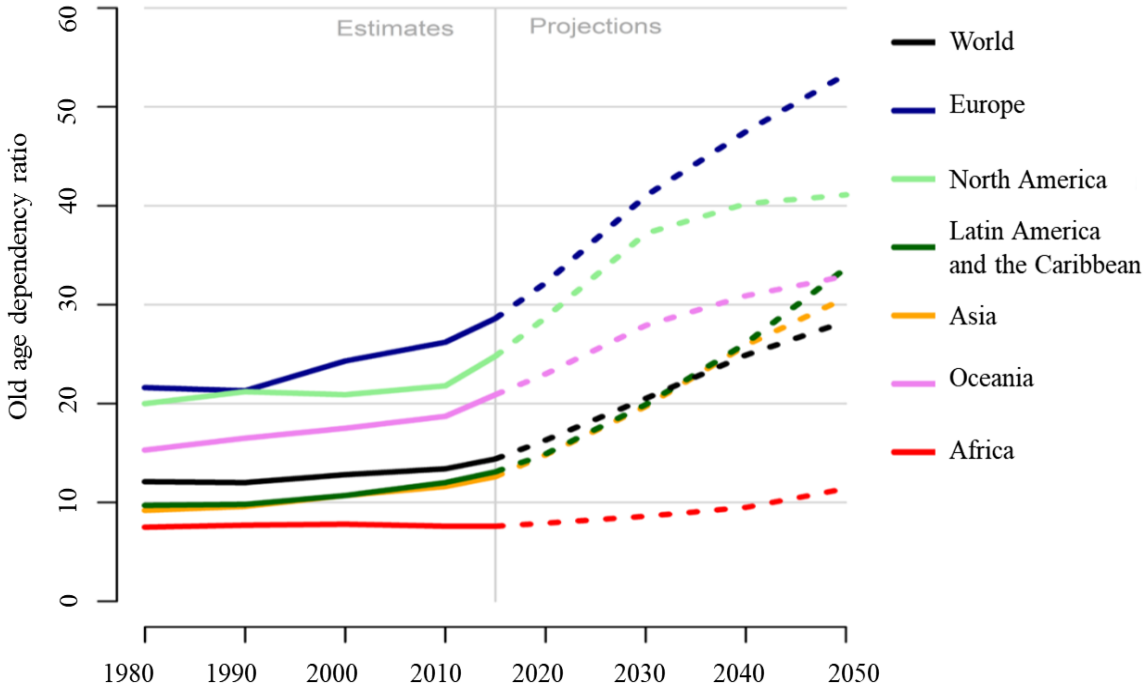

Fig. 1.2: Old age dependency ratio by region, from 1980 to 2050 (reproduced from [1])

185,000 of people undergo an amputation annually [3], caused by diabetes mellitus, dysvascular disease, trauma or malignancy of the bone and joint [4]. Although there is no much information about the global status of the disability and ambulatory, it can be assumed to have a similar, or only a slight difference in the trend. Therefore, not only the ageing but disability also contribute to the increment of dependency.

In addition, following points in the Assistive Technology Act of 1998 in United States are noteworthy [5].

- Disability is a natural part of the human experience and in no way diminishes the right of individuals to -

  (a) live independently;

  (b) enjoy self-determination and make choices;

  (c) benefit from an education;

(d) pursue meaningful careers; and

(e) enjoy full inclusion and integration in the economic, political, social, cultural, and educational mainstream of society in the United States.

It also defines the term assistive technology device [5].

- The term “assistive technology device” means any item, piece of equipment, or product system, whether acquired commercially, modified, or customized, that is used to increase, maintain, or improve functional capabilities of individuals with disabilities.

Accordingly, due to lack of movability owing to the different deficiencies of these individuals with disabilities, their individual life style is affected and the social and economic contribution is deteriorated. Providing a special care or assistance by human beings for these individuals with disabilities further become an additional obligation for the demanding life styles of the healthy individuals having a bad impact on their socio-economic states.

1.1.1 Caretaking and assistance

In order to improve the mobility of these individuals with disabilities, to have a more independent life, common examples of assistive devices that in use are crutches, prostheses, orthoses, wheelchairs and tricycles [6]. Recently, introduction of robotic technologies to the available traditional assistive and care taking methodologies, draws more attention from the community, due to their intuitiveness and the effective in use. Therefore, the goal of assistive robotics, is to develop robotic aids for supporting independent living of persons who have chronic or degenerative limitations in motor and/or cognitive abilities such as the elderly and persons with severe disabilities [7]. Different kinds of assistive robotic devices were developed recently for a variety of applications. Robotic prosthesis [8], exoskeleton robots [9], wheel chair robots [10], companion robots [11], etc.. are some of them.

The focus of this study lies on the assistive robotic devices that can be worn. The main two types of wearable robotic devices are robotic prostheses and exoskeleton robots. In order for better use of these wearable robotic systems, its mechanical design is utmost important. Similarly, in order to control the robots according to their wearer's motion intention, understanding of the wearer's motion intention is also extremely important, yet challenging. In order for this purpose, different non–biological and biological methods are available. Amongst, Electroencephalography (EEG) signals recorded from the scalp of the human head are expected to contain information related to motion intention of the wearer.

The objective of this thesis is to study different approaches to estimate the motion intention using EEG signals, towards control of a wearable robot using EEG signals. EEG signals are dynamic in nature, contain high density of information and higher noise/signal ratio. The research work presented in this thesis attempts to investigate new paradigms to address the issues related to the EEG based motion intention identification. The contribution and the overview of the thesis are explained in the following sections.

1.2 Wearable Robots

As defined by Pons *et. al.* [12], wearable robots can be defined as person oriented robots those worn by human operators, whether to supplement the function of a limb or to replace it completely. When they act to supplement a function of a limb, they are called orthoses or exoskeletons [9], [13], [14]. When they are used to replace a limb completely, they are called prostheses [8], [15], [16].

1.2.1 Upper Limb Exoskeleton

Upper limb exoskeleton robots have joints and links that are corresponded to the joints and links of the human upper limb and are worn parallel to them. Upper limb exoskeleton robots are expected to act as power augment devices, rehabilitation devices, haptic interactions or more recently as body evaluation devices. The number

(a) (b) (c)

Fig. 1.3: Exoskeleton Robots (a)LIMPACT[17] (b) HEXAR[18] (c) SUEFUL – 7[19]

of DoFs the exoskeleton robot may depend on the design of the robot and the corresponding joints of the human body. To date, number of exoskeleton robots have been developed for different applications [17]–[19]. Figure 1.3 shows some of the recently developed upper limb exoskeleton robots. HEXAR [18], which is shown in Figure 1.3(b), was developed with 3 DoFs for power augmentation of the exoskeleton wearer. SUEFUL–7[19] (See Figure 1.3(c)) was developed in SAGA University, Japan for power augmentation of physically weak patients with 7 DoFs.

1.2.2 Upper Limb Prosthesis

Upper limb robotic prosthesis will replace a missing upper limb part of an amputee. It is expected to regain the lost appearance and functions of the missing limb, using the robotic prosthesis. Depending on the amputation level of the upper limb, the prosthesis mainly can be a shoulder prosthesis, transhumeral prosthesis, transradial prosthesis, hand prosthesis or a finger prosthesis. Recently, different types of upper limb prostheses have been developed [20]–[22]. DEKA arm [20] was developed as a shoulder prosthesis with active 10 DoFs. It has 3 configurations for shoulder level amputees, for transhumetal amputees and for transradial amputees. The generation 3 of the prosthetic arm can generate human alike motions and is shown in Figure 1.4 (a). In [21], a transhumeral robotic arm prosthesis shown in Figure 1.4 (b) was proposed

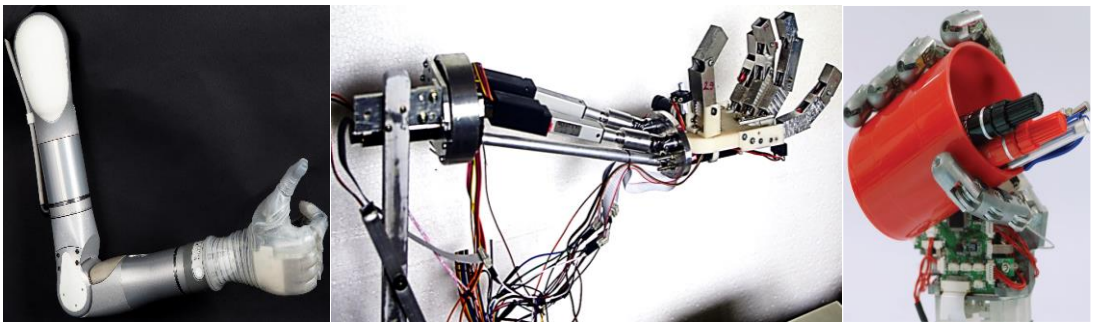

, (a) (b) (c)

Fig. 1.4: Robotic Prostheses (a) DEKA Arm (b) UOM – Arm (c) Smarthand

by a group of researchers in University of Moratuwa of Sri Lanka. It can generate 5 basic grasping modes in the hand, wrist flexion/extension, wrist ulna/radial deviation, forearm supination/pronation and elbow flexion/extension. The smarthand [22] was developed in Italy and is an underactuated five fingered prosthetic hand with 16DoFs, actuated by 4 motors. Smarthand is shown in Figure 1.4 (c).

1.2.3 Control of Wearable Robots

To date, mechanical designs of the wearable robots have achieved the required anthropomorphic features in their designs that might please their users to a certain extent. However, the development of a suitable control strategy to provide required actuation commands to the wearable robot also important in providing a better user experience for the wearable robot user. In order to provide correct commands to the actuators, it is necessary to identify the users' motion intention to move. Once the motion intension is identified, the required support can be generated by the exoskeleton robot or the required motion can be generated by the robotic prosthesis with a perfectly built system.

Among the available techniques to control a wearable robot according to the users' desired motion, biological signal based control techniques have shown a greater success. Amongst, electromyography (EMG) based techniques and the brain signal

based techniques are popular among the researchers. Next sections explain the details associated with EMG and brain signal based motion intention identification methods

A. EMG based control of wearable robots

EMG signals are electrical potential differences that can be measured from the muscle sites. EMG signals mainly can be classified into two types based on the invasiveness [23]. When they are measured from the surface of the muscle non–invasively, they are called surface EMG (sEMG). When a needle is used inside the muscle, it becomes invasive and named intramuscular EMG (iEMG). iEMG provides a better accuracy and repeatability than sEMG [24]. However due to the ease of use and non–invasiveness, sEMG based control of wearable robots is becoming popular. To date, several studies [15], [19] have proposed EMG based control for wearable robots.

EMG based control of a transhumeral prosthesis [15]

Saga University prosthetic arm was developed for the realization of 5DoF upper limb motions for a transhumeral amputee. The hand is controlled using a combination of an EMG based controller (EBC) and a task oriented kinematic based controller (KBC). In a transhumeral amputee, a part of the biceps and triceps are remaining. EMG signals of the amputee's biceps and triceps are used as the input information for the EBC to control elbow flexion/extension and hand grasp/release. Forearm supination/pronation, wrist flexion/extension and ulnar/radial deviation get controlled from the KBC. Motion intention of the amputee is identified via a task classifier using shoulder and prosthesis elbow kinematics. For the scope of this context, only the EBC will be considered. EMG based fuzzy controller is the base for EBC. It proportionally controls the torque of the elbow and hand actuator according to the amount of the EMG signal. The activation of biceps generates the elbow flexion and the activation of triceps generates the elbow extension. Hand grasp is realized when both triceps and biceps are activated simultaneously. The release position of the hand is achieved when the both muscles are not working

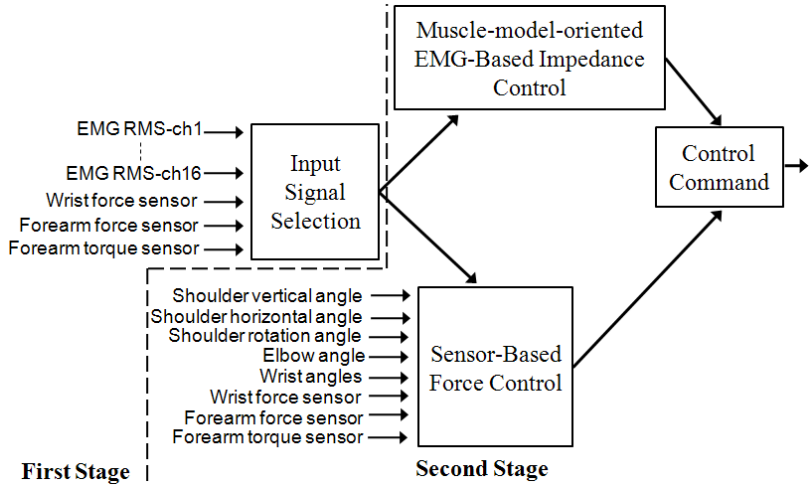

Fig. 1.5: Structure of the Controller for SEUFUL – 7 (reproduced from [19])

SUEFUL–7 [19]

SUEFUL–7 is an upper limb exoskeleton robot with 7 DoF (3 DoFs for Shoulder, 1 DoF for Elbow, 1 DoF for forearm and 2 DoFs for Wrist). In order to obtain the real time control, an EMG based, muscle-model-oriented control method has been proposed. An impedance controller is applied with the muscle-model-oriented control method and impedance parameters are then adjusted in real time as a function of upper-limb posture and EMG activity level [19]. The controller of the SUEFUL–7 [19] uses EMG signals from 16 locations of the user as the primary input information. Also, forearm force, hand force and forearm torque are used as secondary input information for the controller [19]. The structure of the controller is shown in Figure 1.5. The first stage is the input signal selection and the second stage is muscle model oriented EMG based impedance control. Proper input information is selected to the controller according to muscle activity levels in the first stage. Depending on the RMS of the EMG signal, muscle model oriented EMG based control or sensor based force control is selected under the second stage and it is fed as a control command to the robot. This hybrid nature of the control method is a guarantee to activate the SUEFUL–7 even with low EMG signal level. On the other hand, when EMG signals are high, the robot is controlled mainly by the EMG signal generated by user motion.

1.3 Brain Computer Interface Systems

Brain-computer interface (BCI) is a method of communication between the human brain and an external device based on neural activity generated in the brain and is independent of its normal output pathways of peripheral nerves and muscles [25]. Over the recent years, both noninvasive [26]–[34] and invasive [35]–[40] BCI systems have been proposed. Before study about the BCI techniques, it is important to understand the main functions and structure of the brain. Next sections explain the same. A summary of the available BCI systems for motion estimation is shown in Table 1.1, at the end of the section.

1.3.1 Human Brain

The brain is one of the largest and most complex organs in the human body. It is made up of more than 100 billion nerves that communicate in trillions of connections called synapses [41]. The brain is a construction of two hemispheres at the right and left side. Each hemisphere divided into four lobes. These four lobes are shown in Figure 1.6. They are named as frontal lobe, parietal lobe, temporal lobe and occipital lobe. Mostly, all of the functions voluntary functions and majority of the involuntary functions of the body are governed by the different functional areas of the brain. These

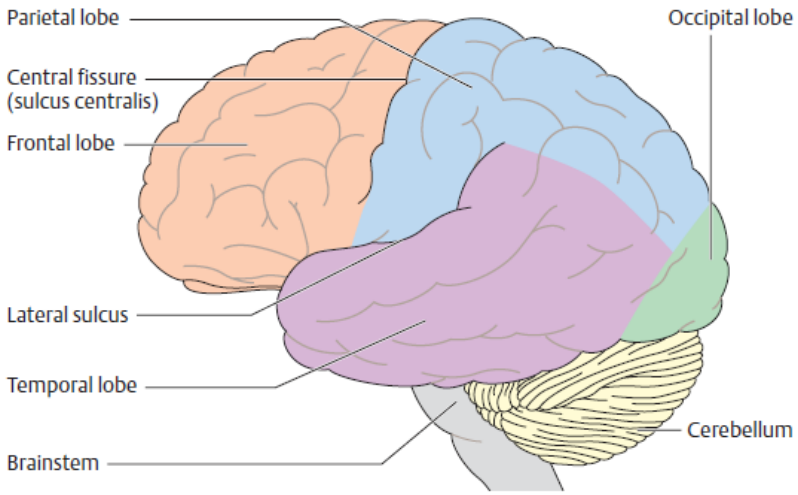

Fig. 1.6 : Lobes of the brain (reproduced from [42])

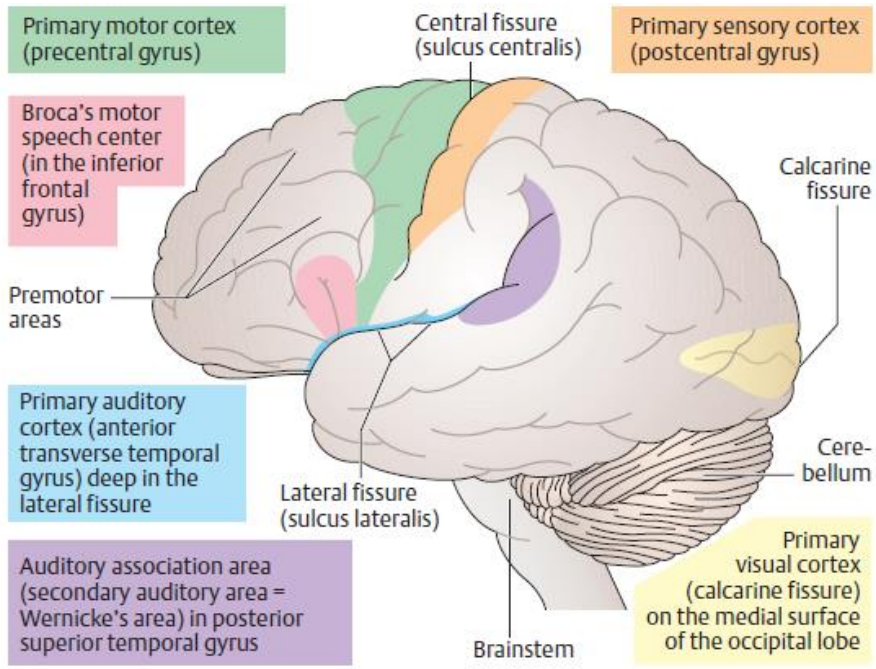

Fig. 1.7: Functional Cortical Areas of the left Cerebral hemisphere (reproduced from [42])

functional cortical areas of the brain are shown in Figure. 1.7. The functions of each area can be determined by their names. Such as motor cortex area is mainly responsible for voluntary motion planning and execution of the body; the visual cortex area is mainly responsible for the visual stimulation recognition [42]. These areas can be divided into two major areas know as primary and secondary [42]. In the primary areas, they contain beginnings and the terminations of the projection pathways [42].

With respect to the current study, it is important to understand more details of the motor cortex area, which governs the voluntary actuations of the limbs. As shown in Figure 1.8, the arrangement of the corresponding functional areas of the motor cortex reassembles a human standing on his head with the feat at the border of the hemisphere [42]. In comparison to the other parts of the body, the upper–limb has a wider range of functional region from shoulder to thumb. However, some recent studies [43]–[45] have reported that in addition to the motor cortex areas, some other areas in parietal cortex also activated during the motor commands.

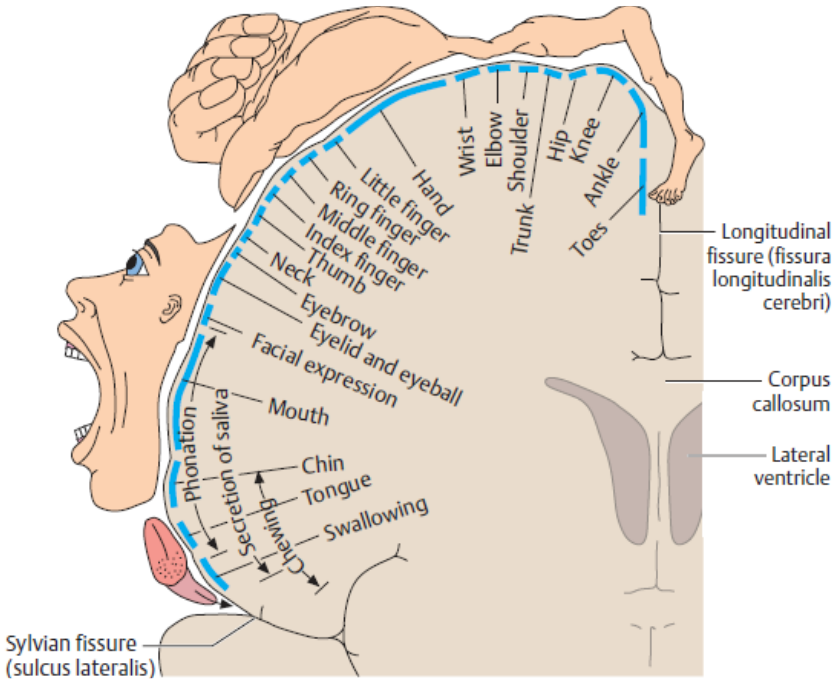

Fig. 1.8: Functional area map of motor cortex for different motor actions of the body (reproduced from [42])

1.3.2 Categorization of BCI techniques

There are various ways of categorizing available BCI techniques, such as used modality, feature extraction method, classification method, etc… In this study, the available BCI techniques are categorized based on the modality. The identified methodology of classification is shown in Figure 1.9. Available modalities can be classified under the two categories based on their invasiveness, noninvasive and invasive. Invasive techniques further can be categorized to technologies using intra–cortical electrode arrays and electrocoricography (ECoG, intracranial electroencephalography). Noninvasive techniques also can be further categorized into electroencephalography (EEG), near infrared spectroscopy (NIRS), mechanomyography (MMG). The further chapters of this thesis use EEG as their modality for the proposed motion intention estimation methodologies. Available EEG based BCI techniques can be categorized into reactive and active BCIs.

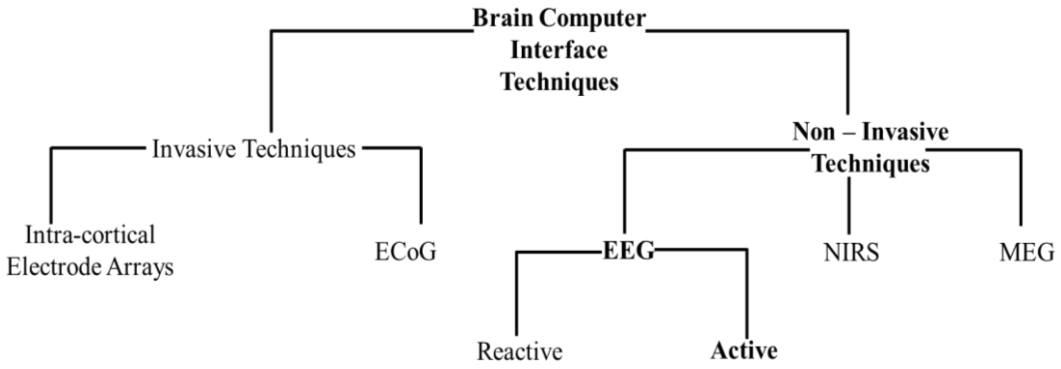

Figure 1.9: Classification of Brain Computer Interface Techniques

1.3.4 Invasive BCI techniques.

Following sections explain the details of the invasive BCI techniques. Initially, intra–cortical electrode arrays based BCI are explained which will be followed by the ECoG based BCIs.

A. Intra–Cortical Electrode Array based BCI

During technology with intra–cortical electrode arrays, a surgical procedure is involving to implant an electrode array into the brain. This electrode array will penetrate through the brain and capable of recording neuronal level potential changes of the brain. Figure 1.10 shows such an implanted electrode in to the human brain. Over the recent years, in animal studies intra – cortical neural activities have been recorded for natural movement [46], a robot arm was controlled in four dimensions for self-feeding tasks [35] and in seven dimensions for orientation and grasping [47]. In addition, using of intra–cortical electrode with human subjects also have been reported [36], [38]. Methods using intra–cortical electrode arrays to record brain activity are superior to existing non-invasive BCI technologies in terms of higher spatial specificity, signal-to-noise ratio, and bandwidth.

Neuro–prosthetic control by an individual with tetraplegia [38]

Collinger *et al.*[38] proposed a BCI systems to control a multi DoF, external prosthetic arm for a patient with tetraplegia. In this method, two intra-cortical micro

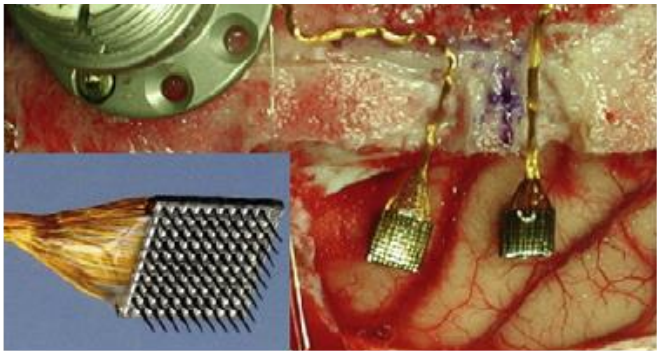

Fig. 1.10: Micro Electrode Array (reproduced from[48])

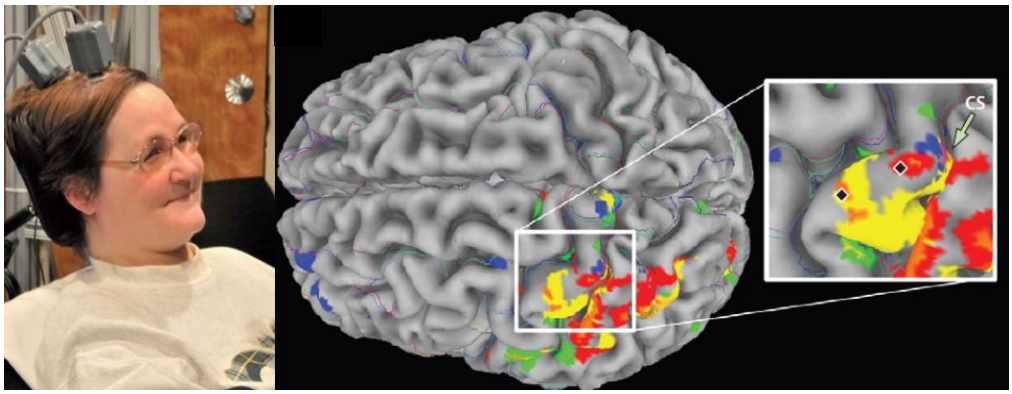

(a) (b)

Fig. 1.11: Patient with tetraplegia (a) access method to the implanted electrodes array (b) activations of the patient's brain – black squares approximate postions of the electrode arrays on the motor cortex (reproduced from [38])

electrode arrays with 96 channels were implanted in the motor cortex areas of the patient's brain. With the information from the intra–cortical micro electrodes, the patient had undergone 13 weeks of training for the BCI which has the goal of controlling an anthropomorphic prosthetic limb with 7 DoFs including 3 DoFs for translation, 3 DoFs for orientation and single DoF for grasping. The study reports the successful control of the prosthetic limb for skillful coordinated reach and grasp movement by the patient. The subject participated in the study and her activated areas of the brain are shown in Figure 1.11(a) and (b), respectively.

Prosthetic arm control by a monkey [35]

Meel *et al.* reports a study on embodied control of a prosthetic arm by monkeys with implanted intra–cortical electrode arrays in to their brain. In this study, monkeys are able use their motor cortical activity to control a mechanized 5 DoF arm replica in a self-feeding task in three dimensions and to proportionally control a gripper on the end of the arm. During the real–time control, the endpoint velocity and gripper command were extracted from the instantaneous firing rates of simultaneously recorded units from the electrode array.

B. Electrocortocogram (ECoG) Based BCI

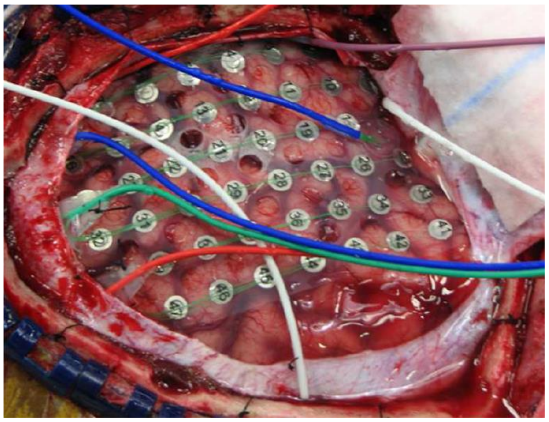

Fig. 1.12: Placement of ECoG electrodes in the cortices (reproduced from [49])

ECoG is also an invasive BCI technique that is in use. In this process, EcoG electrodes are implanted on the brain and they lie on top of the cortex measuring the potential changes on the surface of the cortex. Figure 1.12 shows an implanted electrode on top of the cortices of the brain. Over the recent years ECoG signals have been used in different BCI applications [39], [50], [51]. Similar to the case with intra–cortical electrode arrays, methods using ECoG signals are superior to existing non-invasive BCI technologies in terms of higher spatial specificity, signal-to-noise ratio, and bandwidth.

Trajectory Prediction with ECoG [51]

Nakanishi *et al.* [51], proposed a ECoG based 3 dimensional trajectory prediction methodology to reconstruct the motion of a human limb. In the proposed method, 15 channel and 60 channel electrodes were placed in the sensorimotor cortex of the patient surgically. ECoG signals from the brain and 3D trajectories of the left hand motion were recorded simultaneously. Later, using a sparse linear regression based method, the joint angles and joint trajectories were estimated. This study proves the feasibility of using ECoG based BCI to reconstruct human limb motions in the 3D space, which can be adopted to control the wearable robotic devices according to the user's motion intention.

ECoG based BCI for a patient with tetraplegia [50]

In [50], Wang *et al.* proposed a ECoG based for a patient with tetraplegia to control a cursor in a screen. Initially, 32 channel high density ECoG electrode grid with 28 recording channel was implanted surgically on the left sensorimotor cortex of the patient. Later, using an adaptive motion estimation scheme, the subject attempted to move a cursor on a screen between given targets using the simultaneous signals collected through the ECoG grid, generated for the attempted right arm and hand movements. In the adaptive scheme the cursor control was alternated between the subject and the neural decoder of the proposed BCI. The neural decoder was updated according to the performance of the human subject. The study demonstrate the successful integration of sensorimotor cortex based ECoG signals to predict the motion intentions for a future application in the area of wearable robotics.

Control of upper limb prosthesis with ECoG [39]

Fifer *et al.* [39], have proposed a system based on ECoG for controlling of a modular prosthetic limb. The study comprises of three different components to for neural signal acquisition and processing, behavioral kinematic acquisition, and artificial limb actuation. In the first phase, ECoG signals are acquired from the implanted ECoG electrode array and as features, signal power is extracted for five

different frequency bands. Accordingly, signal power is extracted for μ band, 7 – 13Hz; β band, 16 – 30Hz; low γ band, 30 – 50Hz; high γ band, 70 – 100Hz and 100 – 150Hz frequency bands. Eventually, the integration of the EEG features and the behavioral kinematic data resulted in actuating the modular prosthetic arm of 27 DoF either in three-dimensional virtual or physical space.

1.3.5 Noninvasive BCI techniques

Following sections present details about two main available non– invasive BCI modalities (*i.e.*: Near Infrared Spectroscopy and Electroencephalography).

A. Near Infrared Spectroscopy based BCIs

Functional Near Infrared Spectroscopy (fNIRS) [34] are used by researchers are widely used as noninvasive BCI modality. During fNIRS, it measures the concentration changes of oxy–hemoglobin ([HbO] and deoxy–hemoglobin [HbD]) in the superficial layers of the human cortex. fNIRS lacks the temporal resolution [52]. Massimiliano *et al*.[34], proposed a method based on fNIRS to use in gait rehabilitation. Lee *et al*.[53], proposed a control of a hand exoskeleton

Gait Rehabilitation with fNIRS [34]

Massimiliano *et al*. [34], presented a proof of concept study to assess whether hemodynamic signals underlying lower limb motor preparation in stroke patients can be reliably measured and classified. In the study, fNIRS signals were recorded from seven right-handed chronic stroke patients using a 48 channel recording system. The recorded brain activity corresponded to the preparation of left and right hip movement of seven chronic stroke patients. During the estimation of the intent to move, total hemoglobin signal changes over premotor cortex and posterior parietal cortex were considered as features to train a linear discriminant analysis based classifier.

Hand rehabilitation with NIRS [53]

In [53], a hand rehabilitation robot is operated using a NIRS signals acquired through the scalp of the stroke patients. During the study NIRS signals were recorded from nine channel, of six healthy subjects for open and close motion of the hand. The mean and slope of HbO and HbD signals were selected as features to train two type of classifier. Linear Discriminant Analysis (LDA) and Support Vector Machine (SVM) based classifiers were trained and used to predict the real time motion intention for single DoF (*i.e.:* hand opening and closing). Finally, a single DoF hand exoskeleton robot (see Figure 1.13 (a)) was controlled using NIRS, for the similar motion intention of the user, providing a more intuitive approach for hand rehabilitation. The octode placement for NIRS recordings and experimental setup is shown in Figure 1.13. (b)

(a) (b)

Fig. 1.13: NIRS based hand rehabilitation robot (a) Hand exoskeleton robot (b) experimental setup

B. Electroencephalography based BCIs

EEG measures the electrical activity fluctuations of the brain from the scalp of the human head. Abnormalities of EEG are used to diagnose various kinds of neurological disorders, sleep disorders, brain death, tumors, stroke, etc… in clinical applications. However, due to the easiness of use, noninvasive nature and higher temporal resolution compared to other noninvasive BCI techniques, EEG draws more attention to be used as BCI modality frequently. However, EEG recording are prone

to contaminate with noise produced by: potentials from the brain (cephalic noise) , potentials from the head muscles and skin, eye and tongue (extra cephalic cranial noise), potential form the other body parts such as heart (extra cranial physiological noise), random microscopic fluctuations of the of the electrodes (thermal noise), noise from the movement of the subject (movement artifact), fluctuations of electronic recording components (electronic noise), radiations from the surrounding electrical components (environment noise) and fluctuations in signal conversions for storing (quantization noise) [54], [55]. A higher noise ratio compared to the EEG signal related to the motions makes it challenging to develop EEG based BCIs. Despite, several studies have proposed BCI systems for different applications [26], [28]–[30], [33], [56]–[58].

Control of a prosthesis with EEG [28]

The study [28] reported in 2016 can be considered as astate of the art in control a prosthetic arm using EEG signals from a human. In this study, 13 subjects controlled a prosthetic arm for a robotic arm with high accuracy for performing tasks requiring multiple DoFs. During the study, motor imagery tasks were used to drive two dimensional virtual cursor or robotic arm movement. Accordingly, the imagination of left hand, right hand, both hands, and relaxation corresponds to the respective left, right, up, and down movement of the robotic arm and virtual cursor. In order to control the virtual cursor or the robotic arm, band power features were derived from 62 channel of EEG recorded around the left and right motor cortex areas of each subject. The power activity of the left and right hemispheres were mapped linearly to the velocity of the virtual cursor or to the position of the robotic arm.

BCI for Exoskeleton Control [56]

The study presented in [56] demonstrated the feasibility of detecting motor intention from brain activity of chronic stroke patients using an asynchronous EEG based brain BCI. Here, EEG signals recorded from 64 channels were used to control a single DoF of an upper–limb exoskeleton. Movement related cortical potentials

(MRCP) were used in the calibration stage of the BCI. During the closed loop implementation of the BCI, slope, negative peak amplitude, area, and mahalanobis distance were computed from the segment epochs during the calibration to be used as the features. Thus, in order to improve the system performance in the presence of single-trial variability of MRCPs in the injured brain, the important steps were followed: (1) an adaptive time window was used during extracting features for the BCI calibration; (2) EEG signals are prone to day to day variations. Therefore, training data from two consecutive days were pooled for BCI calibration to increase robustness and (3) BMI predictions were gated by residual EMG activity from the impaired arm, to improve the final decision of the BCI.

Meal Assistive Robot [57]

Perera *et al.* [57] proposed the control of a meal assistive robot using EEG signals that are used to detect the user's intention. In the proposed method, steady state visually evoked potentials (SSVEP) which are related to user's motion intention are detected from the EEG signals. The user can select the robot to feed from given 3 choices of the bowls. Each bowl is represented by a LED matrix blinking at a different frequency. The user has to match the motion intention to the bowl, represented by the LED matrix. Thus, the SSVEP signals are extracted from the EEG, which are generated due to subject watching the blinking of the LED matrix. The robot will be controlled according to motion estimation from the SSVEP signals. Similar approach can be followed to identify the motion intention to control wearable robots also.

Estimation of motion intention for arm Supination/ Pronation [58]

Kiguchi *et al.* proposed a motion intention estimation methodology to be used for control of a prosthetic arm for a transhumeral amputees. Transhumeral amputees do not have enough muscle sites to estimate the distal joint movement by using EMG signals. Therefore, this study proposed a neural network based motion estimation of the supination/pronation using EEG signals from the subjects.

Table 1.1: Summary of BCI systems in use

Study	Country	Modality	Function	Remarks
Collinger *et. al.* [29]	USA	Intra – cortical electrode	7 DoF controlling of a prosthetic arm	13 weeks of training
Meel *et. al.* [26]	USA	Intra Cortical Electrode		Two monkeys were used for the experiments
Nakanishi *et. al.* [42]	Japan	ECoG	Trajectory estimation for 3D space movement	
Wang *et. al.* [41]	USA	ECoG	Cursor Control	Adaptive scheme based on the performance of the patient
Fifer *et. al.* [30]	USA	ECoG	27 DoF modular prosthetic arm control	Band power features were used
Massimiliano *et. al.*[25]	Germany	FNIRS	Estimation of hip movement preparation	Total hemoglobin change selected as feature
Lee *et. al.* [44]	Japan	NIRS	1 DoF hand exoskeleton robot controlling	Hand rehabilitation for stroke survivors
Meng *et. al.* [19]	USA	EEG	Control of a 7 DoF robotic arm	Intial study for multi DoF controlling
Nikunj *et. al.*[45]	USA	EEG	1 DoF control of an exoskeleton	EMG was used to improve the accuracy

1.4 Setup of experimental platform

Following sections explain the basic setup of the experimental platform for this study. Initially, the electrode placement methodologies are explained. It will be followed by a brief explanation to the EEG acquisition system used during the experiment. In addition to the EEG signals, user's motion also recorded during some of the experiments performed. A brief introduction to the mainly used motion capture systems also included in the final section.

1.4.1 Electrode placement for EEG recording

Generally, during the recordings of non–invasive brain signals such as EEG or NIRS, 10–20 international system of electrode placement is used. The nomenclature of this system is depending on the location of the electrode and underlying lobe. 10

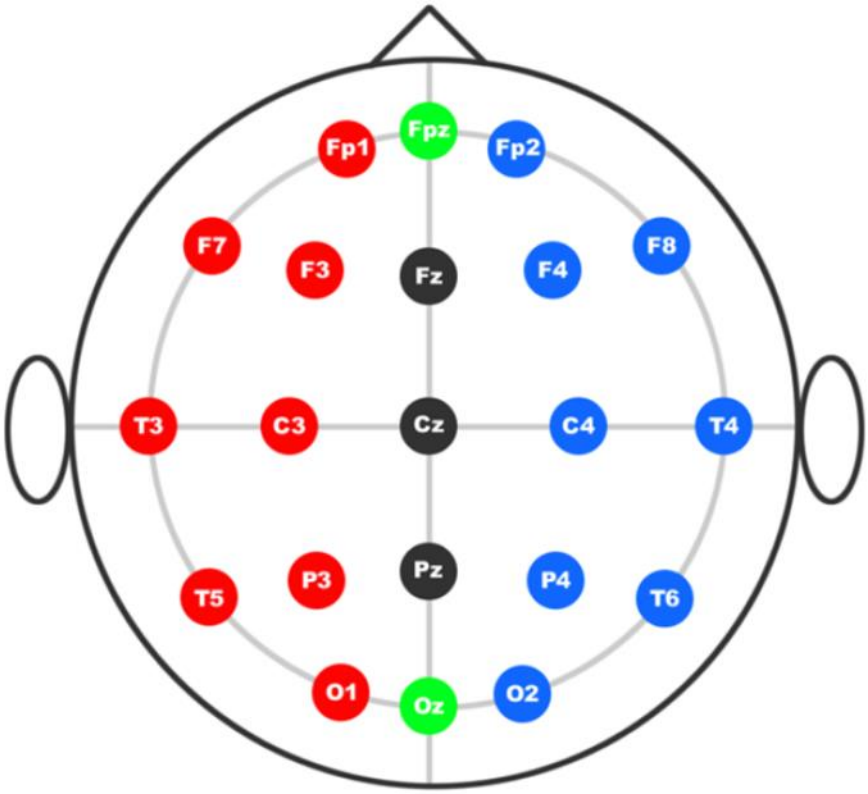

Fig. 1.14: Nomenclature and electrode locations of 10 – 20 electrode system (reproduced from [59])

and 20 refers to the distance between electrodes to be either 10% or 20% of the distance of fron–back or left–right of the brain. Accordingly, F, P, O and T are used in the nomenclature to represent Frontal, Parietal, Occipital, and Temporal lobes. In addition, C is used to the central area. Number are also given to the electrode locations. Zeros are assigned to the mid plane (Cz, Fz, Cz, ….). Right side of the brain is assigned with even numbers (Fp2, F4, C4, ….) while the left side of the brain is assigned with odd numbers (Fp1, F3, C3, ….). The nomenclature and their positions are shown in Figure. 1.14. In addition, 10–20 international system can be extended to different variations, based on the percentages of distances between the electrode locations. Thus, 10–10 international system and the 10–5 international system also can be derived.

1.4.2 Recording of EEG signals

Recording the EEG from the human scalp is usually the initial step of any EEG based BCI. For this purpose, different commercial EEG acquisition systems [60]–[63] are available. EEG signals are detected through electrodes to the acquisition system. However, there should be a certain conductive connection between the electrode and the skin of the scalp to perform the measurements [54]. Accordingly, there are common two type of electrode types in commercially available devices, namely wet type and dry type. Wet type is further classified in to gel type and water type.

In this study, g.LADYbird electrodes, belongs to the gel type from the g.tec co. [60] are used for EEG measurements. The used electrodes are shown in Figure 1.15(a).

(a) (b)

Fig. 1.15: (a) g.LADYbird electrode (b) g.gammacap

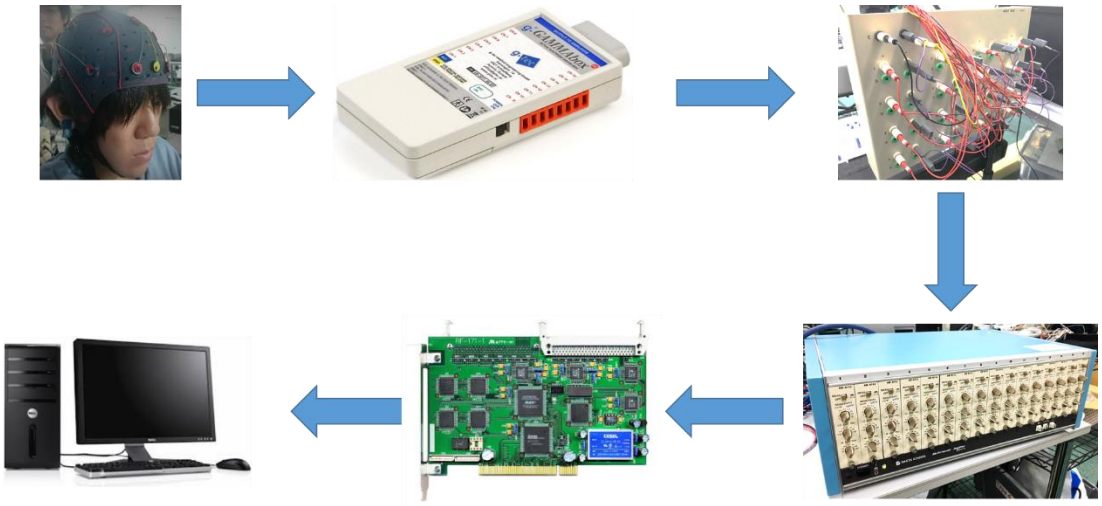

Fig. 1.16: Electrical connection system for the EEG recordings

Electrodes are attached to the g.gammacap [60] (see Figure 1.15(b), from the same vendor), according to selected electrode layout from the. Electrical connection of the EEG recording setup used in this thesis is shown in Figure 1.16. After the detection of the EEG signals from the electrodes, they are sent to the g.gammabox [60] for pre-amplification before send for the electrical filtering and the amplifications. In this study, the systems comprise of equipment form two vendors. Therefore, after the pre – amplification the signals are send to the input box of the nihon kohden [64]. It makes the connection between the g.tec system and the nihon kohden amplifier. From the input box EEG signals are send to the nihon kohden amplifier. The amplifier is connected to the Ritech Interface Board (Model No: RIF-171-1) which is connected to a desktop computer. In the computer EEG signals are stored in csv format using the recording software for further processing and analyzing.

1.4.3 Recording of motion

During the experiments for this study, the user's upper limb motions were recorded for further analysis purposes majorly in identifying the user intended motion. For this purpose, two commercial available motion capture systems were used. One of them was, a v120: Duo (Optitrack) and the other one was Osprey (Motion Analysis

Co.). Both systems used reflective markers attached to the limb segments of the subjects to detect the motion. The movement of the reflective markers are detected by the camera system of each motion capture system and data will be recorded in to the computer. Both motion capture systems operate with their own software for recording data. The data recorded contains coordinate positions of the attached markers, which can be used to calculate the required information such as posision or velcocity, etc…

1.5 Contribution of the thesis

The research work presented in this thesis is mainly focused to study on the EEG based motion intention estimation techniques for control of upper limb wearable robots.

- Propose a new approach to control several DoFs in a wearable robot in real-time by estimating the users motion intention, in terms of the user's intended tasks to perform, by using EEG signals measured from the scalp of the user. A time-delayed feature matrix is introduced to provide inputs to neural network and support vector machine (SVM)-based classifiers that harvest the dynamic nature of the EEG signals for motion intention prediction.
- Propose a EEG based hierarchical approach to achieve multi-DoF control of a transhumeral prosthesis. Initially, the motion intention for arm reaching or hand lifting is identified using a neural network based classifier which is trained with motion-related EEG features. Then elbow motion and hand endpoint motion is estimated using a different neural network based classifiers, which are trained with motion information recorded using healthy subjects.
- Propose and compare two different approaches to estimate the motion intention, in terms velocity. Here, individual joint motions are estimated using a time–delayed feature matrix as input to a neural network based classifier. In addition, end effectors motion is estimated using dynamic feature matrix as input to an autoregressive neural network based classifier.

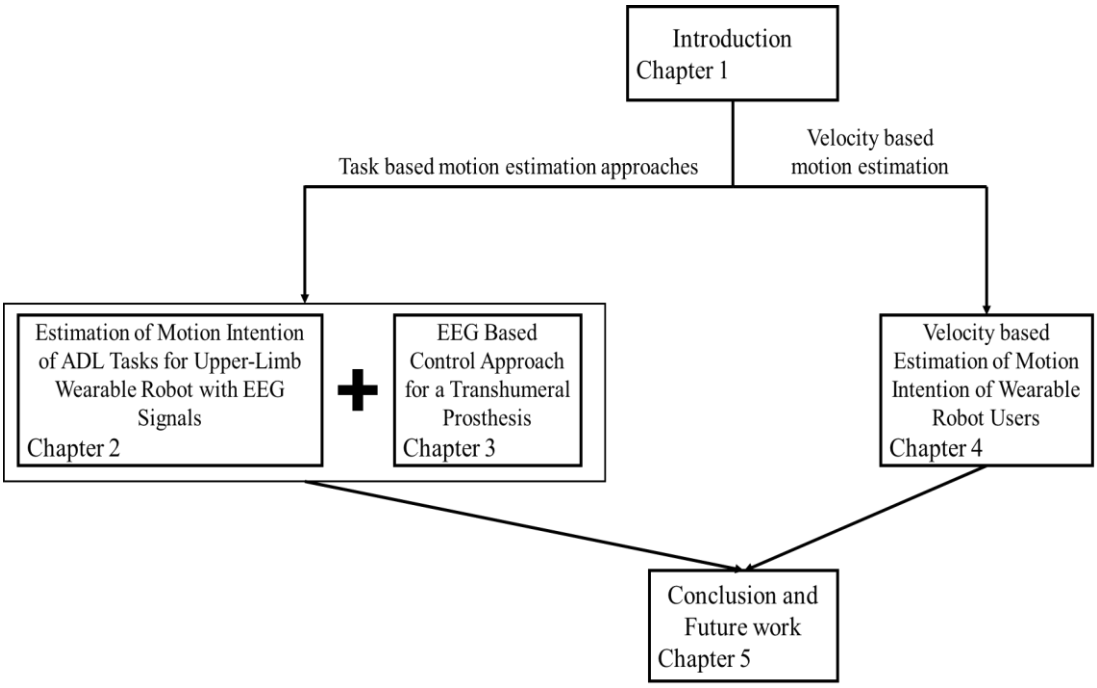

Figure 1.17: Thesis Overview

1.6 Thesis Overview

This thesis consists of five chapters including first chapter. The overall structure of the thesis is illustrated in Figure 1.17. Chapter 2, Chapter 3 and Chapter 4 are dedicated for the aforementioned contributions. Chapter 2 and Chapter 3 focuses on task based motion estimation, whereas Chapter 4 focuses on the velocity based motion estimation. Chapter 1 – Chapter 4 start with an introduction on what would be the contents of the certain chapter in the section, Chapter Overview. The contents of each chapter are organized as follows.

Chapter 2: Estimation of Motion Intention of ADL Tasks for Upper-Limb Wearable Robot with EEG Signals

Chapter 2 is dedicated to propose a task based motion estimation. Initially, the requirement of the proposed study explained with examples from the literature. Then, the proposed approach for the motion intention identification of the activities of daily

living is introduced. It explains the experimental approach to validate the proposed approach. The signal processing techniques, extraction methods and design of the classifiers are explained in detailed. In the results, classification accuracies, latency between the motion onset and the predicted motion for selected classifiers are presented and compared. Finally, the important points of the proposed approach and the results are discussed.

Chapter 3: EEG Based Control Approach for a Transhumeral Prosthesis

Chapter 3 is also dedicated to propose a task based motion intention estimation. The requirement of the current study for the transhumeral prostheses is introduced in the initial section of the chapter. Then the proposed hierarchical structure is presented and its details are explained. It will be followed by an explanation to the experimental approach to confirm the proposed methodology. Then, the signal processing techniques, feature extraction methodologies, and the details of the two stage classification are introduced in respective manner. The results are presented for both proposed stages. At the end, the discussion ins presented.

Chapter 4: Velocity based Estimation of Motion Intention of Wearable Robot Users

Chapter 4 presents the research work related to the velocity based motion intention estimation. Initially, current limitations of the velocity based motion intention estimation are identified. Then, the feasibility of two approaches to estimate the motion intension is studied by introducing individual joint motion based and trajectory based estimation methods. Experimental procedure for both approaches are explained. EEG signal processing, feature extraction and classification methodologies are explained in details. Finally, the results for both methods and the discussion are presented.

Chapter 5: Conclusion and Future Directions

The final chapter includes a summary of the contributions of the thesis, the conclusion, a brief discussion, and suggestions for the future directions.

Reference

[1] "World Population Ageing, Highlights," Department of Economic and Social Affairs, United Nations, 2017.

[2] "Paralysis statistics," *Reeve Foundation*. [Online]. Available: https://www.christopherreeve.org/living-with-paralysis/stats-about-paralysis. [Accessed: 07-Dec-2017].

[3] L. J. Kozak and M. F. Owings, "Ambulatory and inpatient procedures in the United States, 1995," *Vital Health Stat. 13.*, no. 135, pp. 1–116, Mar. 1998.

[4] K. Ziegler-Graham, E. J. MacKenzie, P. L. Ephraim, T. G. Travison, and R. Brookmeyer, "Estimating the Prevalence of Limb Loss in the United States: 2005 to 2050," *Arch. Phys. Med. Rehabil.*, vol. 89, no. 3, pp. 422–429, Mar. 2008.

[5] S. Alper and S. Raharinirina, "Assistive Technology for Individuals with Disabilities: A Review and Synthesis of the Literature," *J. Spec. Educ. Technol.*, vol. 21, no. 2, pp. 47–64, Mar. 2006.

[6] "WHO | World report on disability," *WHO*, 19-Apr-2015. [Online]. Available: http://www.who.int/disabilities/world_report/2011/en/. [Accessed: 19-Apr-2015].

[7] M. J. Johnson, S. Micera, T. Shibata, and E. Guglielmelli, "Rehabilitation and assistive robotics [TC Spotlight]," *IEEE Robot. Autom. Mag.*, vol. 15, no. 3, pp. 16–110, Sep. 2008.

[8] D. Bandara and R. Gopura, "Upper Extremity Prosthetics: Current Status, Challenges and Future Directions," *Seventeenth Int. Symp. Artif. Life Robot.*, 2012.

[9] R. A. R. C. Gopura, D. S. V. Bandara, K. Kiguchi, and G. K. I. Mann, "Developments in hardware systems of active upper-limb exoskeleton robots: A review," *Robot. Auton. Syst.*, vol. 75, no. Part B, pp. 203–220, Jan. 2016.

[10] M. Mokhtari, “The raptor wheelchair robot system,” presented at the International Conference on Rehabilitation Robotics, 2001.

[11] S. Saint-Aime, B. Le-Pevedic, D. Duhaut, and T. Shibata, “EmotiRob: Companion robot Project,” in *RO-MAN 2007 - The 16th IEEE International Symposium on Robot and Human Interactive Communication*, 2007, pp. 919–924.

[12] J. L. Pons, R. Ceres, and L. Calderón, “Introduction to Wearable Robotics,” in *Wearable Robots*, J. L. Pons, Ed. John Wiley & Sons, Ltd, 2008, pp. 1–16.

[13] N. Vitiello *et al.*, “NEUROExos: A Powered Elbow Exoskeleton for Physical Rehabilitation,” *IEEE Trans. Robot.*, vol. 29, no. 1, pp. 220–235, Feb. 2013.

[14] M. Gunasekara, R. Gopura, and S. Jayawardena, “6-REXOS: Upper Limb Exoskeleton Robot with Improved pHRI,” *Int. J. Adv. Robot. Syst.*, vol. 12, no. 4, p. 47, Apr. 2015.

[15] S. K. Kundu, K. Kiguchi, and E. Horikawa, “Design and Control Strategy for a 5 DOF Above-Elbow Prosthetic Arm,” *Int. J. Assist. Robot. Mechatron.*, vol. 9, pp. 61–75, Sep. 2008.

[16] “iLimb: world’s first fully articulating and commercially available bionic hand,” 11-Feb-2014. [Online]. Available: http://www.gizmag.com/go/7661/. [Accessed: 11-Feb-2014].

[17] A. Otten, C. Voort, A. Stienen, R. Aarts, E. van Asseldonk, and H. van der Kooij, “LIMPACT:A Hydraulically Powered Self-Aligning Upper Limb Exoskeleton,” *IEEEASME Trans. Mechatron.*, vol. 20, no. 5, pp. 2285–2298, Oct. 2015.

[18] H.-D. Lee, B.-K. Lee, W.-S. Kim, J.-S. Han, K.-S. Shin, and C.-S. Han, “Human–robot cooperation control based on a dynamic model of an upper limb exoskeleton for human power amplification,” *Mechatronics*, vol. 24, no. 2, pp. 168–176, Mar. 2014.

[19] R. A. R. C. Gopura, K. Kiguchi, and Y. Li, “SUEFUL-7: A 7DOF upper-limb exoskeleton robot with muscle-model-oriented EMG-based control,” presented at the IEEE/RSJ International Conference on Intelligent Robots and Systems, 2009. IROS 2009, 2009, pp. 1126–1131.

[20] L. Resnik, S. L. Klinger, and K. Etter, “The DEKA Arm: Its features, functionality, and evolution during the Veterans Affairs Study to optimize the DEKA Arm,” *Prosthet. Orthot. Int.*, Oct. 2013.

[21] D. S. V. Bandara, R. A. R. C. Gopura, K. T. M. U. Hemapala, and K. Kiguchi, “Development of a multi-DoF transhumeral robotic arm prosthesis,” *Med. Eng. Phys.*, Jul. 2017.

[22] C. Cipriani, M. Controzzi, and M. C. Carrozza, “The SmartHand transradial prosthesis,” *J. NeuroEngineering Rehabil.*, vol. 8, p. 29, May 2011.

[23] M. Asghari Oskoei, M. A. Oskoei, and H. Hu, “Myoelectric control systems—A survey,” *Biomed. Signal Process. Control*, vol. 2, no. 4, pp. 275–294.

[24] E. J. Rechy-Ramirez and H. Huosheng, “Stages for Developing Control Systems using EMG and EEG Signals: A survey,” School of Computer Science and Electronic Engineering University of Essex, United Kingdom, TECHNICAL REPORT CES-513.

[25] A. Vallabhaneni, T. Wang, and B. He, “Brain—Computer Interface,” in *Neural Engineering*, B. He, Ed. Springer US, 2005, pp. 85–121.

[26] K. K. Ang *et al.*, “A Randomized Controlled Trial of EEG-Based Motor Imagery Brain-Computer Interface Robotic Rehabilitation for Stroke,” *Clin. EEG Neurosci.*, vol. 46, no. 4, pp. 310–320, Oct. 2015.

[27] K. Colwell, C. Throckmorton, L. Collins, and K. Morton, “Projected accuracy metric for the P300 Speller,” *IEEE Trans. Neural Syst. Rehabil. Eng. Publ. IEEE Eng. Med. Biol. Soc.*, vol. 22, no. 5, pp. 921–925, Sep. 2014.

[28] J. Meng, S. Zhang, A. Bekyo, J. Olsoe, B. Baxter, and B. He, “Noninvasive Electroencephalogram Based Control of a Robotic Arm for Reach and Grasp Tasks,” *Sci. Rep.*, vol. 6, p. 38565, Dec. 2016.

[29] Y. Hayashi and K. Kiguchi, “A study of features of EEG signals during upper-limb motion,” in *2015 IEEE International Conference on Advanced Intelligent Mechatronics (AIM)*, 2015, pp. 943–946.

[30] A. K. Das, S. Suresh, and N. Sundararajan, “A discriminative subject-specific spatio-spectral filter selection approach for EEG based motor-imagery task

classification," *Expert Syst. Appl.*, vol. 64, no. Supplement C, pp. 375–384, Dec. 2016.

[31] B. Xia *et al.*, "A combination strategy based brain-computer interface for two-dimensional movement control," *J. Neural Eng.*, vol. 12, no. 4, p. 046021, Aug. 2015.

[32] T. Carlson and J. del R. Millan, "Brain-Controlled Wheelchairs: A Robotic Architecture," *IEEE Robot. Autom. Mag.*, vol. 20, no. 1, pp. 65–73, Mar. 2013.

[33] K. LaFleur, K. Cassady, A. Doud, K. Shades, E. Rogin, and B. He, "Quadcopter control in three-dimensional space using a noninvasive motor imagery-based brain-computer interface," *J. Neural Eng.*, vol. 10, no. 4, p. 046003, Aug. 2013.

[34] M. Rea *et al.*, "Lower Limb Movement Preparation in Chronic Stroke: A Pilot Study Toward an fNIRS-BCI for Gait Rehabilitation," *Neurorehabil. Neural Repair*, vol. 28, no. 6, pp. 564–575, Jul. 2014.

[35] M. Velliste, S. Perel, M. C. Spalding, A. S. Whitford, and A. B. Schwartz, "Cortical control of a prosthetic arm for self-feeding," *Nature*, vol. 453, no. 7198, p. 1098, Jun. 2008.

[36] L. R. Hochberg *et al.*, "Reach and grasp by people with tetraplegia using a neurally controlled robotic arm," *Nature*, vol. 485, no. 7398, pp. 372–375, May 2012.

[37] C. E. Bouton *et al.*, "Restoring cortical control of functional movement in a human with quadriplegia," *Nature*, vol. 533, no. 7602, p. 247, May 2016.

[38] J. L. Collinger *et al.*, "High-performance neuroprosthetic control by an individual with tetraplegia," *The Lancet*, vol. 381, no. 9866, pp. 557–564, Feb. 2013.

[39] M. S. Fifer, S. Acharya, H. L. Benz, M. Mollazadeh, N. E. Crone, and N. V. Thakor, "Towards Electrocorticographic Control of a Dexterous Upper Limb Prosthesis," *IEEE Pulse*, vol. 3, no. 1, pp. 38–42, Jan. 2012.

[40] F. Xu, W. Zhou, Y. Zhen, and Q. Yuan, "Classification of motor imagery tasks for electrocorticogram based brain-computer interface," *Biomed. Eng. Lett.*, vol. 4, no. 2, pp. 149–157, Jun. 2014.

[41] M. Hoffman and MD, “Brain (Human Anatomy): Picture, Function, Parts, Conditions, and More,” *WebMD*. [Online]. Available: https://www.webmd.com/brain/picture-of-the-brain. [Accessed: 28-Nov-2017].

[42] A. Faller, M. Schünke, and G. Schünke, *The Human Body: An Introduction to Structure and Function*. Thieme, 2004.

[43] H. G. Yeom, J. S. Kim, and C. K. Chung, “Estimation of the velocity and trajectory of three-dimensional reaching movements from non-invasive magnetoencephalography signals,” *J. Neural Eng.*, vol. 10, no. 2, p. 026006, Apr. 2013.

[44] H. Cui and R. A. Andersen, “Posterior parietal cortex encodes autonomously selected motor plans,” *Neuron*, vol. 56, no. 3, pp. 552–559, Nov. 2007.

[45] H. Cui and R. A. Andersen, “Different Representations of Potential and Selected Motor Plans by Distinct Parietal Areas,” *J. Neurosci.*, vol. 31, no. 49, pp. 18130–18136, Dec. 2011.

[46] D. W. Moran and A. B. Schwartz, “Motor cortical representation of speed and direction during reaching,” *J. Neurophysiol.*, vol. 82, no. 5, pp. 2676–2692, Nov. 1999.

[47] A. Krause, “Brain-Computer Interface Control of an Anthropomorphic Robotic Arm.”

[48] C. Ethier and L. E. Miller, “Brain-controlled muscle stimulation for the restoration of motor function,” *Neurobiol. Dis.*, vol. 83, pp. 180–190, Nov. 2015.

[49] J. L. Roland *et al.*, “Brain Mapping in a Patient with Congenital Blindness – A Case for Multimodal Approaches,” *Front. Hum. Neurosci.*, vol. 7, Jul. 2013.

[50] W. Wang *et al.*, “An Electrocorticographic Brain Interface in an Individual with Tetraplegia,” *PLOS ONE*, vol. 8, no. 2, p. e55344, Feb. 2013.

[51] Y. Nakanishi *et al.*, “Prediction of Three-Dimensional Arm Trajectories Based on ECoG Signals Recorded from Human Sensorimotor Cortex,” *PLOS ONE*, vol. 8, no. 8, p. e72085, Aug. 2013.

[52] S. Fazli *et al.*, “Enhanced performance by a hybrid NIRS-EEG brain computer interface,” *NeuroImage*, vol. 59, no. 1, pp. 519–529, Jan. 2012.

[53] J. Lee *et al.*, “A multichannel-near-infrared-spectroscopy-triggered robotic hand rehabilitation system for stroke patients,” in *2017 International Conference on Rehabilitation Robotics (ICORR)*, 2017, pp. 158–163.

[54] A. Pinegger, S. C. Wriessnegger, J. Faller, and G. R. Müller-Putz, “Evaluation of Different EEG Acquisition Systems Concerning Their Suitability for Building a Brain–Computer Interface: Case Studies,” *Front. Neurosci.*, vol. 10, Sep. 2016.

[55] S. L. Bressler and M. Ding, “Event-Related Potentials,” in *Wiley Encyclopedia of Biomedical Engineering*, John Wiley & Sons, Inc., 2006.

[56] N. A. Bhagat *et al.*, “Design and Optimization of an EEG-Based Brain Machine Interface (BMI) to an Upper-Limb Exoskeleton for Stroke Survivors,” *Front. Neurosci.*, vol. 10, p. 122, 2016.

[57] C. J. Perera, I. Naotunna, C. Sadaruwan, R. A. R. C. Gopura, and T. D. Lalitharatne, “SSVEP based BMI for a meal assistance robot,” in *2016 IEEE International Conference on Systems, Man, and Cybernetics (SMC)*, 2016, pp. 002295–002300.

[58] K. Kiguchi, T. D. Lalitharatne, and Y. Hayashi, “Estimation of Forearm Supination/Pronation Motion Based on EEG Signals to Control an Artificial Arm,” *J. Adv. Mech. Des. Syst. Manuf.*, vol. 7, no. 1, pp. 74–81, 2013.

[59] “10_20_pos_man_v1_0_pdf.pdf.” .

[60] g.tec, “g.tec medical engineering.” [Online]. Available: http://www.gtec.at/Products/Complete-Solutions/g.EEGsys-Specs-Features. [Accessed: 12-Dec-2017].

[61] “EEG Systems.” [Online]. Available: https://www.egi.com/research-division/eeg-systems/geodesic-eeg-systems. [Accessed: 12-Dec-2017].

[62] “Homepage,” *Emotiv*. [Online]. Available: https://www.emotiv.com/. [Accessed: 12-Dec-2017].

[63] “EEG Sensors - EEG Headsets | NeuroSky.” .

[64] “Nihon Kohden Global Site,” *Nihon Kohden Global Site*. [Online]. Available: http://www.nihonkohden.com/index.html. [Accessed: 12-Dec-2017].

Chapter 2

Estimation of Motion Intention of ADL Tasks for Upper-Limb Wearable Robot with EEG Signals

Chapter Overview

In BCIs, encoding of brain information to derive the intended motion of the user in real-time continues to present a problem with respect to the control of wearable robots with multiple degrees of freedom (DoFs). In this chapter, a new approach to control several DoFs in a wearable robot is proposed by estimating the users motion intention in real-time, in terms of the user's intended tasks to perform, by using EEG signals measured from the scalp of the user. A time-delayed feature matrix constitutes of the power band features of EEG signals is introduced to provide inputs to neural network and support vector machine (SVM) based classifiers that harvest the dynamic nature of the EEG signals for motion intention prediction. In order to estimate the motion intention, individual classifiers are trained for each individual subject for both types of classifiers. At the same time, another two different classifiers are trained with data from all the subjects. The estimation results from both types are presented in this chapter and compared. Similarly, prediction latencies are calculated for each technique and are presented here with a comparison. As a conclusion, the experimental results indicate the effectiveness of the proposed methodology in the prediction of user's motion intention. The structure of the chapter is as follows. Initially, the motivation and the requirement of the current study are presented in the introduction. It is to be followed by the methodology which explains the proposed approach and the experimental setup. Then the results are presented to be followed by the discussion.

Chapter 2

2.1 Introduction

A brain-computer interface (BCI) for wearable robots provides a method of communication between the human brain and the robot that is based on the neural activity generated by the brain and is independent of normal output pathways such as the peripheral nerves and muscles [1]. Recently, both noninvasive [2]–[10] and invasive [11]–[16] BCI technologies have been proposed for various purposes. However, the ultimate goal of the BCIs for wearable robots is to enable anthropomorphic movement of wearable robotic devices, such as a prosthesis [17]–[19] or exoskeleton [20]–[22] acting as an assistive device [4], based on the intended motion of the user in real-time for more effective use of these devices in assisting with activities of daily living (ADL) or rehabilitation tasks. These devices correspond to highly dexterous robotic devices with multiple degrees of freedom (DoFs). Therefore, the control signals should be capable of actuating all required DoFs of these robots when wearable robots are controlled. Consequently, several DoFs of motion must be determined using an electroencephalography (EEG) based method or another motion intention identification method. To date, several different motion estimation methods [4], [5], [7], [13], [23]–[27] have been proposed for each specific BCI application.

In one previous study [23], a prosthetic hand was operated with 1 – DoF for its open and closed positions by classifying EEG patterns that occurred while the user imagined left and right hand movements. Palanker *et. al.* [24] proposed an EEG-based control architecture for a wheelchair-mounted robotic arm. Their method used visual stimulation of the subject provided via a visual matrix that includes either a symbolic array or an alphabetic array that corresponds to the required motion. In another previous study [5], Hayashi *et. al.* proposed a neural network-based method to identify the intended motion of the subject. Their method predicted whether the subject's intention involved either moving or not moving the hand within a single degree of freedom (1-DoF). Additionally, several studies [4], [7], [13], [25]–[27] also attempted to identify the intended motion of the subject with respect to the intended task.

Pfurtscheller *et. al.* [25] examined the reactivity of the EEG rhythms (known as mu rhythms) in association with the subject imagining movement of the right hand, the left hand, the foot, and the tongue and attempted to discriminate each individual task using the mu rhythms. Another method based on principal component analysis and a support vector machine (SVM) classifier was proposed by Anirudh *et. al.* [26] to classify the movements of the left and right hands. In an extant study [27], a steady-state visually evoked potential (SSVEP)-based meal assistive robot was proposed. In this method, the subject selected any solid food item that they wanted to eat from three different bowls by looking at the light-emitting diode (LED) matrices corresponding to those bowls, which were blinking at different frequencies. The SSVEP generated was then used to control the multi-DoFs meal assistive robot. In a previous study [4], a motor imagery-based robotic arm control method was proposed to perform reaching and grasping tasks. In this method, the subjects performed motor imagery-based tasks to control different cursor movements on a computer monitor, and the same motor imagery commands were later extended to control a robotic arm with multiple DoFs when performing reaching and grasping tasks.

In most of the studies mentioned above, the motor imagery or motor execution by the subject that triggers the EEG pattern differs from the motion that is generated by the robot. In contrast, the intended motion of the subjects could be predicted using different means. Most studies followed an approach in which they defined a third-party brain trigger for a selected DoF or task. Furthermore, in a few of these studies, the subject operated only a single DoF of the robot or the simultaneous operation of several DoFs was not possible, so this did not provide an intuitive user experience when performing ADLs. Conversely, two different approaches were proposed to identify the intended motion of the user. One method involved prediction of the direction and the speed of the joints that the user wanted to actuate. In this case, a number of predictions of individual joint motions were required to predict the user's upper-limb motion. In this approach, the prediction complexity increases with the introduction of each additional DoF. In another approach, it was possible to identify the ultimate focus of

the user's intended motion and the guide the robotic device from the initial position to the required end position. In this case, it was necessary to predict the intended motion in terms of the user's intended task, and the prediction complexity was independent of the number of DoFs involved. A few of the above studies [4], [5], [23] also attempted to predict some motor tasks. However, with the exception of one study [27], none of the other studies examined or predicted ADLs, although this is more important in the control of wearable robots.

In summary, the available BCI techniques that can be used to operate wearable robotic systems include one or both of the following drawbacks, which do not correspond to the control requirements for wearable robots. Either the techniques do not provide the user with adequate DoFs to allow the required ADL tasks to be performed or the motor imagery/execution that is used to trigger the EEG is not always similar to the output from the robot. Therefore, the robots cannot be controlled intuitively. In addition, EEG signals contain dynamic information about the intended motion, and the available methods do not understand this dynamic information accurately.

This chapter therefore proposes a new approach to control several DoFs of a wearable robot by estimating the expected motion intention of the user in terms of the task to be performed. The study is expected to correspond to an initial study to perform the same tasks using noninvasive BCI techniques, e.g., EEG. Initially, the locations and frequency ranges of the required brain activations are identified for each task during an offline analysis. These brain activations are triggered by the same tasks that would perform by the robot. The information from the offline analysis is used along with a time-delayed feature matrix to provide input to the classifiers, and this helps the classifier to understand the dynamic nature of the EEG features that are introduced in the proposed method. Neural network and SVM-based classifiers are also used to predict the intended motion in real time. Subsequently, the effectiveness of the neural network-based classifier and that of the SVM-based classifier are both compared to

that of the proposed approach. The proposed approach can be used to control several DoFs of a wearable robot to perform a similar intended human motion in real time using a suitable kinematic model for the selected tasks. The next section presents the study methodology and the following sections present the results and a discussion of the study. Finally, our conclusions are presented.

2.2 Method

The key steps in developing a BCI to understand human motion intention can be identified as understanding the activation locations of the brain, understanding the main frequency ranges of brain activations, making the classifier understand the dynamic information included in the EEG signals and finally the estimation of the

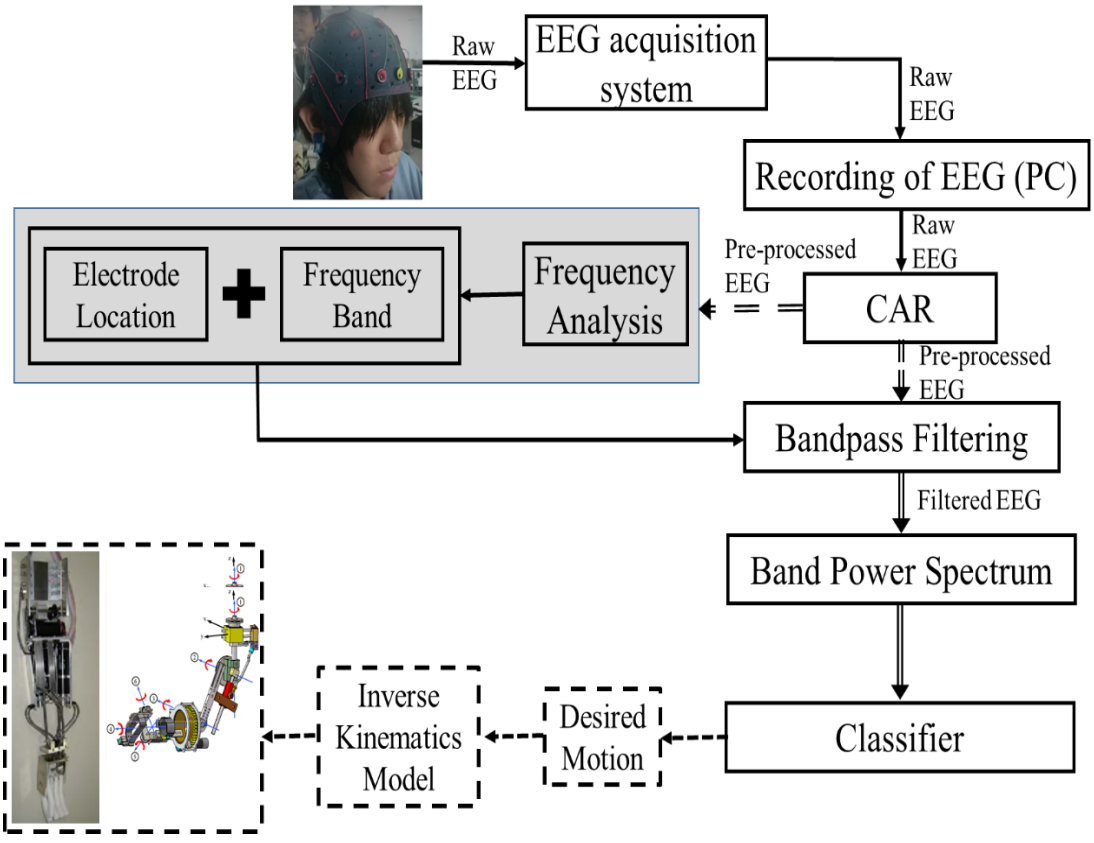

Fig. 2.1: Proposed approach for wearable robot control (dark background – offline analysis ⟶ - raw EEG ⟹ - preprocessed EEG ⟹ - filtered EEG).

human motion intention. accordingly, the proposed methodology for control of the wearable robot comprises a data collection process with a two-stage data analysis process, composed of offline analysis and real-time motion prediction, and an inverse kinematics-based motion generation process to control the robot. The key steps are shown in Figure 2. 1.

Initially, the EEG data are collected from the test subjects for two ADL tasks. The subsequent offline analysis (shown in the dark background area in Figure 2.1) focuses on identification of the brain behavior because different brain regions are activated based on the task to be performed. Additionally, voltages with different frequency ranges are emitted by the brain when different tasks are to be performed by the body. Therefore, one important step in the development of a real-time controller for a wearable robot involves development of a better understanding of the locations in the brain and the range of frequencies that are generated for the tasks to be performed. In the next step, the subject-specific findings from the offline analysis are used to develop a more dynamic prediction methodology for real-time motion prediction. Here in order to identify the dynamic information included in the EEG features, a time series based feature vector is introduced as inputs to the classifiers.

The current study focuses solely on estimation of the intended motion based on each subject's EEG signals. However, as shown in Figure 2.1, the results are to be extended to control a multi-DoF wearable robot using an inverse kinematic model that has been developed appropriately for the expected tasks. To diminish the effects of the noise that is generated among the electrodes and to normalize the recordings across all the channels, a step that is common to both online and offline processes involves initial calculation of the common average reference (CAR) as shown below, where N denotes the number of channels used in the recordings, $X_i(t)$ denotes the raw EEG signal from the i^{th} channel at time t, $X_{car,i}(t)$ denotes the CAR-corrected EEG signal of the i^{th} channel at time t, and $X_k(t)$ denotes the EEG signal of the k^{th} channel for average calculations.

$$X_{car,i}(t) = X_i(t) - \frac{1}{N}\sum_{k=1}^{N} X_k(t) \qquad 2.1$$

Here, all the channels are summed up and the average signal is used as a common reference for each channel. This will average the all the recorded channels over the scalp.

The details of each step in the process are explained in the following sections.

2.2.1 Experimental setup

In this study, EEG signals were recorded for six healthy male subjects who were all aged in the range from 24 to 28 years. A gamma.cap (Gtec Co.) with 16 electrode locations, a g.Gammabox (Gtec Co.) and a biosignal amplifier (Nihon Kohden Co.) were used to record the EEG signals of the test subjects. A standard 10-20 system was followed for placement of the electrodes on each subject's scalp and into the brain cap. Sixteen electrodes were placed at the F3, F4, F7, F8, C3, C4, T3, T4, P3, P4, O1, O2, Fz, Cz, Pz, and Oz positions, as shown in Figure 2.2. The sampling frequency for measurement of the EEG signals was set at 1000 Hz. The left ear lobe was used as the reference point for the EEG recordings.

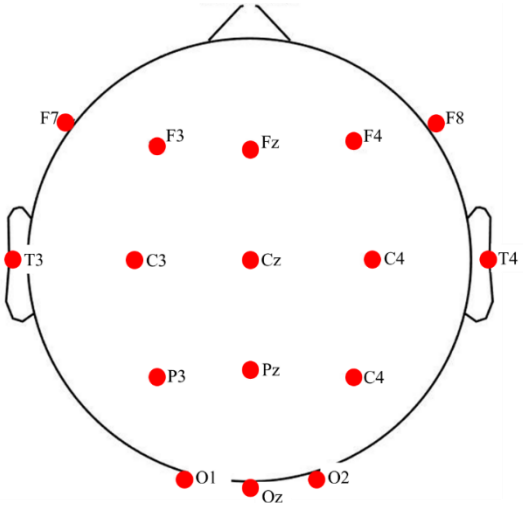

Fig. 2.2:. Selected channel locations according to the 10 – 20 system

The experimental platform is shown in Figure 2.3. In these experiments, the subjects were expected to sit on a chair in front of a table and perform two ADL tasks (i.e., movement of an object (see Figure 2.3(a)) and drinking (see Figure 2.3.(b))). The experiment begins with an audible cue to the subject: “Start.” The subject remained still for the first 10 s of the test. The subject was instructed to relax his hands on his legs when a task was not being performed. An object was placed on the table in front of the subject at 8 s, and the subject was instructed to perform the task of moving the object at 10 s, which involved moving the object from right to left following an audible cue corresponding to “Start.” The subject moved back to their relaxed position after moving the object to their left. Subsequently, there was a 4 s interval prior to the start of the next experiment. A cup was placed on the table in front of the subject at the time of 2 s within this interval. At the end of the 4 s interval, the audible “Start” cue was again given, and each subject performed the required drinking task by moving the cup towards their mouth in a manner similar to the ADL. The subject drank and then replaced the cup in its original position before returning to the rest positon. The subject was intended to perform these tasks at a self-paced rhythm. These procedures were performed 40 times over a period of 357 s. The intervals between each task were

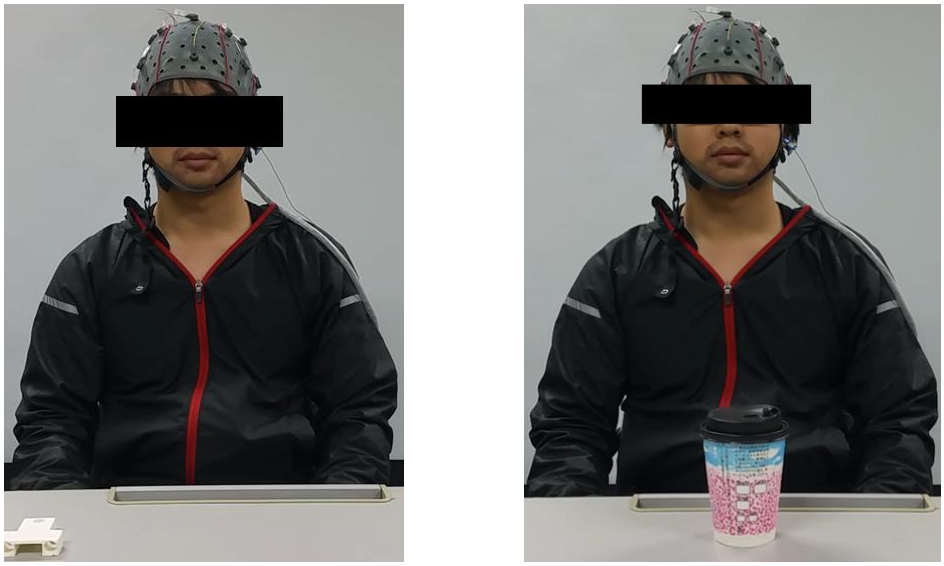

(a) (b)

Fig. 2.3: Experimental setup (a) Moving (b) Drinking

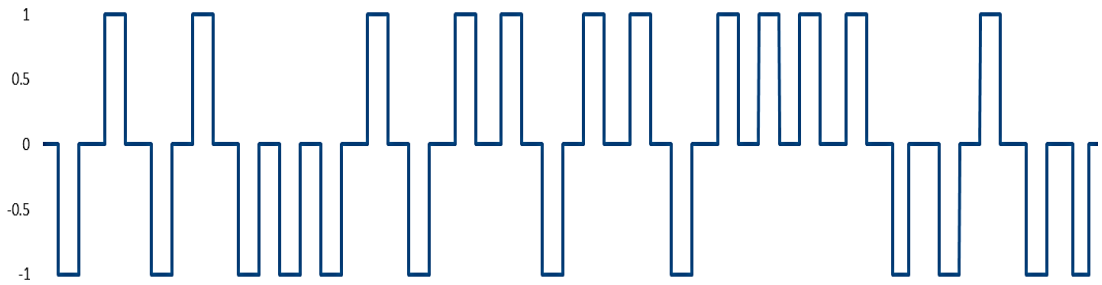

Fig. 2.4: Task schedule for twenty-four tasks in the experiment (1: movement; −1: drinking; 0: resting).

randomly selected to be either 3 s or 4 s in length. The order in which the tasks were performed was also random. The experimental task schedule for 24 of these tasks is shown in Figure 2.4.

The experimental procedure was approved by the institutional ethical review board. All the subjects were given detailed written information about the experiments and were given a chance to clarify any doubts. Then the subject signed a consent form to confirm their consent to participation of the experiment.

2.2.2 Offline analysis

During the offline analysis, the frequency distributions in the raw EEG signals were studied using fast Fourier transforms (FFTs), which are expressed as follows in Eq. (2.2):

$$X[k] = \sum_{t=0}^{N-1} X_{car,i}(t) e^{-2\pi jtk/N} \tag{2.2}$$

where $X_{car,i}(t)$ denotes the time series EEG signal, and N denotes the total number of data points in the signal. FFT analyses were performed individually on each channel for the CAR-calculated EEG signals. It was then possible to identify the locations and the frequency bands of the activated electrodes by examining the FFT analysis results.

2.2.3 Real-time prediction

The results that were obtained during the offline analysis procedure were used to create the feature matrix required for real-time analysis.

A. Feature matrix

The initial step for the real-time prediction process involves extraction of features from the raw EEG signals. In this study, the EEG band power [28], [29] is used as the feature for the prediction algorithm. The EEG power band was calculated based on the results of the offline frequency analysis. Accordingly, the four channel locations that showed the best activation results were selected by observation for use in the real-time analysis in this study. The CAR-calculated EEG signals were then used to calculate the EEG power bands based on the results of the FFT analysis.

One major challenge in EEG-based studies involves understanding of the dynamic information, which changes over time. In this study, a feature matrix of time-delayed inputs is used by the classifiers for this purpose. Therefore, the feature matrix from the selected electrode provides three inputs to the classifier, as shown in Eq. (2.3) below, where $IP_i(t)$ denotes the input to the classifier at time *t* s and $EEG_i(t)$ denotes the EEG band power in the selected i^{th} channel at time *t*:

$$IP_i(t) = \begin{bmatrix} EEG_i(t) \\ EEG_i(t-\Delta t) \\ EEG_i(t-2\Delta t) \end{bmatrix} \tag{2.3}$$

Therefore, the input training matrix dimensions correspond to $\big((3 \times n) \times l\big)$, where *n* denotes the number of electrodes that were selected from the FFT analysis and *l* denotes the number of time steps. The number of rows corresponds to $(3 \times n)$ because each electrode provides three inputs to the classifier at the three different time steps.

The input feature vector for the classifier thus corresponds to Eq. (2.4) below:

$$IP(t) = \begin{bmatrix} EEG_1(t) & EEG_1(t+1) & EEG_1(t+2) & \cdots & EEG_1(l) \\ EEG_1(t-\Delta t) & EEG_1(t+1-\Delta t) & EEG_1(t+2-\Delta t) & \cdots & EEG_1(l-\Delta t) \\ EEG_1(t-2\Delta t) & EEG_1(t+1-2\Delta t) & EEG_1(t+2-2\Delta t) & \cdots & EEG_1(l-2\Delta t) \\ EEG_2(t) & EEG_2(t+1) & EEG_2(t+2) & \cdots & EEG_2(l) \\ \cdots & \cdots & \cdots & \cdots & \cdots \\ EEG_n(t) & EEG_n(t+1) & EEG_n(t+1) & \cdots & EEG_n(l) \end{bmatrix} \quad (2.4)$$

To determine Δt, neural network-based classifications were performed for three randomly selected data sets with different Δt values corresponding to 50 ms, 100 ms, 250 ms, 500 ms, 1 s, and 2 s. Following the evaluation, Δt was selected to be 1s for the entire study because the highest classification accuracy was produced for Δt = 1s.

B. Neural networks

An artificial neuron is an information processing unit and is the building block of neural networks [30]. As in [31], artificial neuron receives input and weights which

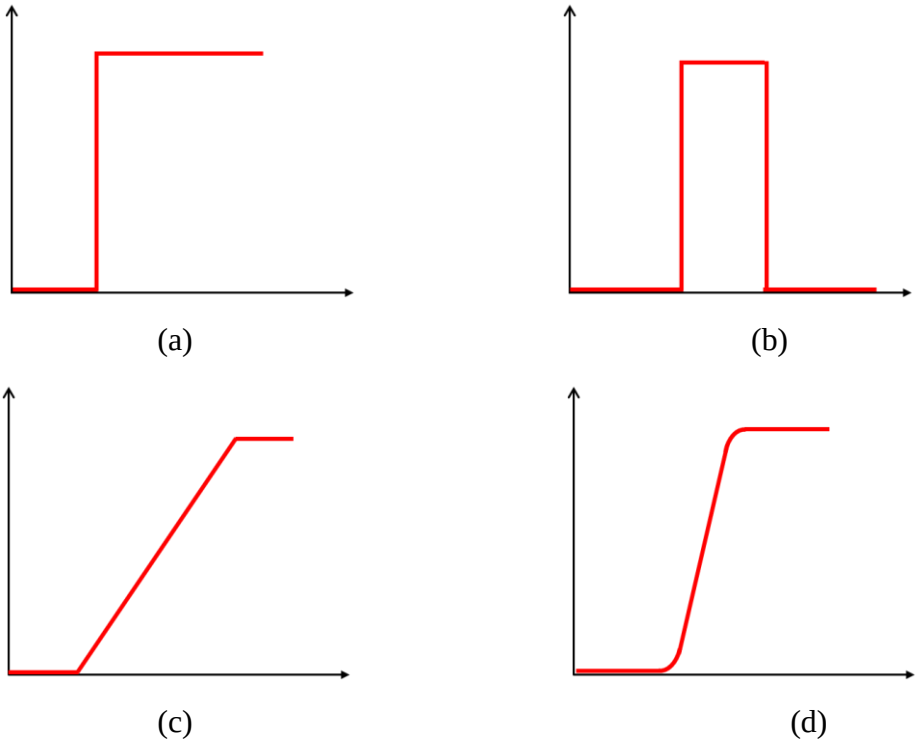

Fig. 2.5: Different activation functions for neural networks (a) Step (b) Arbitrary are used to perform arithmetic summing that will be followed by an activation

function [32]. Accordingly, the network (*N*) will be Step (c) Threshold Linear (d) Sigmoid

$$N = \sum_{i=1}^{n} w_i x_i \tag{2.5}$$

where x_i corresponds to the input to the neuron and w_i corresponds to the weight associated for the branch consist of x_i.

In addition, in order to activate the neuron, several types of activation functions are available. Different types of activation functions in Figure 2.5 (a) – (d) respectively illustrates step function, arbitrary step function, threshold linear function and sigmoidal function. Depending on the function used, it limits the output of the neuron [32].

A feedforward network comprises of different layers, whereas each unit in a layer receives inputs from the units in the immediately preceding layer [32]. Generally, multilayered neural network is built from an input layer, one or more hidden layers and an output layer [32].

In this study sigmoidal transfer function was used as the activation function in both the hidden and output layers to calculate the outputs from each layer. In addition, for the training of the neural network the error-back propagation algorithm was used. Thus, during training the mean squared error between the desired output and the actual network output is minimized iteratively using the gradient decent algorithm.

C. Neural Network based prediction

In this study, seven neural networks were trained; six networks were trained using one individual subject's data and one was trained with the data from all the subjects. Each neural network consists of three layers: the input layer, the hidden layer, and the output layer. The hidden layer contains 30 neurons and was determined by comparison with the results for structures containing 20, 30, 40, and 50 neurons in their hidden layers. The neural network structure is shown in Figure 2.6.

The entire experiment accounts for three different tasks during the training of the neural network, i.e., moving an object, drinking, and resting. With respect to the required training values, 1 was assigned to moving the object, −1 was assigned to drinking, and 0 was assigned to resting, as shown in Figure 2.4. The output during the prediction process from the neural network corresponds to the values ranging from −1 to 1 that are used to represent each of the above tasks. Therefore, six different neural networks were trained for the six subjects using each individual subject's training data. A seventh neural network was trained using a combination of the training data from all the subjects.

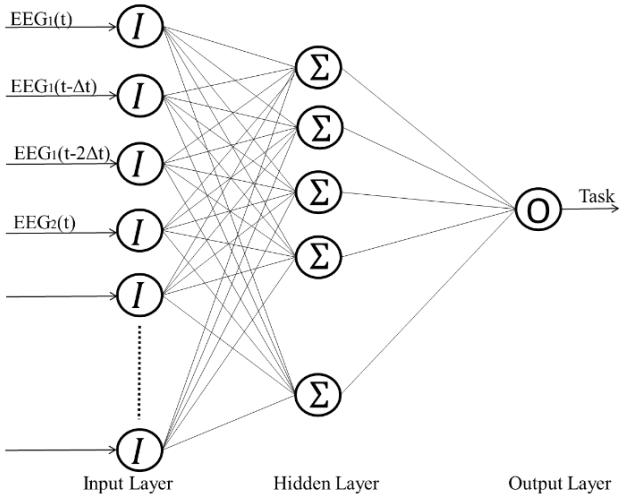

Fig. 2.6: Structure of the trained neural network.

D. Support Vector Machine

The SVM [33] performs classification using linear decision hyperplanes in the feature space. When a linear classifier is defined by a hyperplane's normal vector w and an offset b as in Figure 2.7. Accordingly, as shown in the Figure 2.7, the decision boundary will be

$$x|(w.x) + b = 0 \qquad (2.6)$$

In the Figure 2.7, the dark thick line illustrates the decision boundary. The space

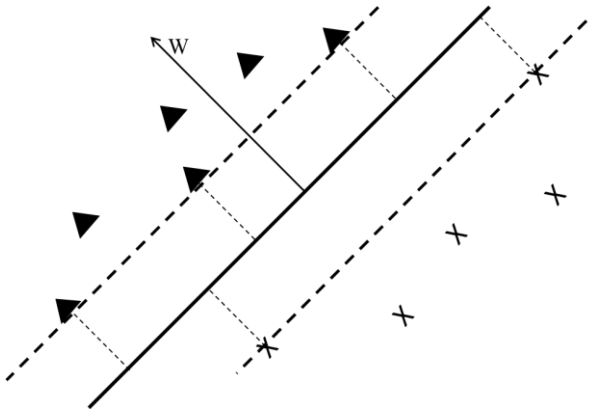

Fig. 2.7: Linear classifier and margins (Reproduced from [33])

on each side of the decision boundary corresponds to a single class of a binary problem. During the training state, these hyperplanes are calculated to separate the training data using different class labels.

However, these data are transformed into a new vector space using a kernel function when it is not possible to separate the training data in a linear manner.

In the linear classification procedure, the hyperplane is calculated as shown in Eq. 2.7, which is upper bounded in terms of the margin as indicated by Eq. 2.8, as shown below [33]:

$$y = sgn((w.x_i) + b) \tag{2.7}$$

$$y\big((w.x_i) + b\big) \geq 1, i = 1, \ldots\ldots, n \tag{2.8}$$

The SVM is also extended to perform multiclass classification. This study focuses on classification of a three-class problem. Given the choice of use of one-against-many and one-against-one approaches in the SVM, this study used the one-against-one approach. This approach is more efficient for use with training data from the i^{th} and j^{th} classes, and the classification problem is solved as shown in Eq. 2.9 below:

Minimize:

$$\frac{1}{2}(w^{ij})^T w^{ij} + C\sum_t(\varepsilon^{ij})_t \quad (2.9)$$

Subject to: $\left(w^{ij}\right)^T \varphi(x_t) + b^{ij} \geq 1 - (\varepsilon^{ij})_t$, if x_i in the i^{th} class,

$$\left(w^{ij}\right)^T \varphi(x_t) + b^{ij} \leq -1 + (\varepsilon^{ij})_t, \text{ if } x_i \text{ in the } j^{\text{th}} \text{ class, and } (\varepsilon^{ij})_t \geq 0.$$

E. SVM-based prediction

The SVM classifier was implemented using the LIBSVM library [34]. A radial basis function was used as the kernel function. Additionally, C and ε were randomly selected to produce superior classification rates. In a manner similar to the neural network approach, six different SVM models were trained for the six subjects using their individual training data and a separate SVM model was then trained using a combination of the training data for all the subjects.

2.3 Results

Results of frequency analysis and the estimation with classifiers are presented respectively in the following sections.

2.3.1 Frequency analysis

The frequency analysis results show the distributions of the magnitudes of the frequencies for each channel. The frequency distributions of channel locations F7 and C5 for subject 1 are shown in Figure 2.8 (a) and Figure 2.8 (b), respectively. Specifically, F7 shows good activation when compared with the performance of C5. For all six subjects, channel locations F7, F8, T3, and T4 showed good activation based on observation and comparison processes. These channels were therefore selected for use in the real-time prediction procedure. The activations were in the frequency range below 4 Hz in all the selected electrode locations above. The selected electrode

locations and their frequency ranges were similar for all six subjects. The EEG signals from the selected channels were high-pass filtered at 4 Hz, and the resulting values were squared to perform the EEG power band derivation. The resulting time-series activations of the EEG patterns at F7 and F8 are shown in Figure 2.9, where *M* denotes the object movement state and *D* denotes the drinking state. A rhythmic activation was observed in both channels for the object movement state. With regard to the drinking state, a certain degree of activation did exist, but no rhythmic pattern was observed. During the resting state, no activation was observed. The derived band power signals were then used to create the input feature matrix for the classifiers and a $(3 \times 4 \times l)$ feature matrix was created and used as the input.

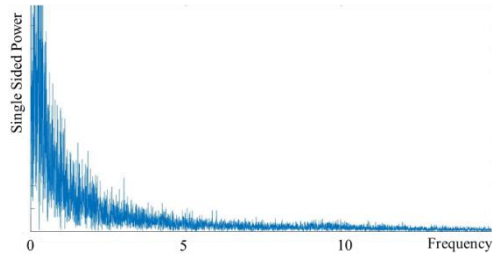

(a)

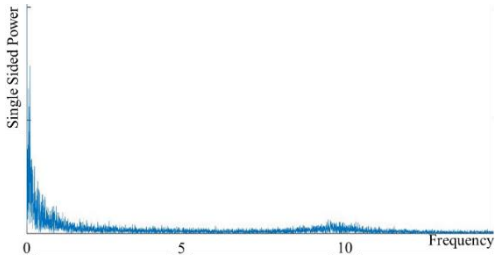

(b)

Fig. 2.8: FFT results for electrodes (a) F7 and (b) C5 for subject 1.

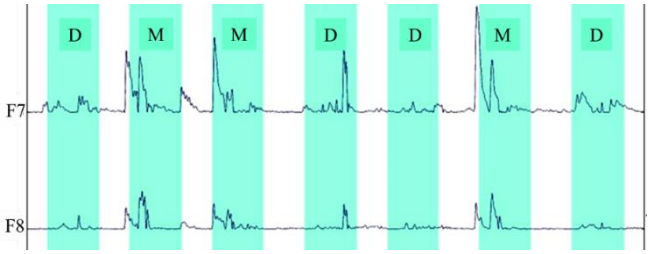

Fig. 2.9: Activation of electrodes F7 and F8 (where D is drinking and M is moving).

2.3.2 Neural network-based prediction

The trained neural networks for the six subjects were then used to predict the intended task. The output from the neural network for the task prediction process of two subjects is shown in Figure 2.10 (a) and (c). This predicts values in the range from 1 to −1 for the expected tasks. The orange color indicates the expected output, and the blue color denotes the real output. The output signal from the neural network was rounded off, and the corresponding resulting output is shown in Figure 2.10 (b) and (c). Similarly, the neural network that was trained using the data from all subjects was also used to predict the intended tasks of the six subjects individually. The results that were obtained from individual trained neural network based prediction are summarized in Table 2.1. The prediction accuracies were calculated based on comparisons of the real and predicted classes at each instant in time. For the individually trained neural networks, the highest accuracy and the average accuracy

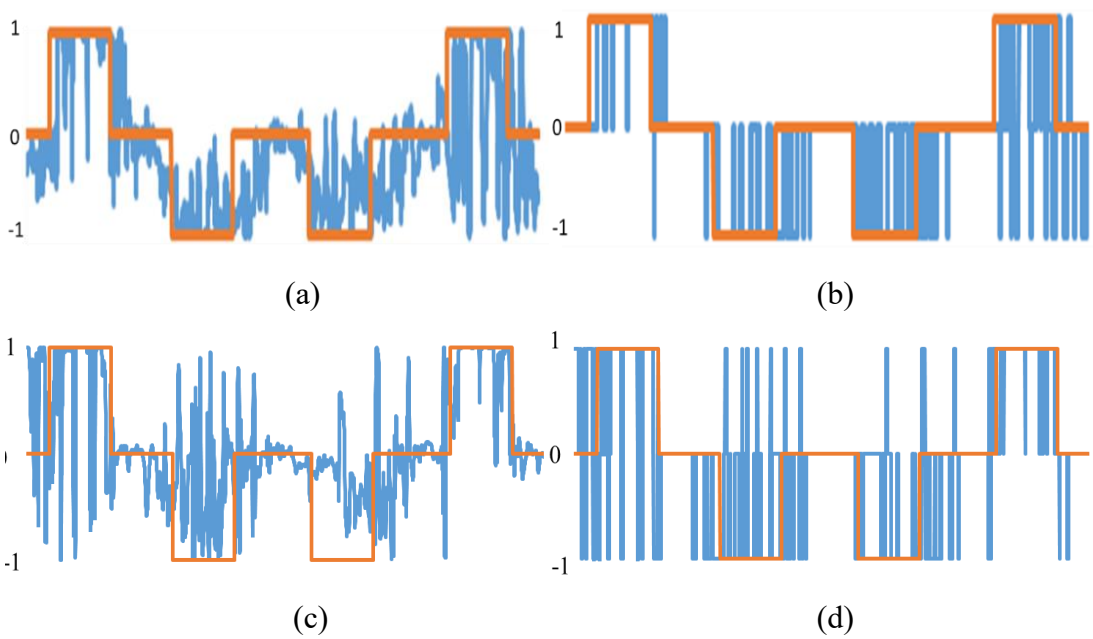

Fig. 2.10: Comparison of actual velocities of elbow flexion/extension with predicted velocities for two subjects. (a) Actual output from the neural network. (b) Corresponding Rounded output. (c) Actual output from the neural network (d) Corresponding Rounded output.

Table 2.1: Results for six subjects produced by the neural networks (Individual Training).

Individual Training				
	Resting	**Moving**	**Drinking**	**Overall**
Subject 1	80.4	61.2	58.2	70.5
Subject 2	69.1	77.7	51.7	67.0
Subject 3	72.2	63.0	56.2	66.2
Subject 4	66.6	73.2	55.8	65.6
Subject 5	67.0	77.4	44.7	64.2
Subject 6	65.4	81.6	33.0	61.5
Average	70.1	72.4	49.9	65.8

for the resting state corresponded to values of 80.4% and 70.1%, respectively. For the object moving state, their highest accuracy and average accuracy values corresponded to 81.6% and 72.4%, respectively. For the drinking state, their highest accuracy and average accuracy values corresponded to 58.2% and 49.9%, respectively. The highest individual accuracy of 70.5% was achieved for subject 1. For all six subjects, the average overall accuracy was 65.8%.

For the neural network that was trained using the data from all six subjects, the

Table 2.2: Results for six subjects produced by the neural networks (Collective Training).

Collective Training				
	Resting	**Moving**	**Drinking**	**Overall**
Subject 1	87.4	69.9	43.6	72.8
Subject 2	75.1	73.1	76.0	74.8
Subject 3	70.1	72.9	68.5	70.4
Subject 4	66.4	80.3	52.1	66.3
Subject 5	70.7	63.4	80.2	71.2
Subject 6	65.2	75.9	36.3	60.8
Average	72.5	72.6	59.5	69.4

results are summarized in Table 2.2. With this type classifier, the highest accuracy and the average accuracy with respect to the resting state corresponded to 87.4% and 72.5%, respectively. For the object moving state, the highest accuracy and average accuracy values corresponded to 80.3% and 72.6%, respectively. For the drinking state, the highest accuracy was 80.2%, while the average accuracy was 59.5%. The highest individual accuracy of 74.8% was recorded for subject 2. The average overall accuracy for all six subjects in this case was 69.4%.

2.3.3 SVM-based prediction

In a manner similar to the neural network-based prediction case, the same data were used to predict the tasks intended by the subjects that used the trained SVM models. Figure 2.11 shows the task prediction results for four subjects. The orange color denotes the expected output, while the blue color denotes the real output. Table 2.3 shows a summary of the results for all six subjects for the SVM models that were trained using data from individual subjects. In this type of classifier, the highest accuracy with respect to the resting state corresponded to 94.5%, while the average

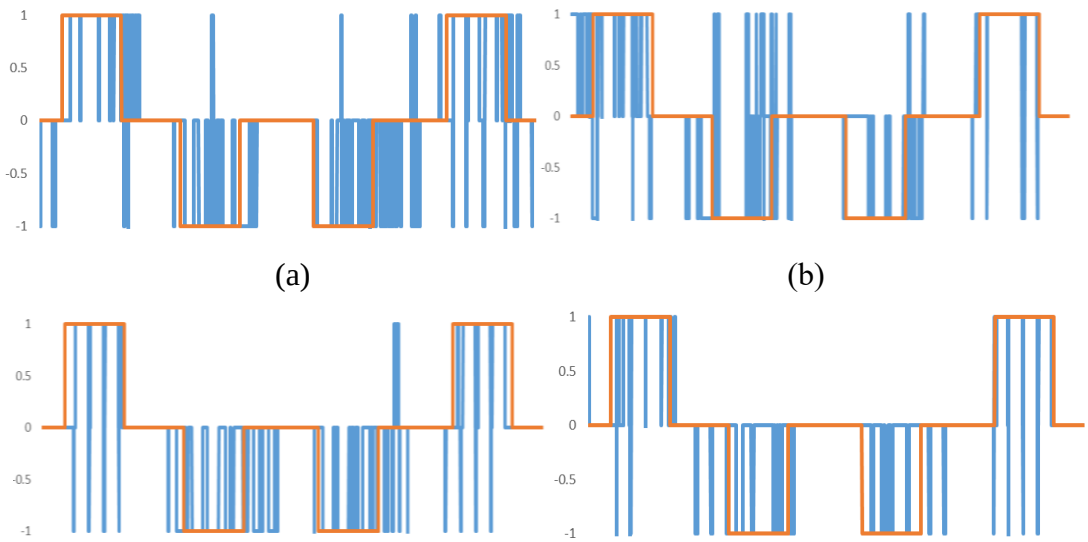

Fig. 2.11: Comparison of actual tasks with predicted tasks for the SVM for four subjects (a) Subject 1 (b) Subject 2 (c) Subject 3 (d) Subject 5

accuracy corresponded to 86.6%. For the object moving state, the highest accuracy was 83.8% and the average accuracy was 77.6%. For the drinking state, the highest accuracy was 59.8% and the average accuracy was 39.1%. Subject 2 showed the highest overall individual accuracy of 74.6%. The average overall accuracy for all six subjects was 73.1 %.

In contrast, for the SVM model (See Table 2.4 for summarized results) that was trained with the data from all six subjects, with regard to the resting state, the highest accuracy was 97% and the average accuracy was 90.4%. Additionally, a highest accuracy value of 84.3% and an average accuracy of 73.4% were recorded for

Table 2.3: Results for six subjects produced by the SVM (Individual Training).

Individual Training				
	Resting	**Moving**	**Drinking**	**Overall**
Subject 1	77.6	77.8	57.2	72.8
Subject 2	78.8	80.3	59.8	74.6
Subject 3	86.5	67.7	54.2	74.3
Subject 4	92.5	83.8	17.5	72.5
Subject 5	94.5	81.5	22	74.1
Subject 6	89.5	74.2	24	70.2
Average	86.6	77.6	39.1	73.1

Table 2.4. Results for six subjects produced by the SVM (Collective Training).

Collective Training				
	Resting	**Moving**	**Drinking**	**Overall**
Subject 1	87.1	73.6	44.4	73.7
Subject 2	92.7	71.0	47.4	76.7
Subject 3	97.0	66.5	4.3	67.6
Subject 4	94.7	77.2	6.7	69.5
Subject 5	80.8	84.3	35.4	70.8
Subject 6	90.1	68.1	27.8	70.0
Average	90.4	73.4	27.7	71.4

the moving state. For the drinking state, the highest accuracy was 47.4%, while the average accuracy was 27.7%. However, the model recorded a lowest accuracy of 4.3% for the drinking state. The highest overall individual accuracy of 76.7% was recorded for subject 2. The average overall accuracy for all six subjects was 71.4%.

2.3.4 Latency

In addition to the accuracy, the latency between the real execution of motion and the prediction was calculated based on the time difference between the real and predicted starting points of the motion. The results for latency for all four type of estimation are summarize in Table 2.5. For the individually trained neural network-based classifier Subject 4 demonstrated the quickest prediction capabilities recording the latency to be only 150ms. The highest latency was recorded was 490ms for Subject 6. Based on the latency of all six subjects, the average latency corresponded to 300 ms.

For the estimations with the neural network recorded with all six subject's data, the quickest prediction capability was demonstrated by Subject 3 who recorded 80ms latency. The highest recorded was 430ms for Subject 5. The overall average latency for this type of neural network prediction was 250 ms.

The quickest estimation when using the SVM models trained for individual

Table 2.5: Latency of real motion onset and estimated motion onset

	Latency			
	NN_IND	**NN_ALL**	**SVM_IND**	**SVM_ALL**
Subject 1	0.45	0.33	0.38	0.40
Subject 2	0.20	0.18	0.47	0.73
Subject 3	0.23	0.08	0.36	0.62
Subject 4	0.15	0.15	1.09	1.25
Subject 5	0.28	0.43	0.51	0.97
Subject 6	0.49	0.28	0.75	0.18
Average	0.30	0.24	0.59	0.69

subjects was recorded to Subject 3 and corresponded to 360ms. The longest latency of 1s and 90ms was recorded for Subject 4. On average, the latency between the real execution of motion and the predicted execution was recorded to be 600 ms when using the SVM trained for individual subjects.

The latency for the SVM model trained with all subject's data recorded a minimum latency of 180ms for the Subject 6. However, the highest value recorded for this type of estimation was recorded from Subject 4 and corresponded to 1s and 250ms. The average latency for all six subjects between the real and predicted motions was 700ms.

2.4 Discussion

This study proposed the use of a task based motion intention prediction method to be used for control of a wearable assistive device. The proposed method was used to predict three task states, i.e., moving, drinking, and resting of the upper extremity, using both neural network and SVM-based classifiers. Each classifier was trained using two different types of data, including data from individual subjects and data from all six subjects. Therefore, four predictions were made for each individual subject. A

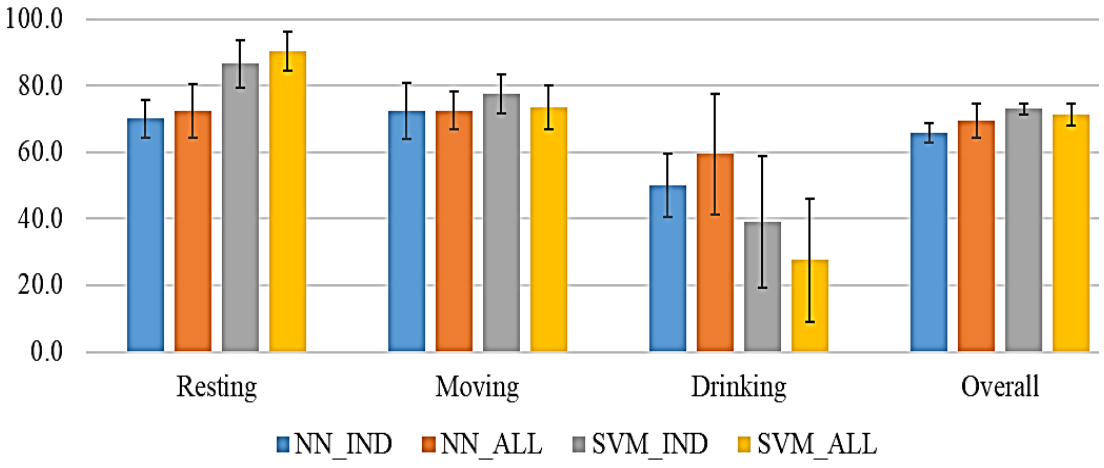

Fig. 2.12: Analysis of results for all six subjects with four different types of prediction.

summary of the results of the four predictions for all six subjects is shown in a column graph in Figure 2.12.

All four prediction methods demonstrated higher rates of accuracy for the object movement and resting states. However, the accuracy rates for the drinking state were low when compared with those for the other two states. This was expected because the input signal for the moving state clearly involves a certain degree of activation, while there were no clear activation signs for the drinking state. However, in neural network-based prediction, when the network was trained using the data from all six subjects, a significantly higher accuracy rate was achieved for the drinking state when compared with the other three prediction methods. Similarly, when it was trained using the data of all six subjects, the neural network-based classifier performs better than the corresponding classifiers that were trained using an individual subject's data for all three classes.

Conversely, when compared with the overall results, the accuracy of the SVM-based classification results exceeded that of the neural network-based classification results. Unlike the neural network-based classifier case, the individually trained SVM models performed better than the SVM model that was trained using the data from all subjects. For the resting state, the SVM achieved a maximum accuracy of 94.5%, while

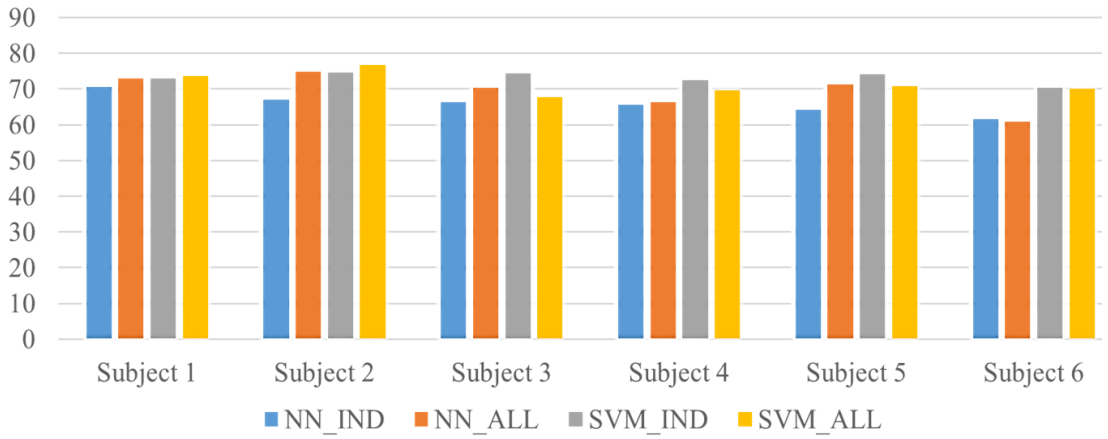

Fig. 2.13: Comparison of results for different subjects

the maximum accuracy for the neural networks was 87.4%. For the object moving state, the accuracies of the SVM and neural network-based classifications were 84.3% and 81.6%, respectively. For the drinking state, the highest accuracies of the SVM and of the neural network-based classifications were 59.8% and 80.2%, respectively. However, for the drinking state, the lowest success rate for the prediction was an accuracy of less than 7% when using the SVM-based classifiers with two subjects, when trained with the data from all subjects. Therefore, the average accuracy for the drinking state for the SVM (39.1%) was lower than that of the neural networks (59.5%).

In addition, a subject based comparison of the overall results is shown in Figure 2.13. For the both instances of the neural network based training, Subject 6 demonstrate the least performance in comparison to the remaining five subjects. Conversely, the best performances of the both instances recorded for different subjects. For SVM based estimation it was the opposite of the neural network based training. The highest performance was demonstrated by the same subject, Subject 2. However, the least performances were demonstrated by two different subjects. Therefore, there is no specific pattern in the performances, subject wise. This could be due to the individual differences in the brain dynamics in humans and the unpredictable adaptation of the performances of the classifies according to the individual differences.

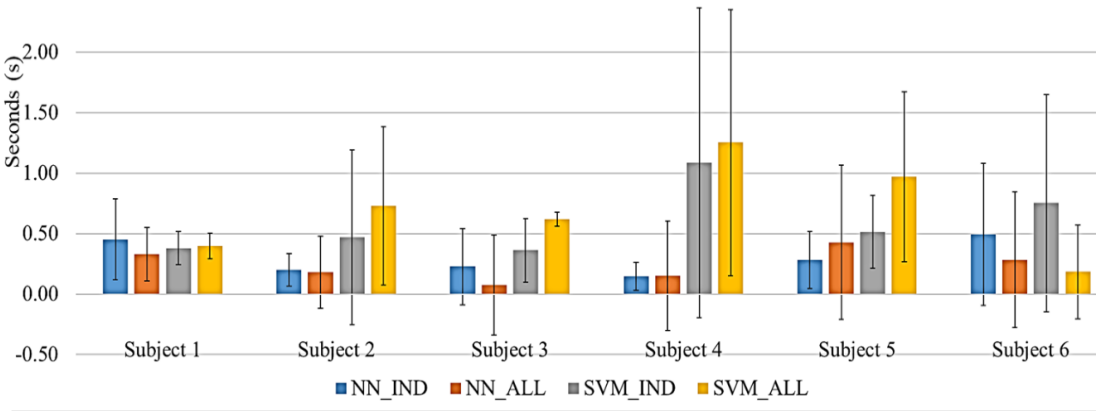

Fig. 2.14: Latency of predicted motion relative to the expected motion for all six subjects.

Summary of the results for the analysis of latency is shown in Figure 2.14. The neural network based estimation provides faster predictions than the SVM based estimation in terms of the latency between the actual motion and the motion predicted by the classifiers. While some prediction latency is inevitable, the latency of the neural network-based classifier is almost half of that of the SVM-based classifier.

Furthermore, the brain activity differences for the two different motor tasks were apparent in the feature plots in Figure 2.9 and hence in the final results with the classifiers. Some studies have shown [38], the difference in the brain activity can be explained by identifying the difference of the two motion tasks in terms of self-involvement. More elaborately, moving task is performed between two random different target points in the space, whereas drinking task is performed between a random point in the space and a point in the body. The later task (drinking) demonstrates more self-involvement according to some studies and involves the forward model [35], [36], by using the efference copy [37] of the motor command to predict the sensory consequences of the ongoing motor act. For similar kind of tasks with higher self-involvement, Blakemore *et. al.* [38] showed the brain activations are attenuated during the task. Accordingly, less brain activation can be expected for drinking tasks, compared to that of the moving task.

Further, another experiment was carried out to confirm the above assumption. Details of the experiments are explained in Appendix i. In the experiment, drinking task was replaced by a similar vertical motion, but between two different points of the space. Results show that similar vertical motion demonstrate a higher brain activation compared to the drinking task, confirming the correctness of the aforementioned assumption experimentally.

Additionally, when compared with the available noninvasive BCIs for control of wearable robotics, the proposed approach allows the wearer to perform two ADL tasks based on the intention of the exact motion through generation of multi-DoF motion for the wearable robot using an inverse kinematic model for the tasks.

Furthermore, the prediction capability of the proposed method for expected motion tasks exceeds or equals that of the currently available noninvasive BCIs for wearable robots.

Future studies will involve the use of hybrid signal modality to provide additional information about the tasks that are performed to obtain the inputs for the classifiers. From this perspective, it will be possible to use the inputs from real-time video signals, head position information measured using inertia measurement units, and functional near infrared spectroscopy signals in conjunction with the EEG signals.

2.5 Conclusions

In this study, a noninvasive BCI approach was proposed to examine the dynamic features of EEG signals that occurred during two ADL tasks. The proposed method was used to predict the task-based motion intentions of users of a wearable robot. Initially, the current statuses of the BCI techniques that were available to perform such tasks were identified. The proposed methodology accommodates the dynamic nature of the EEG signals in its approach through use of time series feature inputs in the classifiers. An offline analysis was performed to identify the activated brain regions and the frequency ranges for each of the intended user motions. The identified signals were then used in real time as inputs to neural network and SVM-based classifiers to predict the intended motions. The experimental results indicated the effectiveness of the proposed method. This study has thus established the feasibility of using a task-based approach to control wearable robots with BCIs.

References

[1] A. Vallabhaneni, T. Wang, and B. He, “Brain—Computer Interface,” in *Neural Engineering*, B. He, Ed. Springer US, 2005, pp. 85–121.

[2] K. K. Ang *et al.*, “A Randomized Controlled Trial of EEG-Based Motor Imagery Brain-Computer Interface Robotic Rehabilitation for Stroke,” *Clin. EEG Neurosci.*, vol. 46, no. 4, pp. 310–320, Oct. 2015.

[3] K. Colwell, C. Throckmorton, L. Collins, and K. Morton, “Projected Accuracy Metric for the P300 Speller,” *IEEE Trans. Neural Syst. Rehabil. Eng.*, vol. 22, no. 5, pp. 921–925, Sep. 2014.

[4] J. Meng, S. Zhang, A. Bekyo, J. Olsoe, B. Baxter, and B. He, “Noninvasive Electroencephalogram Based Control of a Robotic Arm for Reach and Grasp Tasks,” *Sci. Rep.*, vol. 6, p. 38565, Dec. 2016.

[5] Y. Hayashi and K. Kiguchi, “A study of features of EEG signals during upper-limb motion,” in *2015 IEEE International Conference on Advanced Intelligent Mechatronics (AIM)*, 2015, pp. 943–946.

[6] M. Rea *et al.*, “Lower Limb Movement Preparation in Chronic Stroke: A Pilot Study Toward an fNIRS-BCI for Gait Rehabilitation,” *Neurorehabil. Neural Repair*, vol. 28, no. 6, pp. 564–575, Jul. 2014.

[7] A. K. Das, S. Suresh, and N. Sundararajan, “A discriminative subject-specific spatio-spectral filter selection approach for EEG based motor-imagery task classification,” *Expert Syst. Appl.*, vol. 64, pp. 375–384, Dec. 2016.

[8] B. Xia *et al.*, “A combination strategy based brain-computer interface for two-dimensional movement control,” *J. Neural Eng.*, vol. 12, no. 4, p. 046021, Aug. 2015.

[9] T. Carlson and J. del R. Millan, “Brain-Controlled Wheelchairs: A Robotic Architecture,” *IEEE Robot. Autom. Mag.*, vol. 20, no. 1, pp. 65–73, Mar. 2013.

[10] K. LaFleur, K. Cassady, A. Doud, K. Shades, E. Rogin, and B. He, “Quadcopter control in three-dimensional space using a noninvasive motor imagery-based brain-computer interface,” *J. Neural Eng.*, vol. 10, no. 4, p. 046003, Aug. 2013.

[11] M. Velliste, S. Perel, M. C. Spalding, A. S. Whitford, and A. B. Schwartz, “Cortical control of a prosthetic arm for self-feeding,” *Nature*, vol. 453, no. 7198, pp. 1098–1101, Jun. 2008.

[12] L. R. Hochberg *et al.*, “Reach and grasp by people with tetraplegia using a neurally controlled robotic arm,” *Nature*, vol. 485, no. 7398, pp. 372–375, May 2012.

[13] J. L. Collinger *et al.*, “High-performance neuroprosthetic control by an individual with tetraplegia,” *The Lancet*, vol. 381, no. 9866, pp. 557–564, Feb. 2013.

[14] C. E. Bouton *et al.*, "Restoring cortical control of functional movement in a human with quadriplegia," *Nature*, vol. 533, no. 7602, pp. 247–250, May 2016.

[15] M. S. Fifer, S. Acharya, H. L. Benz, M. Mollazadeh, N. E. Crone, and N. V. Thakor, "Towards Electrocorticographic Control of a Dexterous Upper Limb Prosthesis," *IEEE Pulse*, vol. 3, no. 1, pp. 38–42, Jan. 2012.

[16] F. Xu, W. Zhou, Y. Zhen, and Q. Yuan, "Classification of motor imagery tasks for electrocorticogram based brain-computer interface," *Biomed. Eng. Lett.*, vol. 4, no. 2, pp. 149–157, Jun. 2014.

[17] D. Bandara and R. Gopura, "Upper Extremity Prosthetics: Current Status, Challenges and Future Directions," *Seventeenth Int. Symp. Artif. Life Robot.*, 2012.

[18] S. K. Kundu, K. Kiguchi, and E. Horikawa, "Design and Control Strategy for a 5 DOF Above-Elbow Prosthetic Arm," *Int. J. Assist. Robot. Mechatron.*, vol. 9, pp. 61–75, Sep. 2008.

[19] "iLimb: world's first fully articulating and commercially available bionic hand," 11-Feb-2014. [Online]. Available: http://www.gizmag.com/go/7661/. [Accessed: 11-Feb-2014].

[20] N. Vitiello *et al.*, "NEUROExos: A Powered Elbow Exoskeleton for Physical Rehabilitation," *IEEE Trans. Robot.*, vol. 29, no. 1, pp. 220–235, Feb. 2013.

[21] J. M. P. Gunasekara, R. A. R. C. Gopura, T. S. S. Jayawardena, and G. K. I. Mann, "Dexterity measure of upper limb exoskeleton robot with improved redundancy," in *2013 8th IEEE International Conference on Industrial and Information Systems (ICIIS)*, 2013, pp. 548–553.

[22] R. A. R. C. Gopura, D. S. V. Bandara, K. Kiguchi, and G. K. I. Mann, "Developments in hardware systems of active upper-limb exoskeleton robots: A review," *Robot. Auton. Syst.*, vol. 75, Part B, pp. 203–220, Jan. 2016.

[23] C. Guger, W. Harkam, C. Hertnaes, and G. Pfurtscheller, "Prosthetic Control by an EEG-based Brain-," presented at the 5th european conference for the advancement of assistive technology, 1999, pp. 3–6.

[24] M. Palankar *et al.*, "Control of a 9-DoF Wheelchair-mounted robotic arm system using a P300 Brain Computer Interface: Initial experiments," in *IEEE*

International Conference on Robotics and Biomimetics, 2008. ROBIO 2008, 2009, pp. 348–353.

[25] G. Pfurtscheller, C. Brunner, A. Schlögl, and F. H. Lopes da Silva, "Mu rhythm (de)synchronization and EEG single-trial classification of different motor imagery tasks," *NeuroImage*, vol. 31, no. 1, pp. 153–159, May 2006.

[26] A. Vallabhaneni and B. He, "Motor imagery task classification for brain computer interface applications using spatiotemporal principle component analysis," *Neurol. Res.*, vol. 26, no. 3, pp. 282–287, Apr. 2004.

[27] C. J. Perera, I. Naotunna, C. Sadaruwan, R. A. R. C. Gopura, and T. D. Lalitharatne, "SSVEP based BMI for a meal assistance robot," in *2016 IEEE International Conference on Systems, Man, and Cybernetics (SMC)*, 2016, pp. 002295–002300.

[28] E. López-Larraz, L. Montesano, Á. Gil-Agudo, and J. Minguez, "Continuous decoding of movement intention of upper limb self-initiated analytic movements from pre-movement EEG correlates," *J. NeuroEngineering Rehabil.*, vol. 11, p. 153, Nov. 2014.

[29] G. Pfurtscheller and C. Andrew, "Event-Related changes of band power and coherence: methodology and interpretation," *J. Clin. Neurophysiol. Off. Publ. Am. Electroencephalogr. Soc.*, vol. 16, no. 6, pp. 512–519, Nov. 1999.

[30] S. S. Haykin, *Neural Networks and Learning Machines*. Prentice Hall, 2009.

[31] *Pattern Recognition and Prediction with Applications to Signal | David H. Kil | Springer*. .

[32] E. J. Rechy-Ramirez and H. Huosheng, "Stages for Developing Control Systems using EMG and EEG Signals: A survey," School of Computer Science and Electronic Engineering University of Essex, United Kingdom, TECHNICAL REPORT CES-513.

[33] K. R. Muller, S. Mika, G. Ratsch, K. Tsuda, and B. Scholkopf, "An introduction to kernel-based learning algorithms," *IEEE Trans. Neural Netw.*, vol. 12, no. 2, pp. 181–201, Mar. 2001.

[34] C.-C. Chang and C.-J. Lin, "LIBSVM: A Library for Support Vector Machines," *ACM Trans Intell Syst Technol*, vol. 2, no. 3, p. 27:1–27:27, May 2011.

[35] D. M. Wolpert, R. C. Miall, and M. Kawato, “Internal models in the cerebellum,” *Trends Cogn. Sci.*, vol. 2, no. 9, pp. 338–347, Sep. 1998.

[36] J. Decety, “Neural representations for action,” *Rev. Neurosci.*, vol. 7, no. 4, pp. 285–297, Dec. 1996.

[37] E. Von Holst, “Relations between the central nervous system and the peripheral organs,” *Br. J. Anim. Behav.*, vol. 2, pp. 89–94, 1954.

[38] S. J. Blakemore, D. Wolpert, and C. Frith, “Why can’t you tickle yourself?,” *Neuroreport*, vol. 11, no. 11, pp. R11-16, Aug. 2000.

Chapter 3

EEG Based Control Approach for a Transhumeral Prosthesis

Chapter Overview

Robotic prostheses are expected to allow amputees a greater freedom and mobility. The construction of both the mechanical design and the controlling technique are equally important to provide a better user experience for the prosthesis users. Nowadays, several control techniques based on biological signals are available for controlling of the prostheses. Amongst, electromyography (EMG) based control techniques are popular with researchers to understand users motion intention to command the prosthesis to perform the user intended action. However, available options to control robotic prostheses are reduced with increasing amputation level. In addition, for EMG based control of prostheses, the residual muscles alone cannot generate sufficiently different signals for accurate distal arm function. Thus, controlling a multi degree of freedom (DoF) transhumeral prosthesis is challenging with currently available techniques. In this chapter, an electroencephalogram (EEG) based hierarchical two stage approach is proposed to achieve multi-DoF control of a transhumeral prosthesis. During the initial stage of the study, the motion intention for arm reaching or hand lifting is identified using a neural network and k – nearest neighbor based classifiers which are trained with motion related EEG features. The predictions from the classifiers are compared with residual limb motion to generate a final prediction of motion intention. In the next stage, elbow motion and hand endpoint motion is estimated using different neural network based classifiers, which are trained with motion information recorded using healthy subjects. This can then be used to realize multi DoF control of a prosthesis. The experimental results show the feasibility of the proposed method for multi DoF control of a transhumeral prosthesis.

Chapter 3

3.1 Introduction

Transhumeral prostheses are worn by upper elbow amputees to substitute for the loss of functions of the upper limb in performing activities of daily living. Early transhumeral prostheses were body powered and capable of providing elbow flexion/extension, wrist flexion/extension and hand grasping, using a cable operated by glenohumeral articulation of the shoulder [1]. According to the motion intention, the user had to lock joints manually that were not to be operated. Robotic prosthetic devices have been developed to replace these, and to enable more mobility for their users conveniently. Recently, several robotic transhumeral prostheses have been developed [2]–[9]. These devices generate multi degree of freedom (DoF) motion and require identification of the motion intention of the user to properly assist the user.

Many of these prostheses are controlled based on surface electromyogram (EMG) signals from residual muscle sites. An EMG signal is a measureable electric current from a muscle, capable of providing control signals according to the user's motion intention [1]. In [2], in order to control a transhumeral prosthesis, forearm and wrist motions were estimated using an artificial neural network based on shoulder and elbow motions, and hand motion was generated according to fuzzy rules. In [3], DEKA arm was proposed with three modular configurations for transradial, transhumeral and shoulder disarticulated amputees. Here an EMG controller was used in combination with foot controllers and pneumatic bladders for controlling. Lenzi et al. [4] proposed a 5 DoF transhumeral prosthesis for elbow, forearm, wrist, and grasping motions that used an EMG based low level controller. In [10], a neural network based method was proposed to estimate distal arm joint angles to control a transhumeral prosthesis using EMG and shoulder orientation. Despite these advances, there is still a gap to be filled in controlling simultaneous movements in multi DoF transhumeral prostheses. This is made more challenging because as the level of amputation increases, the number of functions to be replaced by the prosthesis increases, yet fewer muscle sites are available to be used for their control. Further, residual muscle sites after an amputation

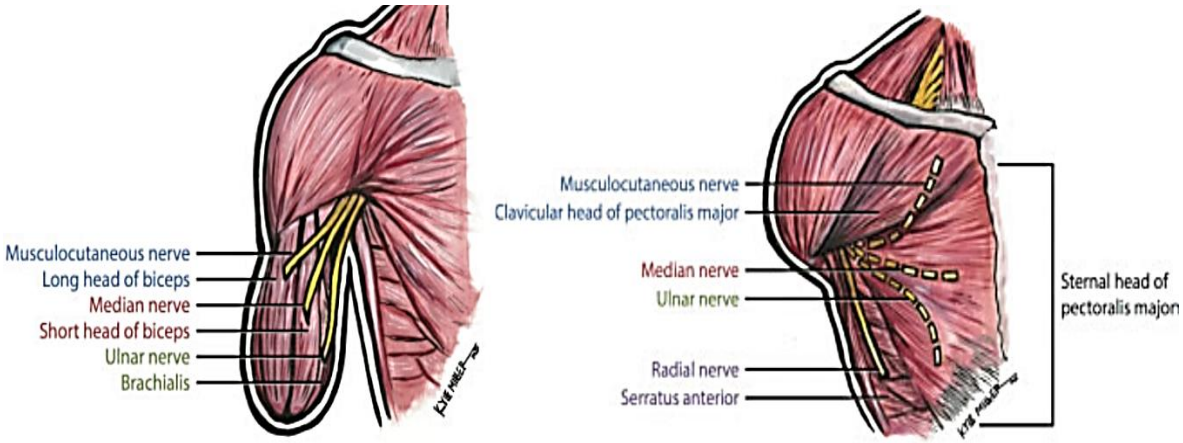

(a) (b)

Fig. 3.1: Targeted Muscle Reinnervation (reproduced from [11])

are not physiologically related to the distal arm functions [1].

A method to control a multi DoF transhumeral prosthetic arm has been proposed based on targeted muscle reinnervation [12]. In this method, the residual nerves of the lost muscles are surgically connected to the residual muscles as illustrated in Figure 3.1 [11]. This allows amputees to contract the reinnervated muscle by attempting to move the missing limb and EMG signals can be detected related to the missing motions. Therefore, EMG signals from these muscles can then be used to control prostheses. However, this method is invasive and some difficulties remain, related to separating the surface EMG signals from different muscles [1]. Owing to the deficiencies in existing methods, electroencephalogram (EEG) is becoming popular among researchers [13], [14] for identifying human motion intention for prosthesis control. EEG records electrical signals from the surface of the human skull that carry information related to all bodily motions. In [13], an EEG based motion estimation method was proposed to control forearm supination/pronation of an artificial arm. Bright et al. [14] proposed a method to control flexion/ extension of a prosthetic finger based on EEG signals. Despite these studies, control methods based on EEG for upper limb prostheses lack the capability to control simultaneous multi DoF motion according to the exact motion intention of the user.

As a solution to this problem, this chapter proposes a new hierarchical approach to control a multi-DoF transhumeral prosthesis using EEG signals in combination with residual upper-limb motion. The proposed approach comprises three main steps: EEG based motion intention identification, collection of motion information from healthy subjects to create a database, and estimation of the motion of a prosthesis based on residual limb motion. For a transhumeral amputee, with the available residual limb it is impossible to physically differentiate between the motion intention for hand reaching motion and that for arm lifting. In a healthy human, hand reaching involves multi-DoF motion of the upper limb, including shoulder, elbow, forearm and wrist motions. For arm lifting, only the shoulder motion will be involved. Amputees are able to perform only shoulder motions for both actions. Therefore, in the proposed approach, EEG signals are used to differentiate between hand reaching and the arm lifting motion intentions. For this purpose, the effectiveness of two different types of classifiers are compared to learn the dynamic EEG signals related to selected motions. Accordingly, neural networks and k – nearest neighbor classifiers are used for motion intention identification. Four different kinds of motion-related EEG features (movement related cortical potentials based amplitude, delta band power, alpha band power and root mean square) in time series are provided as inputs to the classifier. The output from the classifier is used in combination with residual limb motion information to estimate elbow motion and hand trajectory, using two different neural network based classifiers. To train these classifiers, motion information collected from healthy subjects is used.

Using the predicted elbow joint angle and the hand trajectory, it is possible to achieve multi DoF control of transhumeral prostheses for hand reaching or arm lifting. The next section of the chapter introduces the proposed methodology for motion intention identification. Section 3 presents the results of the proposed motion prediction method and the motion analysis. This is followed by the Discussion in Section 4 and the Conclusions in Section 5.

3.2 Methodology

The proposed hierarchical two stage approach for motion intention identification are shown in Figure 3.2. In the initial stage, the users' motion intention to move is estimated using classifiers (neural networks, i.e., multilayer perceptron networks and k-nearest neighbors) trained with the features of EEG signals recorded from the scalp of the user. In the later stage, elbow motion and hand endpoint motion is estimated using different neural network based classifiers, which are trained with motion information recorded using healthy subjects. Details of each stage are explained below.

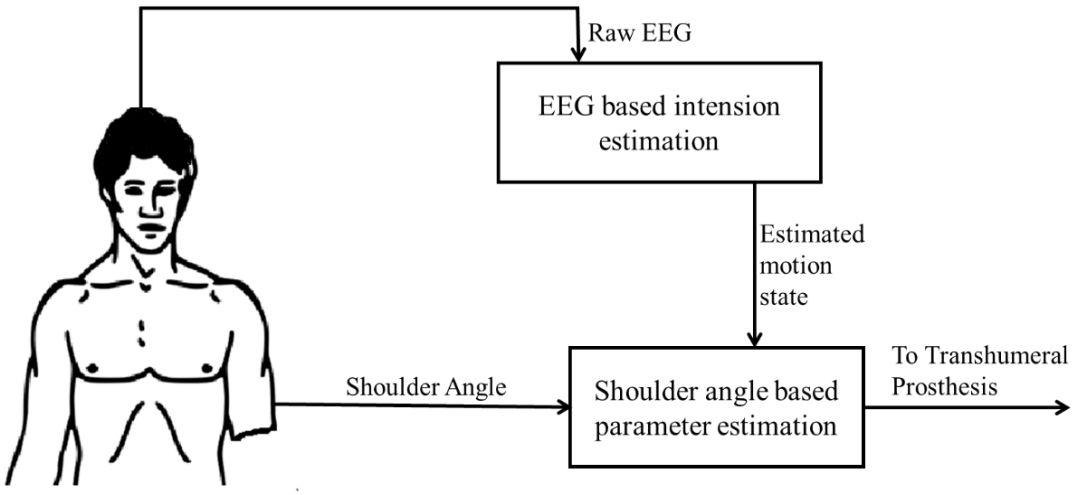

Fig. 3.2: Proposed Hierarchical Approach

3.2.1 EEG based motion intention identification

The main steps and the signal flow chart of the proposed methodology for motion intention identification are shown in Figure 3.3. Initially, brain activations for the desired motions are recorded experimentally, together with the motion data from the participants. Then the data are pre-processed for feature extraction by averaging. Next, extracted features are used to train the motion intention classifier. Finally, the output from the motion intention classifier is compared with the motion state of the

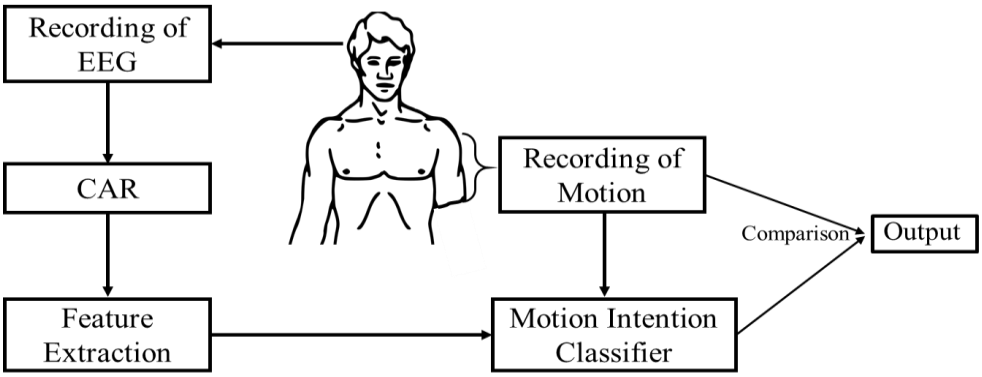

Figure 3.3: Proposed approach for motion identification. CAR – common average reference

residual limb and the final decision is generated. In this study the effectiveness of a neural network based classifier and a k-nearest neighbor classifier are evaluated for the motion intention classifier.

3.2.2 Experimental setup

In the present study, EEG signals were recorded from healthy subjects (4 men, 1 woman, age 24–28). A Gamma.cap (Gtec Co.) with 16 electrode locations, a g.Gammabox (Gtec Co.) and a bio signal amplifier (Nihon Kohden Co.) were used to record the EEG signals from the subjects. Standard 10–20 system was followed to

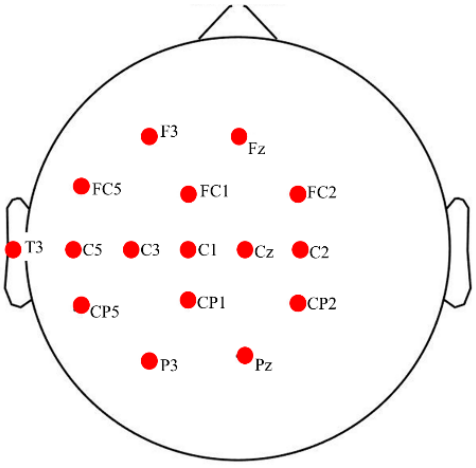

Fig. 3.4: Electrode layout for experiment

(a) (b)

Fig. 3.5: Recording of the motion data (a)Motion Capture System (b)Reflective Markers attached to the upper limb of the subject

Sixteen electrodes were placed at the Fz, F3, FC2, FC1, FC5, C2, Cz, C1, C3, C5, T3, Cp2, Cp1, Cp5, Pz, and P3 positions, as shown in Fig. 3.4. The sampling frequency was set to 500 Hz. The right earlobe was used as the reference for EEG recordings.record the motion of the upper limb, a v120: Duo (Optitrack) motion capture system (See Figure 3.5(a)) was used. Reflective markets were attached to the subject's upper limb in order to identify the corresponding motions with the motion capture systems as shown in Figure 3.5(b). During the experiment, the subject is expected to perform two upper limb motions: arm lifting motion and hand reaching motion. The experiment starts with an audible cue ("start") and the subject remains seated with arms relaxed at the side for the first 10 s, as shown in Figure 3.5(b). During the arm lifting the subject is instructed to perform only shoulder motions by lifting the arm until it is roughly parallel to the ground (See Figure 3.6(a)). The motion is self-phased and afterwards the subject moves the arm back to the resting position. During the hand-reaching motion, the subject is instructed to perform a reaching task (similar to a reaching task in activities of daily living, see Figure 3.6(b)) until the whole arm is fully extended to make it roughly parallel to the ground. The motion is self-phased and

mainly involves shoulder, elbow, forearm and wrist motions. During the experiment, an audible cue is given to instruct the subject to perform the arm lifting. To perform the reaching motion, a different audible cue is given. There is a time gap between the two commands, set at random to 5 s or 6 s, to avoid any periodic effects in the EEG signals. The order of the motions is also set at random. During the experiment, 20 motion instances are carried out, 10 for each motion. The motion schedule for the first 16 motions is shown in Figure 3.7. The experimental procedure was approved by the Kyushu University ethical review board. All subjects were given detailed written information about the experiments and were given a chance to clarify any doubts. Then all subjects signed a consent form to confirm their consent to participation in the experiment.

(a) (b)

Fig. 3.6: Motions used in the experiment. (a) Arm lifting. (b) Hand reaching.

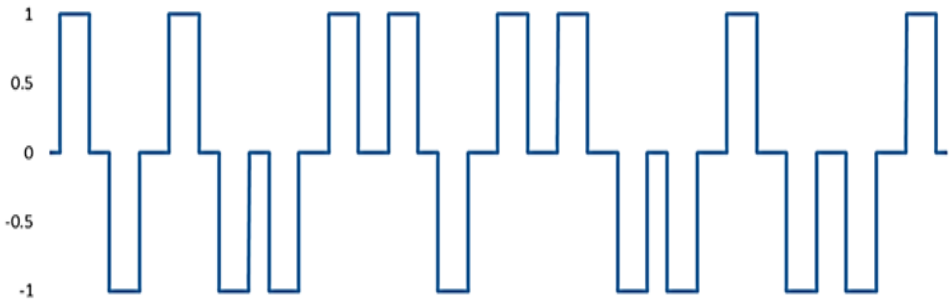

Fig. 3.7: Motion schedule (1 = arm lifting motion, 0 = rest, −1 = hand reaching motion).

3.2.3 Data processing

To minimize the influence of the noise generated among whole electrodes and to normalize the recorded data among every channel, the common average reference (CAR) is calculated with the raw EEG data as follows:

$$X_{car,i}(t) = X_i(t) - \frac{1}{N}\sum_{k=1}^{N} X_k(t) \tag{3.1}$$

where N is the number of channels used in the recordings, $\boldsymbol{X_i(t)}$ is the raw EEG signal from the i^{th} channel at time t, $\boldsymbol{X_{car,i}(t)}$ is the CAR-corrected EEG signal of the i^{th} channel at time t, and $\boldsymbol{X_k(t)}$ is the EEG signal of the k^{th} channel for average calculations. After CAR correction, the data are ready for feature extraction.

3.2.4 Feature extraction

In the present study, four different features are used as inputs to the classifier: movement related cortical potential (MRCP) based amplitude, delta band power, alpha band power and root mean square (RMS).

MRCP can be observed as time domain amplitude fluctuations in the low frequency delta band and has been used recently [15], [16] as a feature which represents motion preparation and execution and contain information related to speed, force and direction of motions [16]. Therefore, information in the MRCP magnitudes can be used to detect movements or intentions to move. Accordingly, amplitudes of low frequency delta band signals are used as an MRCP based feature in this study. CAR-processed EEG signals are passed through a 0.1–2-Hz bandpass filter to prepare them for use in classification. Few studies [13], [17], [18] have used delta band EEG features for motion intention identification. Current study considers the delta band power spectrum and it is obtained by passing the CAR-processed EEG data through a 0.1–4-Hz bandpass filter. The resulting signal is squared to obtain the power spectrum

for the delta band as explained in [19]. Similarly, alpha band features are common to represent movement intention in some studies [19], [20]. For the alpha band power, CAR-processed EEG data are bandpass filtered through 8 – 12Hz followed by the squaring. Using of RMS is also reported in few studies [13]. Accordingly, the effectiveness of RMS will also be evaluated in the study and RMS is calculated as:

$$RMS = \sqrt{\frac{1}{N_a} \sum_{k=t-N_a+a}^{t} e_{ik}^2} \tag{3.2}$$

where e_{ik} is the EEG signal of the i^{th} channel after filtering the k^{th} sample, N_a is the sampling number which is selected based on observations for low noise and high activation, from one of three choices: 100 ms, 200 ms, or 400ms. In the present study, N_a is selected to be 400 ms. In addition, the filtering techniques used for bandpass filter are based on finite impulse response filters, which in general form presents as [21]:

$$y[n] = \sum_{k=0}^{M-1} b_k x(n-k) \tag{3.3}$$

whereas *y(n)* is the output, *x(n)* is the input, b_k is the value of impulse response at k^{th} instant and *k* is the order of the filter and parameters are computed automatically during the implementation of the filter using the EEGLAB [26] tool box for a given signal.

After extracting the features for each subject, the features are plotted for each channel. These plots are observed and two prominently activated channels are selected for classification of the motion. By observation, FC2 and C2 locations were selected for MRCP based amplitudes, RMS and delta power band features. With alpha power band the highest activations were observed for P3 and Pz locations. Sample feature plots for MRCP amplitudes, delta band power and RMS are shown in Figure 3.8(a), Figure 3.8(b) and Figure 3.8(c) respectively.

Using the selected channels, a time-delayed feature matrix is prepared as the input to the classifier as follows for both training and testing phases:

$$Feature\ Matrix = \begin{bmatrix} EEG_i(t) & EEG_i(t+\Delta t) & EEG_i(t+2\Delta t) \\ EEG_i(t-\Delta t) & EEG_i(t) & EEG_i(t) \\ EEG_i(t-2\Delta t) & EEG_i(t-\Delta t) & EEG_i(t) \end{bmatrix} \quad 3.4$$

where, $EEG_i(t)$ is the EEG feature in the selected i^{th} channel at time *t*. The time delay Δt is determined by performing classification on three data sets selected at random for different Δt values of 100 ms, 250 ms, 500 ms, or 1000 ms. After the random evaluation, Δt was selected to be 250 ms for the whole study (for both training and testing) since this value results in the highest classification accuracy. Using time delayed inputs of the same channel to the input matrix, will help the classifier to learn the dynamic information contained in the EEG signals.

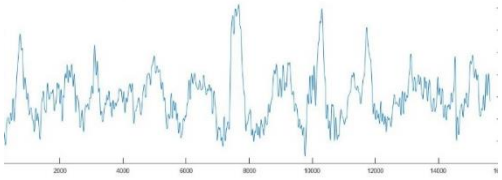

(a)

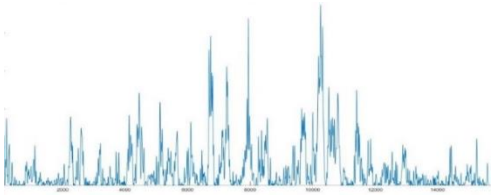

(b)

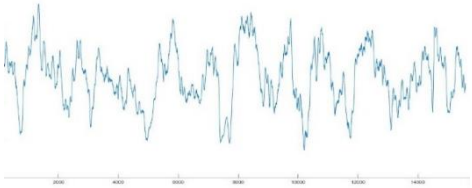

(c)

Fig. 3.8: Feature plots for channel selection. (a) MRCP. (b) Delta band power. (c) RMS.

3.2.5 Neural Network based motion intention estimation

Artificial neural networks have been widely used to solve different classification problems. Generally, a classification problem includes training and prediction phases. Accordingly, during the training phase of this problem, an input feature matrix similar to Eq. 3.3 is fed into a separate feed forward neural network for each subject. Each neural network consists of three layers: the input layer, a hidden layer, and the output layer. The hidden layer contains 30 neurons. The sigmoidal transfer function is used as an activation function in both hidden and output layers, to calculate the output of each layer. The output from the neural network is the estimated motion intention of the user: arm lifting motion, hand reaching motion, or rest. Each neural network is trained using the error back propagation algorithm with feature matrices as the input.

During neural network training a value is assigned to each motion: 1 for arm lifting motion, −1 for hand reaching motion, and 0 for resting, as shown in Figure 3.7. The output prediction from a neural network is also a value from −1 to 1, representing the above classes. For each of the five subject, three different neural networks are trained, one for each feature, for a total of 15 neural networks. A summary of the neural

Table 3.1: Summary of configuration of proposed Neural Networks (NN).

	NN for motion intention prediction	**NN for motion estimation of prosthesis**
Number of NNs	25 (5 per feature for 4 features and combined feature)	10 (5 for elbow angle, 5 for end point estimation)
Input to NN	Feature matrices of EEG features of MRCP, Delta/ alpha Power and RMS	Shoulder Angle of the Healthy Subject from the collected data base
Hidden Layers motion	30	10
Output	Users' motion intention for reaching or lifting motions	Elbow angle and end point position

network configuration is presented in Table 3.1. The trained neural networks are used for prediction of the three motion classes.

3.2.6 k–nearest neighbor classifier based motion intention estimation

k-nn algorithm is a widely used simple classification technique by finding the k number of nearest neighbors in a training data set and then mapping the same during the estimation process. k-nn algorithm is widely presented in following strategies [22].

$$y(d_i) = argmax_k \sum_{X_j \in kNN} y(x_j, c_k) \quad 3.5$$

$$y(d_i) = argmax_k \sum_{X_j \in kNN} Sim(d_i, x_j) y(x_j, c_k) \quad 3.6$$

where, d_i is a test document, x_j belongs to class c_k, Sim(d_i, x_j) is the similarity function for d_i and x_j. In the two strategies, as in [4], the prediction class will be the class that has the largest number of member in the k-nn and as in [5], the prediction will be the class with the maximum sum among the k-nn. However, it should be noted that the value of k is important for the better performance in the classification. Therefore, during the implementation phase of the k-nn classifier with MATLAB, optimization process also runs simultaneously to the classifier. Optimization algorithm automatically determines the best k value and the best metric to be used for the k-nn classifier based on the optimization results, suitable for each training data set of each feature per subject. During the optimization, parameters are optimized to minimize the five-fold cross validation loss. Training and testing data were prepared in a similar manner to the neural network based classification. 20 different k-nn models were trained for all the 5 subject and for the 4 features used. In addition, 5 additional k-nn models were generated by training a single k-nn model for each subject by combining all the four feature matrices. The trained k-nn models were used to estimate the motion intention.

3.2.7 Comparison

The proposed approach includes a step to compare residual limb motions with the neural network output, to improve the accuracy of the prediction. This prevents false triggers when the user does not want to perform any motion. The final prediction of the proposed method is decided based on the result from the comparison. Based only on the movement of the residual limb, it is impossible to identify desired motions. However, the proposed method is capable of identifying user intention to move the upper limb. Thus, the rules of the comparison are shown in Table 3.2.

Table 3.2: Rules of comparison for residual limb motion and the Neural Network (NN) output.

Output from NN	User's desire for motion	Final prediction
Rest	no	Rest
Hand reaching motion	no	Rest
Arm lifting motion	no	Rest
Rest	yes	Rest
Hand reaching motion	yes	Hand reaching motion
Arm lifting motion	yes	Arm lifting motion

3.2.8 Motion analysis

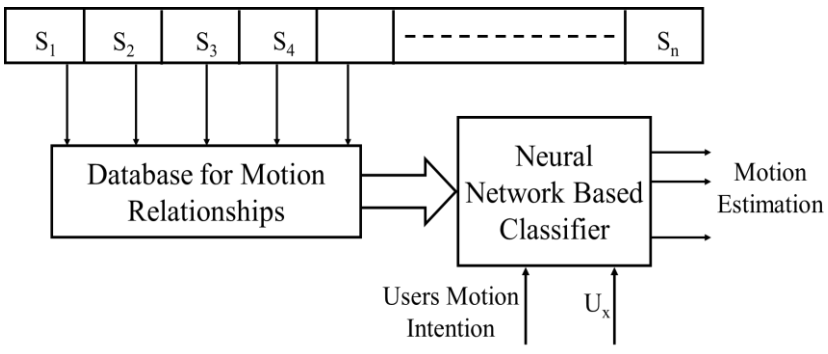

Fig. 3.9: Proposed approach for estimation of identified motion (Sn—healthy individuals, n—1, 2, 3, …, Ux—residual limb joint angle of the transhumeral amputee).

In the approach proposed above, it is insufficient to identify only the motion intention of the transhumeral amputee for prosthetic control. Therefore, after identifying the motion intention of a reaching motion, the method shown in Figure 3.9 is used to estimate the motion of the prosthesis.

A transhumeral amputee with a residual limb is typically only able to make shoulder motions. Therefore, in this method, initially a database is created from the motion information of the desired motions of healthy subjects (S1, S2 …….. Sn) to identify the relationships between shoulder motions and distal motions of the upper limb. With motion capturing, it is possible to record the motion of the upper limb joints experimentally. This information is used to derive the relationships between shoulder motions and distal motions of the upper limb (i.e. shoulder joint angle (Ux) with respect to the elbow joint angle and shoulder joint angle (Ux) with respect to the end point motion of upper limb). Later, information in the database is used to train a different set of neural network based classifiers to estimate the motion of the prosthesis.

Accordingly, 10 different neural networks are trained using the joint relationship information obtained during the motion analysis. Five of them are to estimate the elbow joint angle for each subject, the remaining five are to estimate the hand trajectory for each subject. Each neural network is trained with data from four subjects, with one subject excluded in each instance. The excluded subject is assumed to be the amputee; the remaining four subjects are assumed to be healthy subjects. The neural networks include three layers: input, hidden, and output layers. Each neural network is provided with an input from the estimated motion from the previous classifier (1 = arm lifting motion, 0 = rest, −1 = hand reaching motion) and three inputs of shoulder joint angles positioned at 0 ms, 250 ms and 500 ms. One set of neural networks is trained to estimate the elbow joint angle using the error back-propagation algorithm. The other set is trained to estimate the hand trajectory values for the x and y directions. The hidden layer comprises 10 neurons. Output from the neural networks are the elbow joint angle for the prosthesis to be controlled and hand trajectory values.

For the clarity of the presentation, a summary of the neural network configurations presented in this study are shown in Table 3.1.

3.3 Results

Following sections presents the results for the neural network based and k-nn based classifiers, respectively.

3.3.1 Neural network based motion intention estimation

In total, 20 artificial neural network s were trained to predict the motion intention for lifting and reaching motions of the upper limb using EEG signals. The

Table 3.3: Summarized results for 5 subjects for neural networks.

	Delta band	**Alpha Band**	**MRCP based**	**RMS**	**Combined feature**
Subject 1	72.4	78.1	84.7	79.4	80.9
Subject 2	75.7	72.4	71.1	82.0	71.6
Subject 3	74.5	78.9	78.7	71.0	75.9
Subject 4	66.8	66.1	68.6	74.4	71.3
Subject 5	66.1	70.3	63.9	61.6	62.7
Average	**71.1 ± 3.9**	**73.1 ± 4.8**	**73.4 ± 7.4**	**73.7 ± 7.2**	**72.5 ± 6.0**

outputs from these neural networks were then compared with the residual limb motion, as shown in Table 3.2. The resulting output for subject 1 for the MRCP is shown in Figure 3.10. The results for all five subjects are summarized in Table 3.3. For the delta band power, the highest accuracy of 75.7% was achieved with subject 2. The average accuracy for the delta power bandwas 71.1%. When alpha band power is used, highest accuracy of 78.9% was recorded from the Subject 3. The average was recorded as 73.4%. With MRCP based feature, the highest accuracy of 84.7% was achieved with subject 1, and the recorded average was 73.4%. A highest accuracy of 82.0% was achieved for subject 1 with RMS as the feature. The average for RMS was 63.7%.

When all the features are combined for training, highest accuracy of 80.9% was recorded with Subject 1 and in average an accuracy of 72.5% was recorded.

3.3.2 k-nn based motion intention estimation

Similar to neural network based classifiers, 20 k-nn classifiers were trained to predict the motion intention for lifting and reaching motions. During the prediction, the outputs from the k-nn models were compared with the residual limb motion, as in Table 3.2. Summarized results for the k-nn based motion estimation are shown in Table 3.4. When delta power band was used to estimate the motion intention, the highest accuracy recorded was 63.6% for Subject 1 with an average of 58.7% for the 5 subjects. With alpha power band, Subject 1 recorded a highest accuracy of 59.7% and the recorded average accuracy was 54.8%. MRCP based feature resulted a highest accuracy of 70.0% for Subject 1 and an average accuracy of 60.9% for all five subjects. RMS recoded a highest accuracy of 72.6% for Subject 1. The recorded average was 61.3% for all the five subjects. In addition, when all the features combined to estimate the motion intention, higher accuracy was recorded from Subject 1 and corresponded to 65.8%. The recorded average was 59.6%.

Table 3.4. Summarized results for 5 subjects for k –nn classifiers

	Delta band	**Alpha Band**	**MRCP based feature**	**RMS**	**Combined feature**
Subject 1	63.6	59.7	70.0	72.6	65.8
Subject 2	58.9	53.0	62.8	67.9	55.8
Subject 3	59.6	55.0	62.0	61.6	61.0
Subject 4	57.4	46.5	58.8	56.6	62.6
Subject 5	53.9	57.9	51.0	47.9	52.7
Average	**58.7 ± 3.2**	**54.4 ± 4.6**	**60.9 ± 6.2**	**61.3 ± 8.6**	**59.6 ± 4.7**

3.3.2 Motion relationships

It is important to identify the relationship between the shoulder angle and the elbow angle for prosthetic control. The measured relationship is shown in Figure 3.11

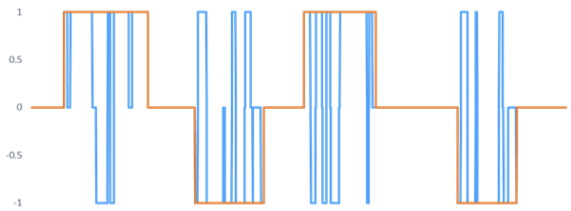

Fig. 3.10: Prediction from the system with MRCP for subject 1 (1 = lifting motion, −1 = reaching motion, 0 = rest, blue line = prediction, orange line = subject motion).

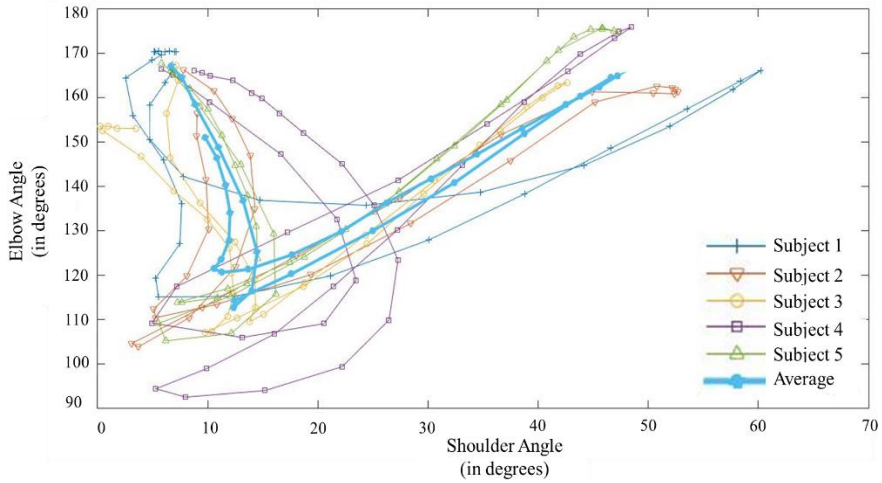

(a)

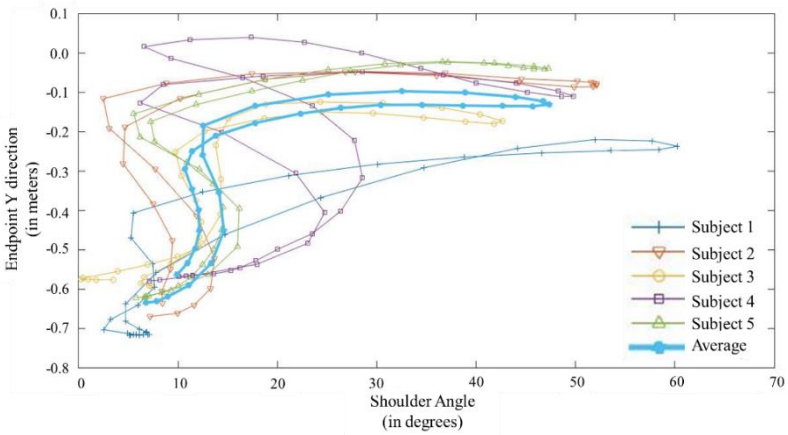

(b)

Fig.3.11: Motion relationships. (a) Elbow flexion/extension angle to the shoulder flexion/extension angle for reaching. (b) Variation of the endpoint with the shoulder flexion/extension angle

(a). The figure shows the variation of the elbow flexion/extension angle with respect to shoulder flexion/ extension angle of the residual limb for each subject. It also shows the average variation for all subjects. For the lifting motion, the elbow angle remains constant at the fully extended position. However, for the reaching motion, the angle initially decreases rapidly and then increases until the elbow is fully extended. It is also important to realize the relationship between shoulder flexion/extension angle and the desired end effector position for prosthesis control. Figure 3.11 (b) shows the variation of the endpoint of each subject with the shoulder joint angle. It also shows the average for all subjects. For the reaching motion the end-effector positon of the hand reaches its maximum point during the initial 20 degrees of shoulder motion.

Throughout the rest of the shoulder motion, the endpoint remains at the same point. In the reverse motion, the endpoint remains at it maximum point until shoulder reaches 20 degrees and it returns to the starting point within the final 20 degrees of shoulder motion.

3.3.3 Motion estimation

Neural network based classifiers trained with the motion relationships of healthy subjects were used to estimate the elbow flexion/ extension and hand trajectory of the transhumeral prosthesis. The generated results are compared with the motion captured experimental results. Similarly, generated elbow flexion/extension results for the subject 1 are shown in Figure 3.12 (a). The joint angle generated by the classifier is similar to that generated experimentally. Similar results were obtained for the other four subjects. Figure 3.12 (b) and Figure 3.12 (c) show that the hand trajectory generated by the classifier is similar to that generated experimentally. For the remaining four subjects, similar results were obtained.

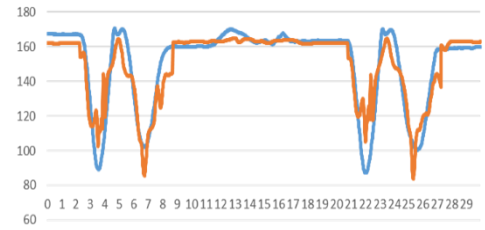

(a)

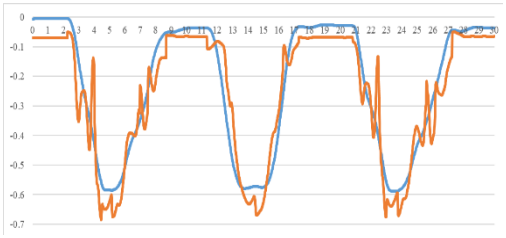

(b)

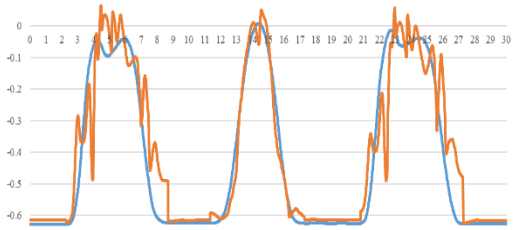

(c)

Fig. 3.12: Comparison of data measured experimentally (blue line) and those generated by the neural network classifier (orange line). (a) Estimated elbow flexion/extension angle. Hand trajectory in the (b) x direction and (c) y direction.

3.4 Discussion

In this study, a hierarchical two-stage motion prediction approach was proposed for control of a transhumeral prosthesis. Initially, the user's motion intention for reaching or lifting of the arm was identified using the EEG recordings from the scalp. For this purpose, four different kinds of EEG features were used to train two different classification techniques. Identified locations for feature extraction were related to motor cortex areas of the brain, which will be activated for motor tasks. Accordingly, as the motion intention classifier, 20 different neural network models

and 20 *k*-nn models were trained with features of MRCP-based amplitudes, delta band power, RMS, and alpha band for the five subjects. Trained classifiers were used to predict three different motion classes: hand reaching, arm lifting, and rest. To improve the reliability of the estimation, the output from these classifiers was compared (gated) with motions of the residual limb. A summary of the results is shown in Figure 3.13. neural network based motion estimation performed much better than the *k*-nn-based motion estimation. With the neural network based estimation, the MRCP-based feature, RMS, and alpha band power showed almost equal average results for all the five subjects. However, alpha band power had the least deviation in the results. A highest accuracy was achieved with the MRCP-based feature for Subject 1 (84.75%); the lowest was with RMS for Subject 5 (61.6%). Conversely, with *k*-nn-based estimation, RMS achieved the highest average accuracy (61.3%) with a higher deviation. When features were combined, the average accuracy was lower than for the other features, except for the delta band power with neural network based motion estimation. With *k*-nn-based motion estimation, models trained with combined features recorded average accuracies higher than those of alpha band power and the delta band power. In this study, analysis was carried out by combining all four feature types. However, there are

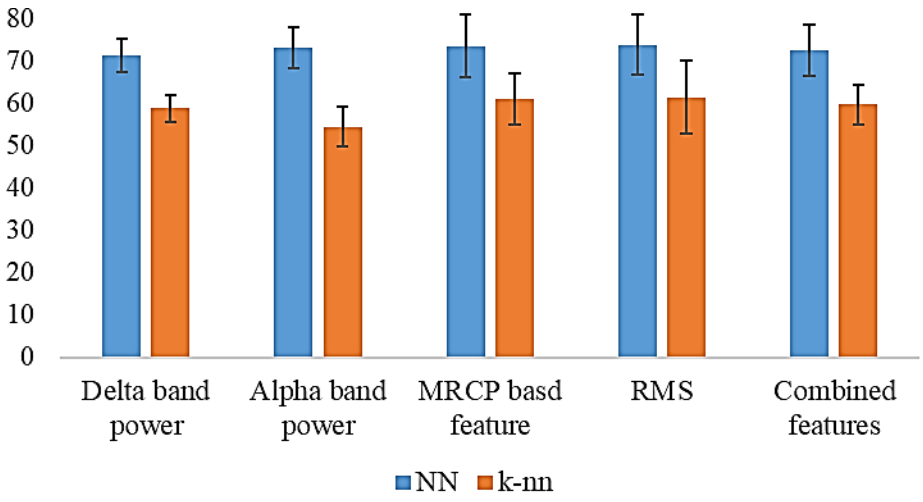

Fig. 3.13: Summary of the results of the motion intention classifiers (error bars show the standard deviation).

number of different possibilities for combining the features, such as combining two or three different features. In the scope of this study, it does not consider these possibilities.

In addition, the chance levels were computed for the five subjects; they have the values of 46.9%, 49.0%, 53.4%, 36.9%, and 37.5% from Subjects 1–5, respectively. Percentage accuracy values recorded with the neural-network-based estimation are significantly higher than the recorded chance levels for all five subjects. Furthermore, a p-value < 0.05 recorded based on the binomial test suggests that the results obtained are statistically significant.

Furthermore, Figure 3.14 and Figure 3.15 summarize and compare the results of the motion intention estimation before gating with the residual limb motion and the after gating with the residual limb motion. Figure 3.14 and Figure 3.15 shows the results of neural network based estimation and results of the k–nn based estimation, respectively. Evidently, the proposed gating method has resulted in significant improv-

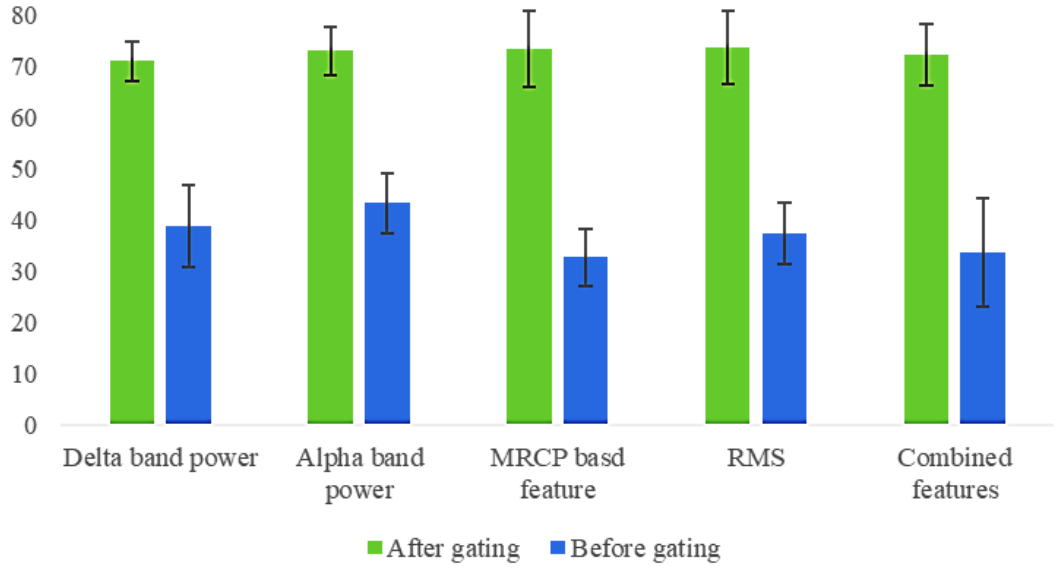

Fig. 3.14: Comparison of the estimation results for neural network based estimation before and after the gating method

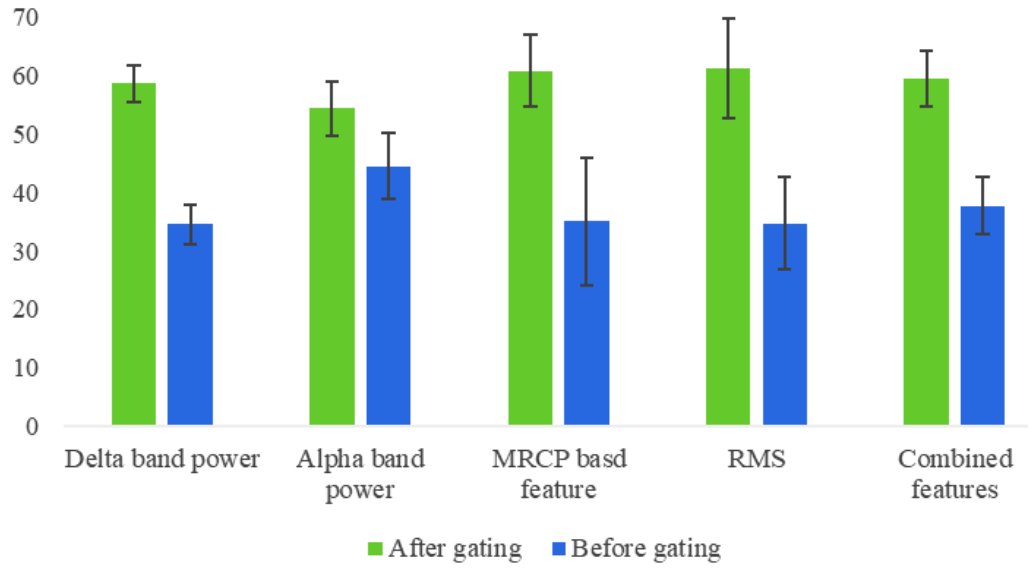

Fig. 3.15: Comparison of the estimation results for k–nn based estimation before and after the gating method

ement in the estimation results avoiding false triggers of the either of the motions. However, only when the estimation before the gating method is considered, alpha power band based feature show better results compare to the other four different feature sets. However, after gating with neural network based estimation, the results achieve closer value compare to the results before gating. This is due to the avoidance of the false triggers during the resting period of the upper-limb motion. Furthermore, it was observed that alpha power band based estimation produced more false triggers during the resting period compared to other feature types. Despite, the proposed gating methods has contributed to the performance enhancement of the motion intention identification in this study.

The relationships among residual shoulder angle, elbow joint angle, and end effector position were also investigated. These relationships were used to estimate the end effector position and the elbow joint angle of the amputee using the residual shoulder angle. Ten individual neural networks were trained with healthy subjects to estimate the end effector position and the elbow joint angle. These results show that it

is feasible to control the elbow joint of a transhumeral prosthesis, once the motion intention is identified. It is also possible to control multi-DoF motion of the prosthesis for reaching tasks. However, this requires a properly developed inverse kinematic model for the prosthesis, using the relationship between the endpoint and the residual shoulder angle. Thus, the proposed method demonstrates the capability of using the proposed approach to control multiple DoFs of a transhumeral prosthesis.

However, this proof of concept study was performed with healthy subjects. In [23], Estelle et al. showed that amputees show deteriorated activations of the EEG signals compared with healthy subjects during motor execution tasks of absent movements of the individual joints of the phantom limb. In the current study, during arm lifting and reaching movements, both phantom arm movement and the residual limb movements are collaborated. It is not clearly understood what will be the response of the brain in such a scenario. On the other hand, some studies [24], [25] have shown that the involvement of the brain to perform task-based upper limb motions such as reaching, pointing, etc., is different from the individual joint motions. On this note, we assume that the current study is applicable to upper limb amputees.

3.5 Conclusions

In this chapter, a new approach was proposed to control a multi-DoF transhumeral prosthesis taking into account the motion intention of the user based on EEG signals. It consists of three major steps: EEG based motion intention identification, collection of motion information from healthy subjects to create a database, and estimation of the motion of the prosthesis based on residual limb motion. The motion intention was predicted for two major upper-limb functions: arm lifting and hand reaching. Based on the motion intention prediction and the residual limb shoulder angle, appropriate multi DoF motion of the arm prosthesis can be realized. To predict the motion intention, three different features were used to provide input to the neural network based classifier. Time delayed inputs were provided to the classifier to yield dynamic information of the different features. The prediction from the

classifier was compared with the residual motion to generate a final prediction of motion intention. The results prove the feasibility of the proposed approach to control multi DoF motion of a transhumeral prosthesis using EEG signals.

References

[1] A. E. Schultz and T. A. Kuiken, “Neural interfaces for control of upper limb prostheses: the state of the art and future possibilities,” *PM R*, vol. 3, no. 1, pp. 55–67, Jan. 2011.

[2] S. K. Kundu, K. Kiguchi, and E. Horikawa, “Design and Control Strategy for a 5 DOF Above-Elbow Prosthetic Arm,” *Int. J. Assist. Robot. Mechatron.*, vol. 9, pp. 61–75, Sep. 2008.

[3] L. Resnik, S. L. Klinger, and K. Etter, “The DEKA Arm: Its features, functionality, and evolution during the Veterans Affairs Study to optimize the DEKA Arm,” *Prosthet. Orthot. Int.*, Oct. 2013.

[4] T. Lenzi, J. Lipsey, and J. W. Sensinger, “The RIC Arm #x2014;A Small Anthropomorphic Transhumeral Prosthesis,” *IEEEASME Trans. Mechatron.*, vol. 21, no. 6, pp. 2660–2671, Dec. 2016.

[5] K. B. Fite, T. J. Withrow, X. Shen, K. W. Wait, J. E. Mitchell, and M. Goldfarb, “A Gas-Actuated Anthropomorphic Prosthesis for Transhumeral Amputees,” *IEEE Trans. Robot.*, vol. 24, no. 1, pp. 159–169, Feb. 2008.

[6] “A ‘Manhattan Project’ for the Next Generation of Bionic Arms - IEEE Spectrum,” 11-Feb-2014. [Online]. Available: http://spectrum.ieee.org/biomedical/bionics/a-manhattan-project-for-the-next-generation-of-bionic-arms. [Accessed: 11-Feb-2014].

[7] C. Toledo, L. Leija, R. Munoz, A. Vera, and A. Ramirez, “Upper limb prostheses for amputations above elbow: A review,” presented at the Health Care Exchanges, 2009. PAHCE 2009. Pan American, 2009, pp. 104–108.

[8] “Motion Control, Inc. U3+ Arm Myoelectric Prosthesis,” 13-May-2014. [Online]. Available: http://www.utaharm.com/ua3-plus-myoelectric-arm.php. [Accessed: 13-May-2014].

[9] D. S. V. Bandara, R. A. R. C. Gopura, K. T. M. U. Hemapala, and K. Kiguchi, “Development of a multi-DoF transhumeral robotic arm prosthesis,” *Med. Eng. Phys.*, Jul. 2017.

[10] A. Akhtar, N. Aghasadeghi, L. Hargrove, and T. Bretl, “Estimation of distal arm joint angles from EMG and shoulder orientation for transhumeral prostheses,” *J. Electromyogr. Kinesiol.*, vol. 35, pp. 86–94, Aug. 2017.

[11] J. E. Cheesborough, L. H. Smith, T. A. Kuiken, and G. A. Dumanian, “Targeted Muscle Reinnervation and Advanced Prosthetic Arms,” *Semin. Plast. Surg.*, vol. 29, no. 1, pp. 62–72, Feb. 2015.

[12] T. A. Kuiken *et al.*, “Targeted Muscle Reinnervation for Real-Time Myoelectric Control of Multifunction Artificial Arms,” *JAMA J. Am. Med. Assoc.*, vol. 301, no. 6, pp. 619–628, Feb. 2009.

[13] K. Kiguchi, T. D. Lalitharatne, and Y. Hayashi, “Estimation of Forearm Supination/Pronation Motion Based on EEG Signals to Control an Artificial Arm,” *J. Adv. Mech. Des. Syst. Manuf.*, vol. 7, no. 1, pp. 74–81, 2013.

[14] D. Bright, A. Nair, D. Salvekar, and S. Bhisikar, “EEG-based brain controlled prosthetic arm,” in *2016 Conference on Advances in Signal Processing (CASP)*, 2016, pp. 479–483.

[15] I. K. Niazi, N. Jiang, O. Tiberghien, J. F. Nielsen, K. Dremstrup, and D. Farina, "Detection of movement intention from single-trial movement-related cortical potentials," *J. Neural Eng.*, vol. 8, no. 6, p. 066009, Dec. 2011.

[16] N. A. Bhagat *et al.*, "Design and Optimization of an EEG-Based Brain Machine Interface (BMI) to an Upper-Limb Exoskeleton for Stroke Survivors," *Front. Neurosci.*, vol. 10, p. 122, 2016.

[17] A. Vuckovic and F. Sepulveda, "Delta band contribution in cue based single trial classification of real and imaginary wrist movements," *Med. Biol. Eng. Comput.*, vol. 46, no. 6, pp. 529–539, Jun. 2008.

[18] L. Kauhanen *et al.*, "EEG and MEG brain-computer interface for tetraplegic patients," *IEEE Trans. Neural Syst. Rehabil. Eng.*, vol. 14, no. 2, pp. 190–193, Jun. 2006.

[19] G. Pfurtscheller and F. H. Lopes da Silva, "Event-related EEG/MEG synchronization and desynchronization: basic principles," *Clin. Neurophysiol.*, vol. 110, no. 11, pp. 1842–1857, Nov. 1999.

[20] H. Jasper and W. Penfield, "Electrocorticograms in man: Effect of voluntary movement upon the electrical activity of the precentral gyrus," *Arch. Für Psychiatr. Nervenkrankh.*, vol. 183, no. 1–2, pp. 163–174, Jan. 1949.

[21] E. Punskaya, "Design of FIR Filters," University of Columbia, 2009.

[22] "An improved K-nearest-neighbor algorithm for text categorization," *Expert Syst. Appl.*, vol. 39, no. 1, pp. 1503–1509, Jan. 2012.

[23] E. Raffin, P. Giraux, and K. T. Reilly, "The moving phantom: Motor execution or motor imagery?," *Cortex*, vol. 48, no. 6, pp. 746–757, Jun. 2012.

[24] F. Filimon, “Human cortical control of hand movements: parietofrontal networks for reaching, grasping, and pointing,” *Neurosci. Rev. J. Bringing Neurobiol. Neurol. Psychiatry,* vol. 16, no. 4, pp. 388–407, Aug. 2010.

[25] R. Caminiti, P. B. Johnson, and A. Urbano, “Making arm movements within different parts of space: dynamic aspects in the primate motor cortex,” *J. Neurosci. Off. J. Soc. Neurosci.*, vol. 10, no. 7, pp. 2039–2058, Jul. 1990.

Chapter 4

Velocity based Estimation of Motion Intention of Wearable Robot Users

Chapter Overview

EEG signals are known to carry a higher amount of information that represent physiological and psychological behavior of a human. However, having a higher information density and a higher noise ratio compare to other types of BCI modalities, it is challenging to extract the only motion related information from the EEG signals. However, in the Chapter 3 and Chapter 4 the estimated parameters were related to the intermittent motion intention of the human. Accordingly, a task or a certain focused motion intent was estimated by using a collection of information over the time series information. Conversely, when it comes to the velocity estimation, the estimation parameter become a continuous time series prediction. Therefore, during the estimation of the velocity, EEG signals should be capable of providing necessary adequate information to perform the time series estimation. In this chapter the feasibility of using two different approaches to estimate the user's motion intention in terms of velocity are evaluated. In the first method user's motion is estimated in the form of individual joint based velocity for 2DoFs. This will enable the control of similar number of DoFs of the robot. In the latter method, user's motion intention is estimated in the form of the velocity of the hand trajectory. This will enable full control of the DoFs of the robot corresponding to generate the similar hand trajectory motion. In this chapter, the experimental procedures for the evaluation of the proposed approaches and the results are presented.

Chapter 4

4.1 Introduction

Chapter 3 and Chapter 4 proposed the motion estimation methods of wearable robotic wearers, in terms of the expected task to be performed to be used for the intuitive control of the wearable robot. In this case, the predictions have to be made intermittently based on the time series data from the EEG signals for predefined number of tasks. However, with that kind of control the user's motion range get limited only to the estimated tasks by the controller. On the other hand, if it possible to estimate the individual joint movements or at least the end point movement in terms of continuous time series signal such as velocity it would be the best estimation to control a wearable robot similar to a real life situation. Recently several invasive [1], [2] and noninvasive [3], [4] attempted velocity based motion estimation using different BCI techniques.

In [1], the endpoint velocity and gripper command were extracted from the instantaneous firing rates of simultaneously recorded units from a micro electrode array implanted to a monkey control a 5 DoF robotic arm. Nakanishi *et. al.* [2] porposed a joint angles and joint trajectories estimation method using the ECoG electrodes implanted to a human brain. In their method, , 15 channel and 60 channel electrodes were placed in the sensorimotor cortex of the patient surgically to estimate the 3D trajectories of the left hand motion.

In using the noninvasive techniques, Kiguchi *et. al.*[3] proposed a neural network based 1 DoF joint parameter estimation methodology with EEG signals. In this study, the joint angle, angular velocity and angular acceleration of the supination/ pronation were estimated using different features of EEG signals to train neural network based classifiers. In [4], Jun *et. al.* proposed a method to estimate the hand movement velocity from EEG signals during a drawing task. In their method, power band features of EEG were derived from 0.1 – 4 Hz band and 24 – 28 Hz band to reconstructed hand movement velocity by Kalman filtering and a smoothing algorithm.

Chapter 4

In contrast to the task based estimation approaches presented in previous chapters, velocity based motion estimation demands the estimation of time series parameter continuously from motion onset to the end of the motion. From the aforementioned studies, invasive techniques demonstrate the better estimation capabilities compared to the noninvasive techniques. During the invasive techniques, the signal recording is more localized to the exact area of the brain and the recording technology is capable of recording low level activities of the brain activation using the micro electrode arrays or the ECoG techniques.

Conversely, EEG signals record more global level activity of the human brain from the scalp and a single recording from a single channel of EEG might be an electrical activity change owing to a bunch of low level brain activities. Even though some of the aforementioned studies have shown some success on decoding single DoF motions, multi DoF estimation of motion is yet to be achieved.

Accordingly, this chapter is intended to study the feasibility of using two new approaches to predict the user's motion intention. Initially the user's motion intention to move 2 DoF of the upper limb is estimated in terms of velocity for the wrist flexion/ extension and elbow flexion/ extension motions. In the next method the velocity of the motion path of the user's hand end point is estimated using the EEG signals. In the first method, the activation of the brain is identified in an offline study and the results are used to train a neural network based classifiers to estimate the 2 DoF motion velocity. During the estimation of the hand end point velocity, In order to recognize the dynamic information of the EEG signals, root mean square (RMS) based feature matrix introduced as input to the nonlinear autoregressive network with an exogenous input. Experiments were carried out to test and prove the proposed methodology are presented in this chapter. Next sections respectively present the details of the EEG measurement, methodology and results. Final section is dedicated for conclusion.

4.2 Methodology

The attempted methodologies to study the feasibility for velocity based prediction

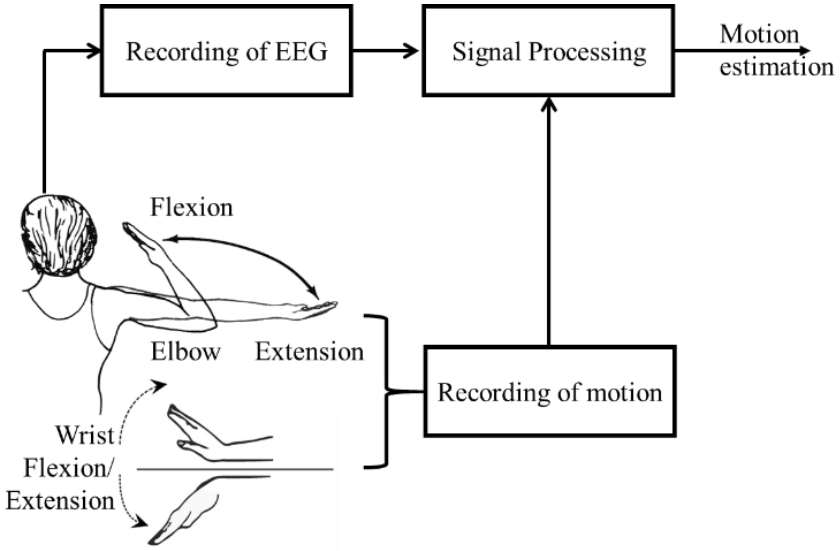

(a)

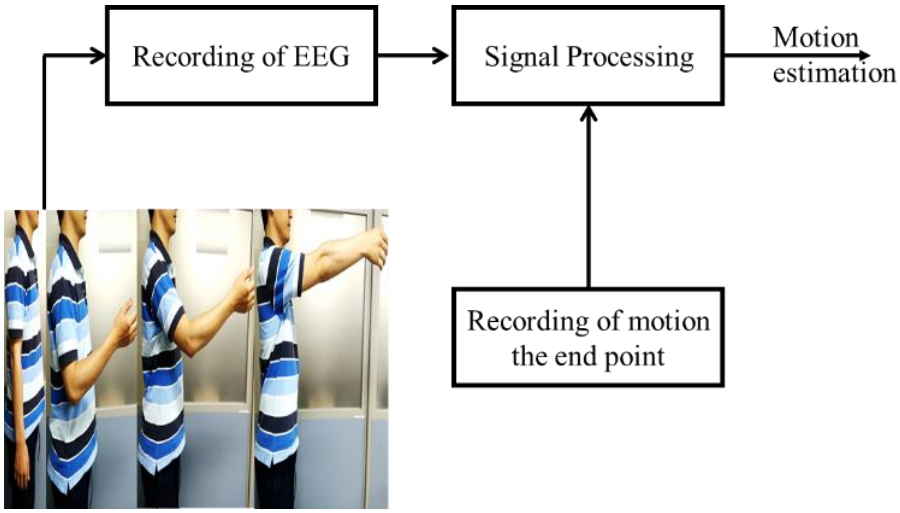

(b)

Fig. 4.1: Velocity estimation approaches (a)Joint based velocity estimation (b)End – point velocity estimation

4.2.1 Joint based velocity estimation

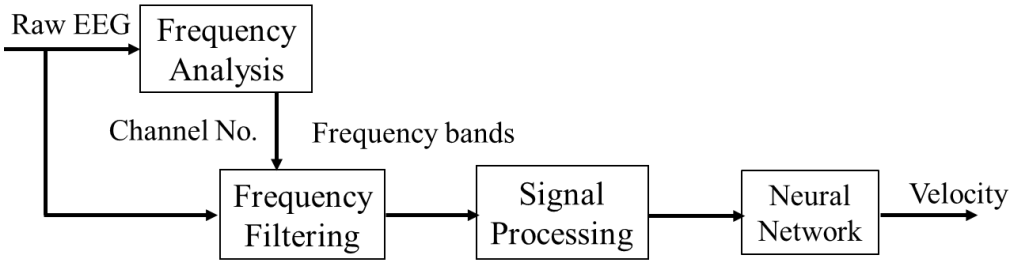

Fig. 4.2: Proposed approach for motion intention estimation

is shown in Figure 4.1. In the first method shown in Figure 4.1. (a) two of the motions of the user's upper limb is selected, in order to attempt multi DoF estimation. Accordingly, elbow flexion/ extension and wrist flexion/ extension motions were selected. In the later method user's hand end point motion is estimated using the EEG signal, as illustrated in Figure 4.1.(b). Identifying the user's end point motion also can enable the multi DoF controlling of a wearable robot. In the following sections the experimental method and the signal processing techniques are explained in detail.

Proposed approach for the joint based estimation is shown in Figure 4.2. Initially, raw EEG signals are recorded from the human scalp simultaneously with the motion capture data. Then the EEG signals are analyzed in an offline study, in order to understand the motion related activation. During the estimation, the results from the offline analysis are used to process the signals to feed into a neural network based classifier. Details of each step are explained below.

A. Experimental Setup

In this study, EEG signals are recorded at 15 locations on the human scalp using gamma.cap (Gtec Co.) and amplifier (Nihon Kohden Co.) systems. Locations of the electrodes are placed according to the standard 10-20 system. Fifteen electrodes are placed at Fp1, Fp2, F3, F4, C3, C4, P3, P4, F7, F8, T3, T4, Fz, Cz and Pz positions as shown in Figure 4.3(a). Setup of the motion capture system and the marker placement on the subject's upper limb is shown in Figure 4.3(b). The sampling

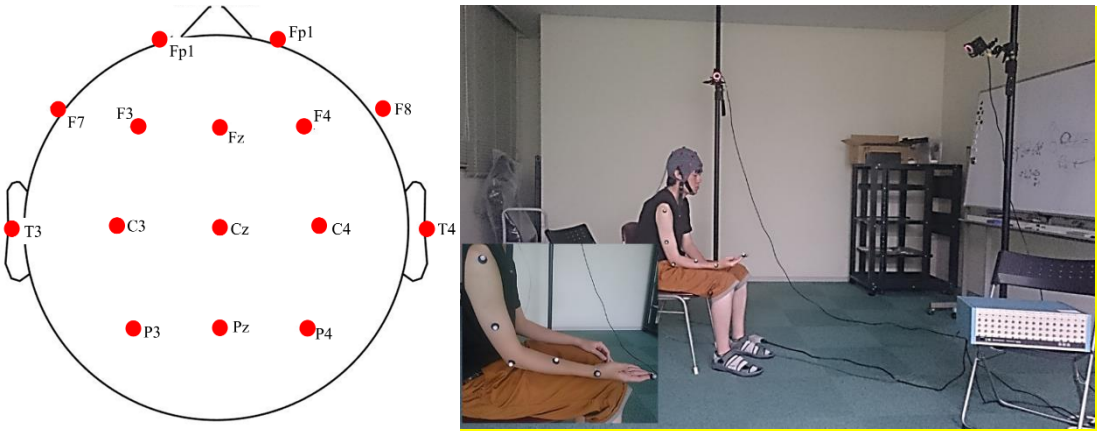

(a) (b)

Fig. 4.3: Experimental setup (a) Electrode layout (b) Recording environment with motion capture system

frequency of the measurement of EEG signals is 500 Hz. During the experiments, subjects perform wrist flexion/extension together with elbow flexion/ extension. Simultaneously to the EEG measurement joints angle of the user was recorded with Osprey (Motion Analysis Co.) motion capturing system. Subjects carried out the motion for 5 seconds after 5 seconds interval and is one cycle. Duration of 1 trial is 120s and 10cycles of motion. Two healthy male subjects (age: 24 and 31) participated for the experiments.

B. Signal Processing

In the first step, in order to remove the influence of the noise that is generated among whole electrodes and to average the recording over the scalp, Common Average Reference (CAR) is calculated as in Eq. 4.1.

$$e_{car,i}(t) = e_i(t) - \frac{1}{N}\sum_{k=1}^{N} e_k(t) \qquad 4.1$$

where N is the number of channels used in the recordings, $\boldsymbol{e_i(t)}$ is the raw EEG signal from the i^{th} channel at time t, $\boldsymbol{e_{car,i}(t)}$ is the CAR-corrected EEG signal of the i^{th}

channel at time *t*, and $\boldsymbol{e_k(t)}$ is the EEG signal of the k^{th} channel for average calculations. After CAR correction, the data are ready for further analysis.

Depending on the performed task, different brain regions are activated. Furthermore, different frequency ranges are emitted from brain for different tasks of the body. Better understanding of the location and the range of frequencies generated for the upper-limb tasks is one of the important steps on estimating the desired motion of the wearable robot users. Accordingly, proposed approach to detect the human motion intention comprises of two analysis steps, offline analysis and real-time analysis as shown in a block diagram in Figure 4.2.

Initially, power spectrum of the EEG signal is calculated based on the Fast Fourier Transform (FFT) analysis on the signal after CAR for each electrode separately as a method of analyzing the frequency as in Eq. 4.2.

$$X[k] = \sum_{t=0}^{N-1} X_{car,i}(t) e^{-2\pi jtk/N} \tag{4.2}$$

where $X_{car,i}(t)$ denotes the time series EEG signal, and *N* denotes the total number of data points in the signal. These results from the frequency analysis can be used in real-time motion estimation.

Accordingly, the activated locations of the brain and the frequency ranges are identified during the during the frequency analysis. In real-time analysis, only the signals from identified electrode locations are considered. Selected signals are passed through a frequency filter with the boundary conditions defined according to the activated frequency bands. Resulting signal is then squared to enhance the time series properties of the EEG for subject's motion intention. These time series data contain the information of the user's motion intension for elbow and wrist motions.

The obtained data is used to construct the training matrix for the neural network

based classifier. Accordingly, the feature matrix is provided with three inputs from a selected channel which allows the features to contain dynamic information of EEG. Thus the feature matrix looks like $EEG_1(t)$, $EEG_1(t-\Delta t)$ and $EEG_1(t-2\Delta t)$, where $EEG_1(t)$ stands for the EEG signal of a selected channel at a given time *t* s.

The feature matrices are used to train two separate feed forward neural networks. Each neural network consists of three layers, input layer, hidden layer and output layer. Hidden layer contains 10 neurons. Sigmoidal transfer function is used in both hidden and output layers in order to calculate the output of each layer. Each neural network is trained using error-back propagation algorithm. Each neural network provides the velocity of the elbow and wrist motions as their outputs separately.

4.2.2 Trajectory based velocity estimation

Proposed approach for the trajectory based velocity estimation is shown in Figure 4.4. Initially, raw EEG signals are recorded from the human scalp simultaneously with the motion capture data. Then the Root Mean Square (RMS) values based EEG features are obtained. The features are used to train a neural network based classifier. Details of the followed step are explained below.

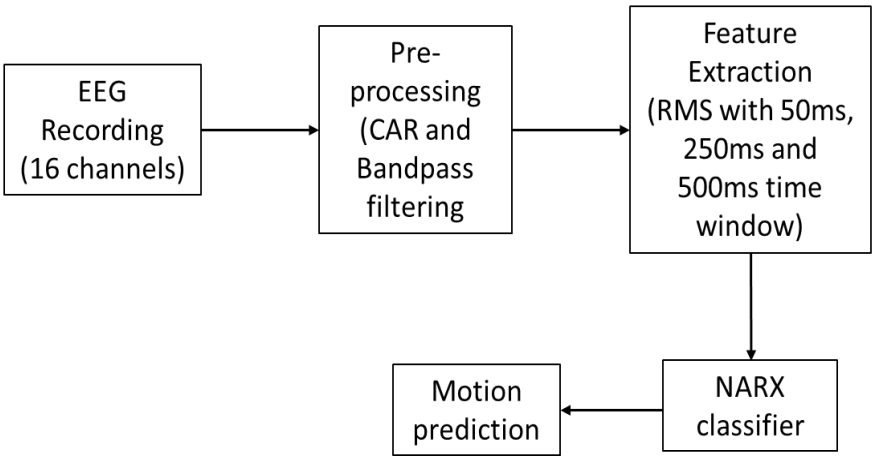

Fig. 4.4: Proposed approach for motion estimation

A. Experimental Setup

In this study, EEG signals are recorded at 16 locations on the human scalp using gamma.cap (Gtec Co.) and amplifier (Nihon Kohden Co.) systems. Locations of the electrodes are placed according to the standard 10-10 system. Sixteen electrodes are placed at Fz, F3, FC2, FC1, FC5, C2, Cz, C1, C3, C5, T3, CP2, CP1, CP5, P3 and Pz positions as illustrated in Figure 4.5 (a) . The sampling frequency of the measurement of EEG signals is 500 Hz.

(a) (b)

Fig. 4.5: Experimental Conditions (a)Electrode Layout (b) Different motion steps of reaching motion

During the experiments, subjects perform arm extension motion similar to a reaching motion in daily motions. The basic motion pathway is shown in Figure 4.5 (b). This motion is mainly a combination of movements of the shoulder, elbow and wrist motions of the subject. Simultaneously to the EEG measurement, motion of the subject's hand end point motion is recorded with v120: Duo (Optitrack) motion capturing system. During the experiment, subjects are given an audible cue "start" to start a single reaching motion cycle. Starting position of the arm is fully extended elbow and perpendicular to the ground. The subject is given the audible cue at every 5s or 6s interval randomly. Duration of 1 trial is 130s and 20 cycles of motion is carried out. One healthy male subjects and one female subject (age: 24, 28 and 26) participated for the experiments.

B. Signal Processing

Recorded EEG data are CAR processed similar to the same process in 4.1.1 B

using the Eq 4.1. After CAR, the resulting signal is band pass filtered in the delta range (i.e – 0.1Hz – 4Hz).

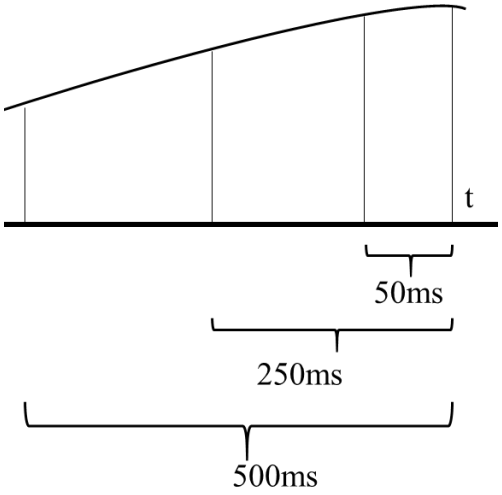

Fig. 4.6: Representation of RMS in multiple time widows

In order to extract features for training of the classifier, RMS values are extracted from the filtered delta band signals as in Eq. 4.3,

$$RMS = \sqrt{\frac{1}{N_a}\sum_{k=t-N_a+a}^{t} e_{ik}^2} \qquad 4.2$$

where, e_{ik} represents the EEG signals of i^{th} channel after filtering at t^{th} sampling. N_a is the selected window length for RMS calculation.

Motion preparation and movement execution and post motion information of EEG signals are important in estimating the user's motion intention. Therefore, in order to gather the dynamic features for the classification three different N_a values were used to calculate the RMS values. Accordingly, 50ms, 250ms and 500ms time windows were used for the RMS calculation, at the given time ts. As shown in Figure 5.6, extracting the RMS from 3 different time windows let the feature matrix to contain different time series information, which can be used to make the classifier understand

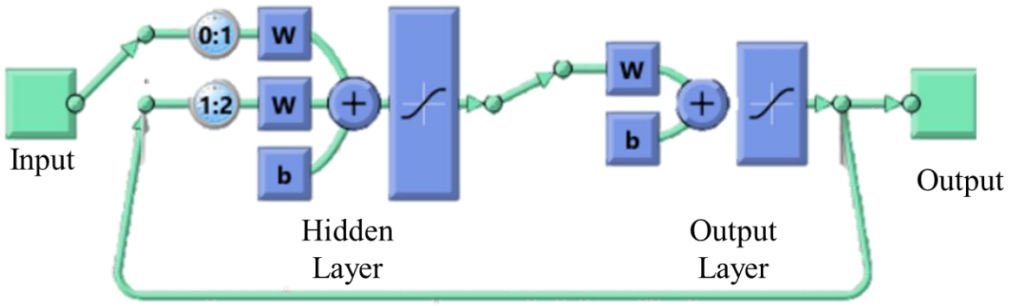

Fig. 4.7: Structure of the neural network used for trajectory estimation

the motion related dynamic EEG information. Input to the classifier is constructed as three inputs from a selected channel that comprises of the three different RMS values.

Thus the set of features make a $3 \times n$ input matrix to the classifier where n in the selected number of channels. Channel selection is carried out by observation of the feature plots. In this study nonlinear autoregressive network with an exogenous input is used as the classifier. This is a type of recurrent neural network with an input from the output of the network and comprises of three layers: input, hidden and output. Hidden layer contains 36 neurons. The output from the neural network will be the velocity of the hand end position. Three different networks are trained for three different subjects with experimental data and used for the prediction of velocity of the end point of the hand.

4.3 Results

Offline analysis results and motion estimation results for the individual joint based velocity estimation are presented below which will be followed by the results for the trajectory based velocity estimation results.

4.3.1 Joint based velocity estimation

Power spectrum analysis results reveal the activation of brain locations and the activated frequency ranges for the different motions performed. Thus obtained results

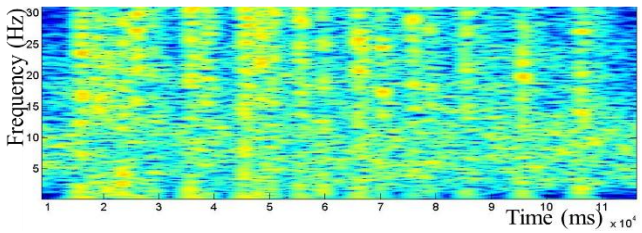

(a)

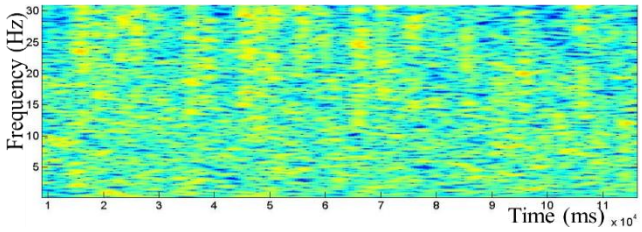

(b)

Fig. 4.8: Power spectrum analysis (a) P3 (b) F4

for P3 and F4 of subject 1 are shown in Figure 4.8(a) and Figure 4.8(b), respectively. In comparison, in the range of 0.1 – 4 Hz P3 shows a good activation for the motion onsets that that of the F4. In a similar manner the power spectrum for all 16 channels were observed. Similar to the activation shown in Figure 4.8(a) for P3, the other locations of C3, F7 and T3 show a good activation compared to the other channels. Most of the time frequency range below 4Hz shows a better activation in the above selected electrode locations. Electrode locations and frequency ranges are similar among all subjects.

According the results from the above analysis, EEG signals from the selected channels are band pass filtered at the range of 0.1 – 4Hz. The values of the resulting time series are then squared. Such obtained time series signals are shown in Figure 4.9. The activations of EEG patterns for F7 and T3 are respectively shown in Figure 4.9(a) and 4.9(b), respectively.

The feature matrix comprises of these time series signals are fed into the aforementioned neural networks. During the estimation of motion intention, resulting predicted velocities are shown in Figure 4.10. In the Figure blue color lines represent the actual recorded velocity and the orange color line shows the estimated velocity

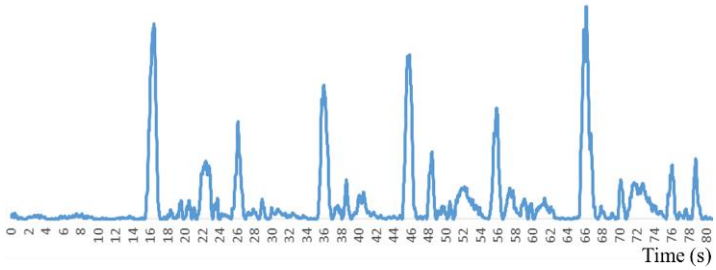

(a) F7

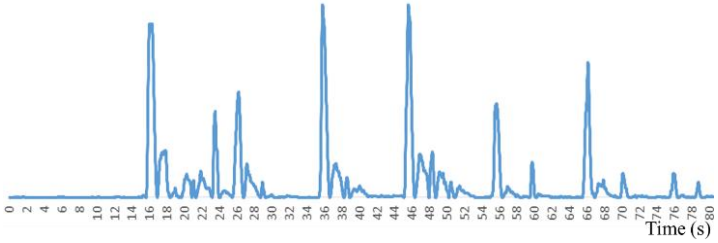

(b) T3

Fig. 4.9: Time series data of selected electrodes

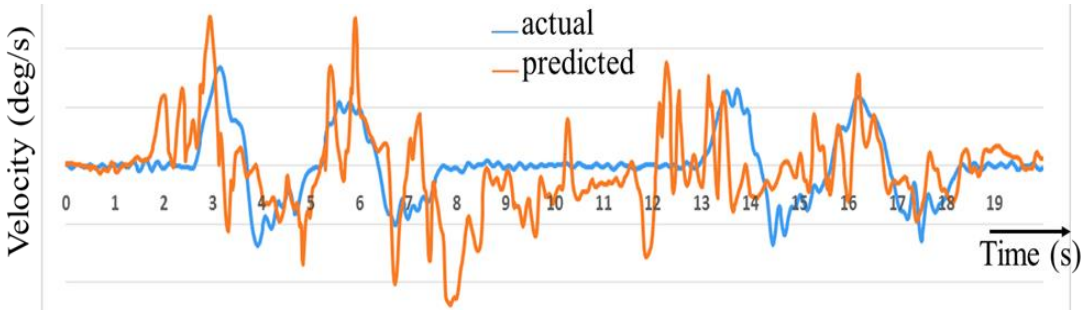

(a)

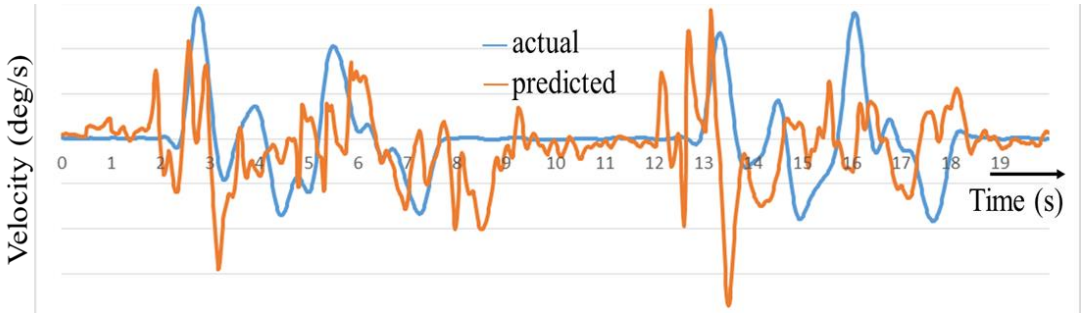

(b)

Fig 4.10: Comparison of actual velocity with predicted velocity (a) Elbow flexion/ extension (b) wrist flexion/ extension

from the classifier. Figure 4.10(a) and (b) respectively shows the comparison of elbow flexion/extension velocity and wrist flexion/ extension velocities. According to the graphs it can be observed that the direction of the motion intention of the user can be predicted accurately for the both upper limb motions.

4.3.2 Trajectory based velocity estimation

Initially, the feature plots for all the 16 channel are obtained. The feature plots are then observed to identify the best activated locations to be used for the estimation of motion intention. Thus based on the activation of the channels, for all subjects FC5, C5, T3 and CP1 locations are selected to provide input to the classifier. Feature plots for CP1 at 500ms time window are illustrated in Figure 4.11. In order for training, selected 4 channel locations make a feature matrix with 12 inputs to the classifier. Trained classifiers are used to estimate the end point velocity of the hand. Similarly predicted end point velocity of both subjects are illustrated in Figure 4.12. The results show that the proposed method can predict the end point velocity of the human hand similar to the real velocity for the 1 st subject as in 4.12(a). The results of the subject

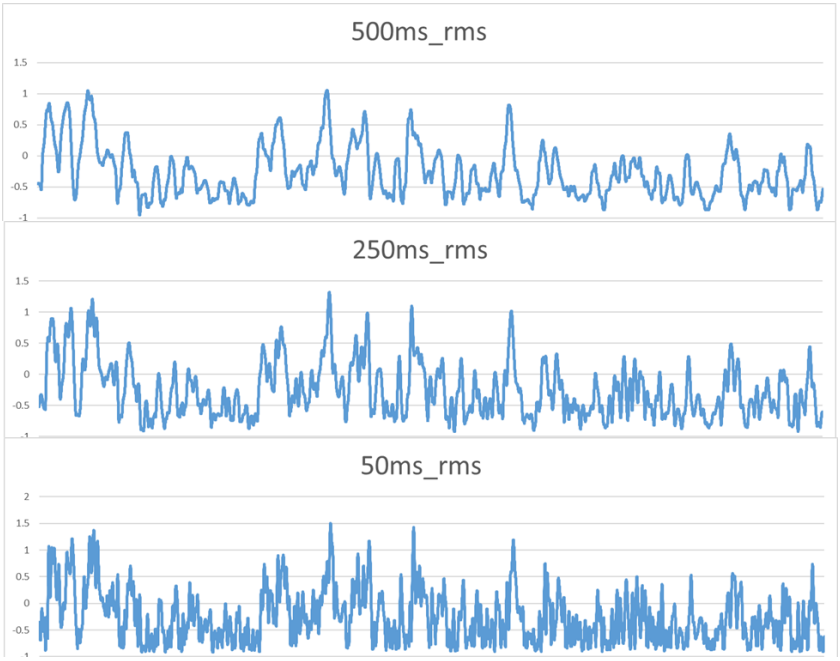

Fig 4.11: Feature Plot for CP1

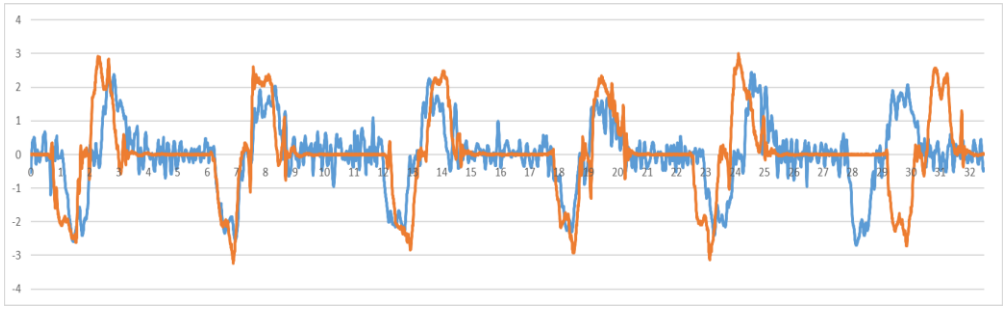

(a)

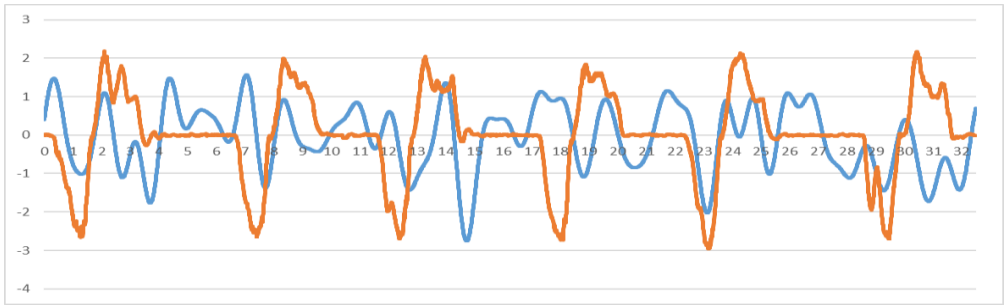

(b)

Fig 4.12: Comparison of predicted velocity with real velocity of end point of hand (blue – prediction, orange – real) (a) Subject 1 (b) Subject 2, (smoothed for clarity)

2 are smooth for better clarity in Figure 4.12(b) and show the estimation is capable of providing the direction of the motion.

4.4 Conclusion

Based on the final estimation based using the BCI, two different motion identification approaches can be identified. In this chapter the feasibility to use two different techniques to estimate the motion in terms of velocity was studied. Initially, individual joint based velocity was estimated for 2 DoF of upper limb motion. At first activated brain region and the frequency ranges for the intended user motions are identified in an offline study. The identified signals are used in real-time as input to the neural network to estimate the motion intention. Results demonstrated the feasibility of using the proposed approach for identification of the motion direction for multi DoF motions.

In the second step, the velocity of the hand trajectory was estimated for reaching task. In this method, to gather the dynamic information of the EEG signals RMS values of multiple time windows were used as features to the classifier. The features were used to train a nonlinear autoregressive to estimate the end point velocity of the human hand, in order to achieve the multi-DoF controlling of an upper-limb wearable robot. The results can be used with an inverse kinematic model of a human upper-limb to successfully control multi-DoF upper-limb exoskeleton robot.

In comparison, hand trajectory based motion estimation demonstrates better prediction capabilities than the individual joints based motion estimation. This may be expected, as in general humans do not actuate the joints individual to perform a motion involving multi DoFs. Instead humans focus on the motion of the end point of the hand most of the time for upper limb related motions. Therefore, EEG signals too can be expected to contain information related to the motion of the hand end point in comparison to the information related to individual joint motion. Furthermore, by estimating the motion intention of the end point it would be possible to achieve multi DoF controlling irrespective of the actual number of DoFs involving in the final motion. On the other hand with individual joint based estimation, prediction will be needed to be made for all the DoFs involving.

REFERENCES

[1] M. Velliste, S. Perel, M. C. Spalding, A. S. Whitford, and A. B. Schwartz, "Cortical control of a prosthetic arm for self-feeding," *Nature*, vol. 453, no. 7198, p. 1098, Jun. 2008.

[2] Y. Nakanishi *et al.*, "Prediction of Three-Dimensional Arm Trajectories Based on ECoG Signals Recorded from Human Sensorimotor Cortex," *PLOS ONE*, vol. 8, no. 8, p. e72085, Aug. 2013.

[3] K. Kiguchi, T. D. Lalitharatne, and Y. Hayashi, "Estimation of Forearm Supination/Pronation Motion Based on EEG Signals to Control an Artificial Arm," *J. Adv. Mech. Des. Syst. Manuf.*, vol. 7, no. 1, pp. 74–81, 2013.

[4] J. Lv, Y. Li, and Z. Gu, “Decoding hand movement velocity from electroencephalogram signals during a drawing task,” *Biomed. Eng. OnLine*, vol. 9, p. 64, Oct. 2010.

[5] Y. Hayashi and K. Kiguchi, “A study of features of EEG signals during upper-limb motion,” in *2015 IEEE International Conference on Advanced Intelligent Mechatronics (AIM)*, 2015, pp. 943–946.

[6] D. S. V. Bandara, A. Jumpei, and K. Kazuo, “A Non-Invasive BCI Approach for Predicting Motion Intention of ADL Tasks for an Upper-Limb Wearable Robot,” *Int. J. Adv. Robot. Syst.*

[7] T. D. Lalitharatne, A. Yoshino, Y. Hayashi, K. Teramoto, and K. Kiguchi, “Toward EEG control of upper limb power-assist exoskeletons: A preliminary study of decoding elbow joint velocities using EEG signals,” in *2012 International Symposium on Micro-NanoMechatronics and Human Science (MHS)*, 2012, pp. 421–424.

Chapter 5

Conclusion and Future Work

5.1. Conclusion

Wearable robotic systems such as exoskeletons or prostheses play an important role in providing the necessary assistant to the physically handicapped people by assisting to perform their day to day activities. This is a prevailing and demanding requirement towards improving the independency of handicapped community to have a better quality of life and is a great deal of importance for the socio – economic stability of the society. In order to provide a better user experience for the wearable robotic user, the mechanical design of the robot and the controlling of the robot according to the intended motions of the user is utmost important. Therefore, in this thesis the feasibility of using some novel approaches to estimate the user's motion intention with non – invasive, EEG signals are evaluated.

The thesis is structured with five chapters. At the beginning of the first chapter, it presents the prevailing requirement of assistive technologies to improve the independency. The it is dedicated to discuss the presently available motion estimation techniques including EMG signals and BCIs. It also provides an understanding to the human brain. At the final section of the first chapter, it provides a brief introduction to the flow and contents of the thesis. Next two chapters of the thesis are dedicated to present the research work towards developing task based motion intention estimation techniques.

In the second chapter, two activities of daily living tasks are estimated together with the resting state. Initially, EEG signals were recorded from six healthy male subjects simultaneously, for drinking, moving and resting states of the motion. In an

offline analysis of the EEG signals, the activation regions of the brain and the activation frequency ranges were identified. Then using a feature matrix made from power band features of the identified locations in a time series, SVM and neural network based classifiers were trained to estimate the user's intent for the motion. During the training of the classifiers, two types of data were used for the training. One set of training was carried out using data from the individual subjects. Another training was carried out using a single set of data, which comprises of data from all the six subjects. The later type of training data was used to study the generalizability of EEG signals over the subjects. Using the trained classifiers, subject's intended tasks were estimated. The estimation results were compared to the actually performed tasks and accuracy was calculated. In addition, the latency between the actual motion onset and the predicted motion was calculated. In terms of accuracy, SVM based classifiers performed better than the neural network based classifiers for both types of training data. With SVM, the SVM models trained with individual subject's data had better estimation capabilities compared to the SVM model trained with the data from the all six subjects. Conversely, the estimation capabilities of the neural network based classifiers improved drastically, for the neural network trained with the data from all the six subjects compared to the neural networks trained with individual subject's data. In terms of estimation time delay, neural network based classifiers showed better results compared to the same with the SVM based classifiers. Above results demonstrated feasibility of estimating the motion in terms of performed task. When the application is limited an individual or few individuals SVM based estimation algorithm can be used to achieve a better accuracy with the tradeoff of the estimation delay. However, where there are enough data for classifier training, neural network based algorithm may be used to generalize the estimation with better accuracy and quicker estimation capabilities.

Third chapter of the thesis proposed a motion intention estimation approach to estimate the motion intention of above elbow amputees to control a transhumeral

prosthesis for reaching tasks. The study comprised of EEG based motion intention identification which will be followed by the estimation of motion of the elbow and hand endpoint. During the EEG based motion identification, EEG signals were used to differentiate the motion between arm lifting, resting and reaching tasks. For a transhumeral amputee, the residual limb motion is similar for both arm lifting and reaching tasks. MRCP, band power and RMS features were derived from the raw EEG data, which were then used to train 15 different neural network for the 5 subjects for the 3 types of features. Later the prediction result from the neural network was gated with the motion state of the residual limb to avoid false triggers. Results demonstrated the feasibility of differentiating the three motion states, resting, arm lifting and reaching. Once a reaching motion is successfully identified, during the next step the limb motion parameters are estimated for elbow and hand end point movements. In this step, initially a database is created to identify the relationship between the motion of elbow angle to the shoulder joint and the end point motion to the shoulder joint angle during the reaching motion of the healthy subjects. Later this data is used to train a neural network based classifier. During the implementation, residual limb shoulder angle of the transhumeral amputee is fed in to the neural network to estimate the corresponding elbow and hand end point motion which can be used to control the tranhumeral prosthesis. Results demonstrated successful generalized usability of the data recorded from the healthy subjects to estimate the motion of the transhumeral amputees for reaching motion.

During the task based estimation, three types of classifiers were used namely, neural network based classifiers with sigmoidal transfer function, support vector machine classifier with radial basis function as kernel and k–nearest neighbor classifier with optimization technique to select better k value and the matrix. In the first study, both SVM and neural network are nonlinear classifiers. However, the SVM outperforms the neural network classifier. This could be due to the nature of the radial basis function used as the kernel function of the SVM classifier. RBF kernel considers

the normal distribution of a data point when defining the boundary of the data point to generate the hyper plane for the whole data set. Therefore, the SVM with RBF kernel represents the data set better than the sigmoidal function used with the neural network based classifier.

On the other hand, in the second study, neural network based classifier out performs the k-nn based classifier. This could be due to the nature of the EEG data, which used as input to the both classifier. In general, k-nn is good at representing lower dimensional data, compared with the data representation at high dimensional data. However, EEG is usually knowing to contain high dimensional data and due to this reason k-nn performs less compared with the neural network based classifier.

In the next chapter, velocity based motion intention approaches are studied. In this chapter two types of velocity based motion intention approaches are introduced. In one method it estimates the velocity of the individual joints for 2 DoFs. In the second method the velocity of the hand endpoint is estimated. In contrast to the task based estimation approaches, velocity based approached demand continuous time series estimation which may be challenging with the existing signal acquisition and processing technologies. During the estimation of the individual joint based motion, EEG data is recorded for simultaneous motions of elbow and wrist joints. In an offline analysis, the activated regions of the brain and the activated frequency bands are identified. Based on the results, power band data is used in a time series to train a neural network based classifier to estimate the two motions. Even though the results were not quantified, they demonstrated the feasibility of using EEG to estimate multi DoF motion by estimating individual joint parameters. During the trajectory estimation, EEG signals were recorded simultaneously to upper limb reaching motions. RMS features were extracted in different time windows for the same channel locations. RMS from the multiple time windows were combined in the feature matrix to make a time series data to be fed into an autoregressive network to estimate the motion intention. The estimated motion from the classifiers were compared with the desired

trajectory. Results demonstrated the capability of estimating the trajectory velocity using the proposed approach. In comparison, trajectory velocity based estimation approach performed better than the approach proposed for the estimation of individual joint based velocity.

5.2 Future Work

The studies presented in this thesis are still in their preliminary stage and can be improved in number of ways to be used with wearable robotic users. As mentioned in the second chapter, still not a lot of motion intention identifications studies had not focused on estimating the activities of daily livings (ADL) of the users. The study proposed in this chapter evaluates the concept with two activities of daily living. However, the study can be further extended to identify more ADL tasks in a future study. At the same time, the ADL tasks may be categorized into few categories based on the type DoF involving, movement direction or other identified criteria. Then the motion intention estimation can be made in terms of category of the motion. A different sensor modality can be employed to identify the exact motion intention out of the estimated category of the ADL task.

In addition, the studies proposed here are carried out with healthy subjects as the testing platform. Further, the maximum number of subjects participated in this study are limited to 6 subjects. Although there is no exact definition on how many subjects should be used to validate the application of a certain BCI, it would be important to carry out the validation of the same approaches different classes of subjects such as more gender distribution in the subjects, more age distribution in the subjects, more ethnical distribution in the subject, different health condition in the subjects and more importantly a representation from the real end users of the proposed BCI systems.

Moreover, robust methods for recording and analyzing EEG data should be developed. When using the invasive techniques such as intra cortical micro electrode

arrays or ECoG, the implants are placed on a small area of the brain and the techniques have shown the capability of providing necessary information for motion estimation. In a similar manner, during the acquisition of EEG electrodes can be placed in a denser manner to record the brain activity. Later during the analysis, techniques to identify the motion related EEG features from the dense recordings can be investigated in the future.

Furthermore, there are different modalities in use to identify user motion intension, not only BCI based but also from different types of sensors. In order to improve the accuracy of the EEG based BCI, further research can be performed to investigate better combination of different sensor technologies such as NIRS, EMG, inertia measurement units, visual information from the cameras, motion capture systems, etc…

Appendix i

Purpose of the experiment: To study the effect of body image on the brain activation of different tasks

In Chapter 2, an approach to estimate the human motion intention was proposed in terms of intended tasks for moving and drinking. For moving, a higher brain activation was observed compared to that of the drinking. As explained in the discussion of Chapter 2, when there is an individual involvement to the performing task, the brain activation is attenuated. This experiment is performed to confirm the above phenomenon.

Experimental Setup

In this experiment EEG signals were recorded from 8 locations of the brain from a healthy male subject. A gamacap with 8 locations and ploymate mini, wireless Bluetooth EEG system was used to record the EEG signals. Electrodes were placed according to the international 10 – 20 system at F7, F3, F4, F8, T7, C3, C4 and T8 locations (See Figure 1). The sampling frequency for measurement of the EEG signals

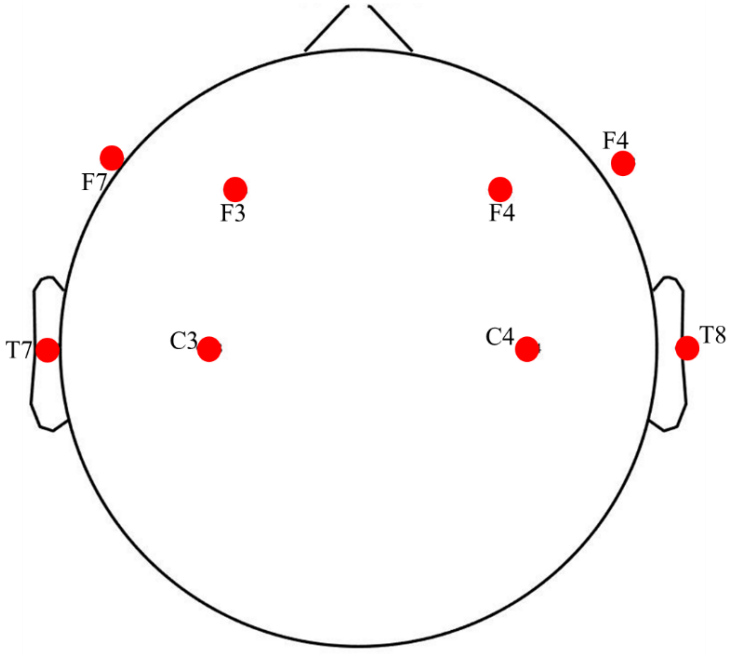

Figure 1. Electrode Layout

Appendix i

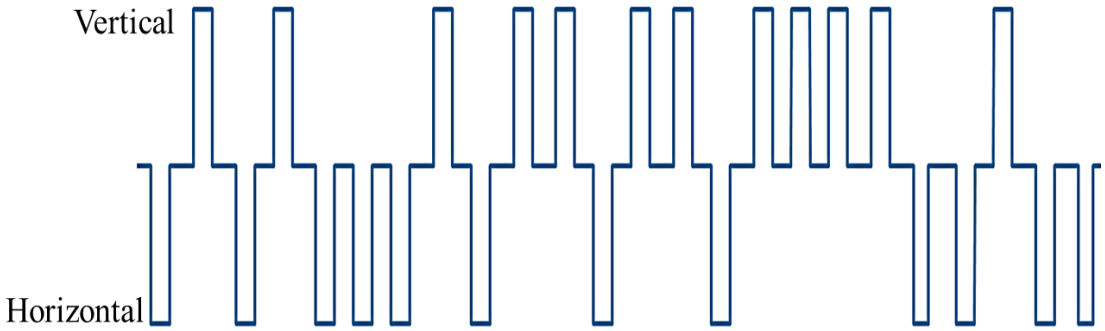

Figure 2. Motion Schedule

was set at 1000 Hz. The left ear lobe was used as the reference point for the EEG recordings.

The subject sits on a chair in front of a table and perform two different moving tasks vertical and horizontal. Horizontal movement tasks are similar to movement tasks explained during the section 2.2.1. Vertical movement tasks are expected to replace the drinking tasks. This is because drinking as a vertical movement task, the end point of the motion corresponds to a point in the body. On the other hand, the

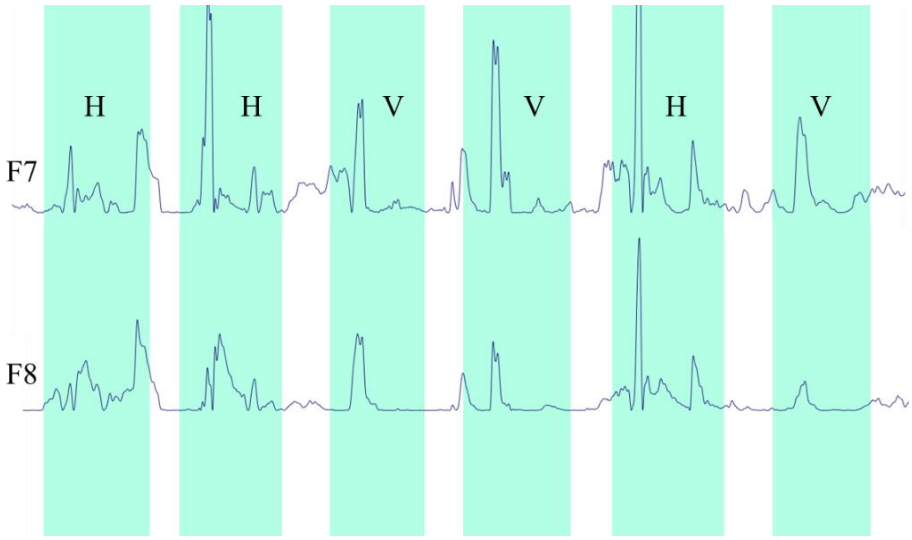

Figure 3. Activation of electrode location of F7 and F8 (H – horizontal, V – vertical movement)

subject moves a small object between two vertical points in the space during the vertical movement task in this experiment. The other experimental procedures and schedules are similar to the information presented in section 2.2.1. Figure 2 shows the motion schedule of vertical and horizontal movements.

Signal Processing:

Main purpose to study the brain activity for the two movement tasks and compare them with the brain activations for the initial experiment as shown in the Figure 2.9. Therefore, same techniques followed during the signal processing of the 2nd chapter was followed during this study. Accordingly, at first the common average reference was computed. Then the resulted signal was used to obtain the power band between 0.1Hz – 4 Hz. Similar power band was obtained in chapter 2 also.

Results:

Resulting brain activations related to the band power 0.1Hz – 4Hz are shown in Figure 3 for F7 and F8 locations of the human brain. Motion time ranges for vertical and horizontal movements are marked as H and V in the figure, respectively. During the both horizontal and vertical motions, higher brain activations can be observed.

Discussion:

Main focus of this study was to make sure, human body related motions attenuate the brain activations. In the initial observation with the drinking task, brain activations were attenuated compare to that of the horizontal movement as presented and explained in the Chapter 2. Two differences in the drinking and horizontal movement of an object are two tasks are in two different planes, horizontal and vertical; and horizontal movement occurred between two points in the space, but drinking task is between a point in the space and the mouth, a point related to the body. Therefore, to study the brain activity difference, the drinking task was replaced by a vertical movement task, which will occur between two different point in the space,

unlikely to the drinking task. When the same brain features are observed, vertical movement tasks show better activations compared to that of the drinking tasks. Therefore, as explain the discussion in the chapter 2, it can be deduced, that the brain activations will get attenuated when a point or points of the body involved with a motion task.

Appendix ii

Consent to Participate in a Research Study

Kyushu University ● Fukuoka, Japan

Title of Study:	**A Non-Invasive BCI Approach for Predicting Motion Intention of ADL Tasks for an Upper-Limb Wearable Robot**

Investigators:

Name:	**D.S.V Bandara**	**Dept:**	Department of Mechanical Engineering
Name:	**Jumpei Arata**	**Dept:**	Department of Mechanical Engineering
Name:	**Kazuo Kiguchi**	**Dept:**	Department of Mechanical Engineering

Introduction

- You are being asked to be in a research study of estimation of motion intention of upper – limb with EEG signals.
- You were selected as a possible ant because, the experiment will be performed with healthy subjects.
- We ask that you read this form and ask any questions that you may have before agreeing to be in the study.

Purpose of Study

- The purpose of the study is to estimate the subject's motion intention to move the upper – limb, using brain signals of the subject. The results from the study are expected to be used for developing a EEG based controller for an upper – limb wearable robot
- Ultimately, this research may be published as a journal paper in a peer reviewed journal.

Description of the Study Procedures

In this study, Gamma.cap (Gtec Co.) with 16 electrode locations, a g.Gammabox (Gtec Co.) and bio signal amplifier (Nihon Kohden Co.) will be used to record the EEG signals from the subjects. A standard 10-20 system will be followed to place the electrodes on the scalp and into the brain cap. Sixteen electrodes will be placed at selected positions shown in the Fig. 1. The left ear lobe was used as the reference for EEG recordings.

Appendix ii

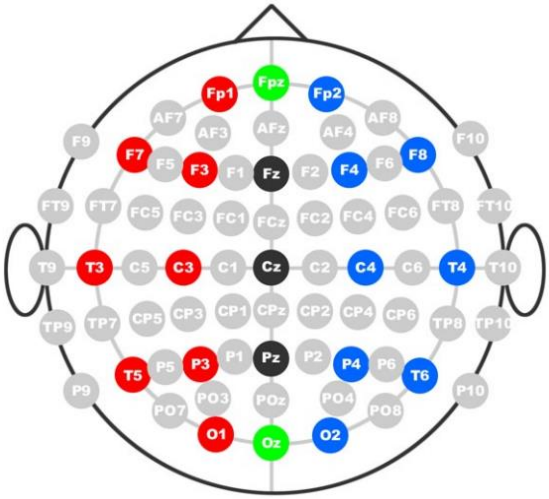

Figure 1: Locations for placement of electrodes

In the experiments, the subjects are expected to perform tasks of activities of daily living (ADLs) (such as, object moving, drinking, moving arm, etc...).

As an example, let's assume two tasks are selected and they are object moving and drinking.

The experiment begins with an audible cue to the subject "Start." The subject remained still during the first 10 s. The subject will be instructed to relax his hands on the legs when a task is not performed. An object will be placed on a table in front of the subject at 8 s, and the subject will be instructed to perform the task of object moving at 10 s by moving the object from right to left with an audible cue corresponding to "Start." The subject will have to move back to the relaxed position after moving the object to the left side. Subsequently, a 4 s interval exists prior to the start of the next task. A cup will be placed on the table in front of the subject at 2 s in the interval. At the end of 4 s in the interval, the audible cue "Start" will be given, and the subject will perform the drinking task by moving the cup toward the mouth in a manner similar to the ADL. The subject will simulate drinking and place the cup in the original position and returned to the rest positon. The subject is supposed to perform tasks at a self-paced rhythm. These procedures will be performed 40 times for 357 s. The interval between each task was randomly selected as either 3 s or 4 s. The order of the tasks will also be random. In such way the experimental schedule will be based on the selected number of ADLs.

In addition to the EEG measurements, simultaneously motion of the subject's body parts will be recorded with v120: Duo (Optitrack) motion capturing system.

Appendix ii

Risks/Discomforts of Being in this Study

- There are no reasonable foreseeable (or expected) risks. The whole experiment is design to be riskless. The electrodes will be attached to a brain cap and the brain cap will be put on to the head. Therefore, the electrode does not have a direct contact to the skin. A water soluble gel (g.Gammagel, Gtec Co.) will be used between the electrode and the skin. In addition, to be used with the motion capturing system markers will be placed on the body joint with adhesive tapes.

Benefits of Being in the Study

- There are no benefits of participation for the participants.

Confidentiality

- This study is anonymous. We will not be collecting or retaining any information about your identity. We might record a video or take pictures of the experiment. However, the face of the subject will not be reveled in the videos or the photos

Right to Refuse or Withdraw

- The decision to participate in this study is entirely up to you. You may refuse to take part in the study *at any time* (even in the middle of an experiment) without affecting your relationship with the investigators of this study or Kyushu University. Your decision will not result in any loss or benefits to which you are otherwise entitled.

Right to Ask Questions and Report Concerns

- You have the right to ask questions about this research study and to have those questions answered by me before, during or after the research. If you have any further questions about the study, at any time feel free to contact Prof. Kazuo Kiguchi at kiguchi@mech.kyushu-u.ac.jp or by telephone at xxx –xxxx - xxxx. If you like, a summary of the results of the study will be sent to you.
- If you have any problems or concerns that occur as a result of your participation, you can report them to the Prof. Kazuo Kiguchi at the number above.

Consent

- Your signature below indicates that you have decided to volunteer as a research participant for this study, and that you have read and understood the information

provided above. You will be given a signed and dated copy of this form to keep, along with any other printed materials deemed necessary by the study investigators.

Subject's Name (print): _____

Subject's Signature: _____ Date: _____

Investigator's Signature: _____ Date: _____

Appendix iii

```
% Calculates windowed (over- and non-overlapping) RMS of
a signal using the specified windowlength
%

function y = rms(signal, windowlength, overlap, zeropad)

delta = windowlength - overlap;

%% CALCULATE RMS

indices = 1:delta:length(signal);
% Zeropad signal
if length(signal) - indices(end) + 1 < windowlength
    if zeropad
        signal(end+1:indices(end)+windowlength-1) = 0;
    else
        indices  =  indices(1:find(indices+windowlength-1
<= length(signal), 1, 'last'));
    end
end

y = zeros(1, length(indices));
% Square the samples
signal = signal.^2;

index = 0;
for i = indices
    index = index+1;
    % Average and take the square root of each window
    y(index) = sqrt(mean(signal(i:i+windowlength-1)));
end
```